

Copyright Warning & Restrictions

The copyright law of the United States (Title 17, United States Code) governs the making of photocopies or other reproductions of copyrighted material.

Under certain conditions specified in the law, libraries and archives are authorized to furnish a photocopy or other reproduction. One of these specified conditions is that the photocopy or reproduction is not to be “used for any purpose other than private study, scholarship, or research.” If a user makes a request for, or later uses, a photocopy or reproduction for purposes in excess of “fair use” that user may be liable for copyright infringement,

This institution reserves the right to refuse to accept a copying order if, in its judgment, fulfillment of the order would involve violation of copyright law.

Please Note: The author retains the copyright while the New Jersey Institute of Technology reserves the right to distribute this thesis or dissertation

Printing note: If you do not wish to print this page, then select “Pages from: first page # to: last page #” on the print dialog screen

The Van Houten library has removed some of the personal information and all signatures from the approval page and biographical sketches of theses and dissertations in order to protect the identity of NJIT graduates and faculty.

ABSTRACT

The Collapse of the Cypress Viaduct During the Loma Prieta Earthquake of October 17, 1989

by

Mohamed M. Eid

The Loma Prieta earthquake of October 17, 1989 in California was one of the most disastrous earthquakes in U.S history. It caused damage to commercial, residential, and industrial structures, transportation and utilities.

This study includes investigations about the Cypress Viaduct collapse reported by:

1. California Governor's Board of Inquiry [4].
2. National Institute of Standards and Technology (NEL) [1].
3. The Author.

Investigators in the first report concluded that the collapse was due to horizontal ground motion. In the second one, it was due to the vertical ground motion.

In the author's investigation, a detailed static and dynamic analyses are performed to determine the cause of the failure. Static analyses are performed to determine the moment and shear capacities of the critical sections. Also to predict the mode and sequence of failure. Dynamic analyses are performed employing the finite element software ADINA to investigate the effect of ground motion on the Viaduct.

**THE COLLAPSE OF THE CYPRESS VIADUCT DURING
THE LOMA PRIETA EARTHQUAKE OF OCTOBER 17, 1989**

by
Mohamed M. Eid

A Thesis
Submitted to the Faculty of
New Jersey Institute of Technology
in Partial Fulfillment of the Requirement for the Degree of
Master of Science
Department of Civil Engineering
October, 1992

APPROVAL PAGE

The Collapse of the Cypress Viaduct During
the Loma Prieta Earthquake of October 17, 1989

by

Mohamed M. Eid

8/10/92

Dr. M. Ala Saadeghvaziri, Thesis Adviser
Assistant Professor of Civil Engineering, NJIT

Dr. William R. Spillers, Committee Member
Professor of Civil and Environmental Engineering and
Chairperson of the Department, NJIT

5/2/92

BIOGRAPHICAL SKETCH

Author: Mohamed M. Eid

Degree: Master of Science in Structural Engineering

Date: October, 1992

Date of Birth:

Place of Birth:

Undergraduate and Graduate Education:

- Master of Science in Civil Engineering, New Jersey Institute of Technology, Newark, NJ, 1992
- Bachelor of Science in Civil Engineering, School of Engineering, Cairo University, Cairo, Egypt, 1982

Major: Civil Engineering

ACKNOWLEDGMENTS

The work presented in this Thesis was carried out under the direction of Dr. M. A. Saadeghvaziri, whose valuable guidance, and assistance are gratefully acknowledged.

Also, thanks are due for the financial support provided to the author by the G. E. foundation through “The Young Faculty Grant” awarded to Dr. M. A. Saadeghvaziri.

TABLE OF CONTENTS

	Page
1 INTRODUCTION	1
1.1 General	1
1.2 Seismological Considerations	2
1.3 Description of the Cypress Viaduct (I-880)	3
1.3.1 B1 Bents	4
1.3.2 B2 Bents	7
1.3.3 B3 Bents	7
1.4 Site Conditions	10
1.5 Damage and Collapse of The Cypress Viaduct	11
1.5.1 Damage to B1 Bents	15
1.5.2 Damage to B2 Bents	16
1.5.3 Damage to B3 bents	17
1.6 Damage to Expansion Joints	17
1.7 Damage to Foundations	23
2 INVESTIGATIONS BY CALIFORNIA GOVERNOR’S BOARD OF INQUIRY AND NATIONAL INSTITUTE OF STANDARDS AND TECHNOLOGY	24
2.1 Report by California Governor’s Board of Inquiry [4]	24
2.1.1 Static Analyses	24
2.1.2 Dynamic Analyses	26
2.1.3 Conclusion	28
2.2 Report by National Institute of Standards and Technology [1]	29
2.2.1 Description of Collapse by Motorists	29

	Page
2.2.2 Dynamic and Static Results	29
2.2.3 Conclusion	32
2.3 Summary	33
3 STATIC ANALYSES	34
3.1 General	34
3.2 General Assumptions	34
3.3 Analyses of B1 Bent	35
3.3.1 Gravity Loads	35
3.3.2 Seismic Loads	35
3.3.3 Analyses at Critical Sections	37
3.3.4 Analyses at Section 1–1	37
3.3.5 Analysis at Section 2–2	47
3.3.6 Analysis at Section 3–3	48
3.4 Analyses of B2 Bent	51
3.5 Analyses of B3 Bents	55
3.6 Conclusion	59
4 DYNAMIC ANALYSES	60
4.1 Analyses of B1 Bent	60
4.1.1 Two Dimensional Model	61
4.1.2 Three Dimensional Model	71
4.2 Analyses of B2 Bent	90
4.3 B3 bents	95
4.4 Nonlinear Analysis	100
4.4.1 General	100

	Page
4.5 Comparison of Static and Dynamic Analyses	101
4.5.1 B1 Bents	101
4.5.2 B2 Bents	106
4.5.3 B3 Bents	107
5 CONCLUSION	108
BIBLIOGRAPHY	109

List of Tables

Table	Page
2.1 Fundamental Frequencies	26
3.1 Seismic Forces Causing Flexural Damage at Section 1-1	45
3.2 Seismic Forces Causing Shear Failure at Section 2-2	48
3.3 Seismic Forces Causing Flexural Damage at Section 3-3	50
3.4 Seismic Forces Causing Flexural Damage at Section 1-1	53
3.5 Seismic Forces Causing Shear Failure at Sections 1-1 and 2-2	55
3.6 Seismic Forces Causing Flexural Damage at Section 1-1	56
3.7 Seismic Forces for Shear Failure at Sections 1-1 and 2-2	56
4.1 Fundamental Frequencies	61
4.2 Maximum Lateral Displacements	63
4.3 Seismic Shear and Axial Forces	67
4.4 Seismic Forces	67
4.5 Fundamental Frequencies	72
4.6 Maximum Lateral Displacements	73
4.7 Seismic Shear and Axial Forces	73
4.8 Seismic Forces	81
4.9 Vertical Accelerations (Bent Height = 46 ft)	81
4.10 Participation Factors of Frequencies (Time = 13.52 Sec)	81
4.11 Fundamental Frequencies	90
4.12 Maximum Lateral Displacements	91
4.13 Seismic Shear and Axial Forces	91
4.14 Seismic Forces	91
4.15 Vertical Accelerations (Bent Height = 46 ft)	92

Table	Page
4.16 Fundamental Frequencies	96
4.17 Maximum Lateral Displacements	96
4.18 Seismic Shear and Axial Forces	96
4.19 Seismic Forces	97

List of Figures

Figure	Page
1.1 Plan of the Cypress Viaduct.	4
1.2 Typical Dimensions of Type B1 Bent.	5
1.3 Reinforcement Details of Type B1 Bent.	6
1.4 Lower Level Joint Detail of Type B1 Bent.	7
1.5 Typical Dimensions and Rfts of Type B2 Bent.	8
1.6 Typical Dimension and Rfts. of B3 Bents.	9
1.7 Map of Oakland Showing Near-Surface Geology.	12
1.8 Cracking Below the West Shear Key, Bent 55	14
1.9 Cracking Below the East Shear Key, Bent 56	14
1.10 The Collapse Between Bents 84 and 90	18
1.11 Failure of the West Side of Bent 90	18
1.12 Close-up of the West Side of Bent 90	19
1.13 East Shear Key of Bent 108 After the Collapse	19
1.14 Collapse of Bents 72–76	20
1.15 Rotation at the Upper Part of Bent 80	20
1.16 Nearly Undamaged Upper West Column of Bent 71 on the Ground	21
1.17 Lower Shear Key of the Upper West Column of Bent 71	21
1.18 Upper Part of Bent 97 (West Side)	22
1.19 View of the Standing Bents 96 and 97	22
2.1 Gravity and Seismic Forces.	25
2.2 Lower Column-to-Girder Joint.	31
3.1 Seismic Forces for Type B1 Bent	36
3.2 P-M Interaction Diagram (Section 1–1)	38

Figure	Page
3.3 P-M Interaction Diagram (Section 3–3)	39
3.4 Analysis of the Upper Frame.	40
3.5 Upper Column Just Below the Shear Key.	40
3.6 Analysis of the Lower Frame.	41
3.7 Forces Acting on Section 1–1.	43
3.8 Analysis at Section 3–3.	49
3.9 Analysis of B2 Bents	52
3.10 P-M Diagram (Section 1–1)	54
3.11 Analysis of B3 Bents.	57
3.12 P-M Interaction Diagram (Section 1–1)	58
4.1 Horizontal Ground Acceleration (Peak = 0.29g)	62
4.1 Vertical Ground Acceleration (Peak = 0.06g)	62
4.3 2–D Model of B1 Bent.	63
4.4 First Transverse Mode Shape	64
4.5 First Vertical Mode Shape	65
4.6 Second Transverse Mode Shape	66
4.7 Lateral Displacement (Node 1)	68
4.8 Lateral Displacement (Node 3)	68
4.9 Seismic Shear Force at Shear Key (Node 2)	69
4.10 Seismic Axial Force at Shear Key (Node 2)	69
4.11 Vertical Displacement (Node 2)	70
4.12 Vertical Displacement (Node 4)	70
4.13 3–D Model of B1 Bent.	71
4.14 Cross Section of Upper and Lower Decks.	72
4.15 3–D Model of B1 Bents	74

Figure	Page
4.16 First Longitudinal Mode Shape	75
4.17 First Transverse Mode Shape	76
4.18 First Torsional Mode Shape	77
4.19 First Vertical Mode Shape	78
4.20 Second Vertical Mode Shape	79
4.21 Second Transverse Mode Shape	80
4.22 Lateral Displacement (Node 1)	83
4.23 Lateral Displacement (Node 3)	83
4.24 Seismic Shear Force at Shear Key (Node 2)	84
4.25 Seismic Axial Force at Shear Key (Node 2)	84
4.26 Seismic Forces (Node 2)	86
4.27 Vertical Displacement (Node 2)	87
4.28 Vertical Displacement (Node 4)	88
4.29 Vertical Displacement (Node 5)	88
4.30 Vertical Acceleration (Node 5)	89
4.31 Vertical Acceleration (Node 6)	89
4.32 3–D Model of B2 Bent.	90
4.33 Lateral Displacement (Node 1)	93
4.34 Lateral Displacement (Node 3)	93
4.35 Seismic Shear Force (Node 1)	94
4.36 Seismic Axial Force (Node 1)	94
4.37 3–D Model of B3 Bents.	95
4.38 Lateral Displacement (Node 1)	98
4.39 Lateral Displacement (Node 3)	98
4.40 Seismic Shear Force (Node 1)	99

Figure	Page
4.41 Seismic Axial Force (Node 1)	99
4.42 Tensile Stress Distribution in the Lower Girder-to-Column Joint . . .	102
4.43 Stress Vectors in the Upper Column (Below Shear Key)	103
4.44 Strain Distribution in the Lower Joint	104
4.45 Damage to B1 Bents	105
4.46 Collapse of B1 Bent	106

CHAPTER 1

INTRODUCTION

1.1 General

At 5.04 p.m., on October 17, 1989, an earthquake with a surface-wave magnitude (M_s) of 7.1 occurred with its epicenter located about 10 miles northeast of Santa Cruz and 60 miles south-southeast of San Francisco. The earthquake ruptured a segment of the San Andreas fault below the Santa Cruz mountains, and the rupture propagated about 25 miles both northwest and southeast within 10–seconds period. This earthquake, named the Loma Prieta earthquake, was the largest on the San Andreas fault since the great San Francisco earthquake of 1906 [1]. The fault displacement differed significantly from the dominant horizontal movements that have characterized historical surface ruptures on most segments of the San Andreas fault. The Southern Santa Cruz Mountains segment of the San Andreas fault was identified in 1988 as having a 30 percent probability of rupturing in a magnitude 6.5 earthquake within the next 30 years.

Although strong shaking lasted only about 10 to 15 seconds, the damage was severe to the dwelling and masonry buildings near the epicenter, to the buildings in Santa Cruz and Los Gatos, and to the elevated highway structures in the bay area including the collapse of a section of I-880 in Oakland which claimed 42 lives, and the collapse of a 50–foot link span of the San Francisco Oakland Bay Bridge. Damage occurred throughout an 3,000 square miles area. The statistics of the earthquake are:

1. About 70 deaths; 4000 injuries.
2. Approximately 10 billion property damage.

3. Over 12,000 people displaced from their homes.

1.2 Seismological Considerations

The Richter magnitude (M_l) of the earthquake assessed by the seismographic stations at the university of California at Berkeley was 7.0. The average surface waves magnitude (M_s) was estimated as 7.1 [2].

The earthquake was along a section of the San Andreas fault where major earthquakes have occurred in historical times, on October 8, 1865 and February 9, 1980 with magnitudes estimated to be 6.5 and 7.0, respectively. There was no evidence that deep tectonic movement propagated to the surface; this was probably due to the relatively great depth of the earthquake hypocenter (about 11 miles).

The most recent significant earthquakes in the epicentral area were recorded on June 27, 1988 ($M_l = 5.4$), and September 11, 1989 ($M_l = 3.4$).

Foreshocks with (M_l) greater than 2.7 was recorded in the immediate epicentral area in the 24 hours before the October 17 main shock.

An aftershock sequence began immediately with over 300 aftershocks with $M_l > 2.5$ recorded at the Berkeley Seismographic Station in the six days following the mainshock. About 25 earthquakes were recorded in the same time with $M_l > 4$; the largest of these being one with $M_l = 5.2$ on October 19.

Strong motion records shows that at epicentral area the maximum peak horizontal acceleration was 0.64g and the maximum peak vertical acceleration was 0.66g [2]. In San Francisco, at the San Francisco International Airport, the maximum peak horizontal acceleration was 0.33g. In this earthquake, structures in most of the San Francisco Bay area received only light to moderate shaking of duration less than 5 seconds (above 0.1g).

No ground motion records were available at the site of the Cypress Structure [3]. But in Oakland, four strong motion records from sites near the collapsed Cypress Structure were available and they are:

1. Oakland Outer Harbor Wharf (1.5 miles to the west).
2. A two-story office building in Oakland (1.5 miles to the southeast).
3. Emeryville (1 mile to the north).
4. 2-story office building in Oakland (1.5 miles to the southwest)

Acceleration records from these three sites had peak horizontal accelerations of 0.29g, 0.26g, 0.26g, and 0.18g, respectively. And peak vertical accelerations of 0.06g, 0.06g, 0.04g, and 0.16g. The geologic conditions at the first three stations and the freeway are similar beneath the surface, though they are different near the surface, suggesting a level of shaking at the Cypress freeway similar to the first three sites.

The peak horizontal acceleration in areas surrounding Oakland was 0.1g, which indicates that the earthquake was amplified by almost 3 times in Oakland. This amplification was caused by the deep clay deposits in that area.

1.3 Description of the Cypress Viaduct (I-880)

The Cypress Viaduct, located approximately 0.6 mile to the west of downtown Oakland, was the first continuous double-deck freeway structure in California, which was completed in 1957. Each deck carried 4 lanes of traffic. The bents were constructed, approximately, 80 ft apart and were supported on pile foundations [4].

There were 11 different bent configurations used in the Cypress Structure, Only 3 primary bent types (B1, B2, and B3) were present in the majority of the collapsed section. In this study we will focus on these 3 bent types.

Figure 1.1 shows a plan of the freeway with the damaged (uncollapsed) section extending from Bent 27 to Bent 62. The collapsed section extends from Bent 63 to Bent 112. Only Bents 96 and 97 remained standing in the collapsed section.

Expansion joints for the upper and lower decks are provided every three spans.

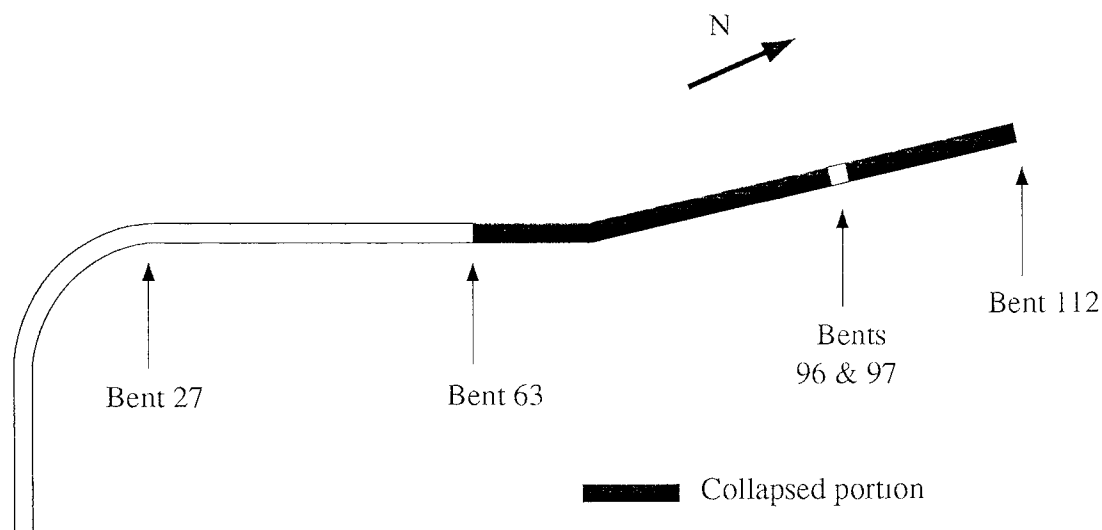


Figure 1.1 Plan of the Cypress Viaduct.

1.3.1 B1 Bents

Twenty nine of the total 48 collapsed bents were type B1. The typical bent dimensions are shown in Figure 1.2. It is also shown in the figure that the upper frame is connected to the lower frame by shear keys (hinges) [4].

The columns of the lower frame are also connected to pile caps by shear keys. B1 bent reinforcement details are shown in Figures 1.3 and 1.4.

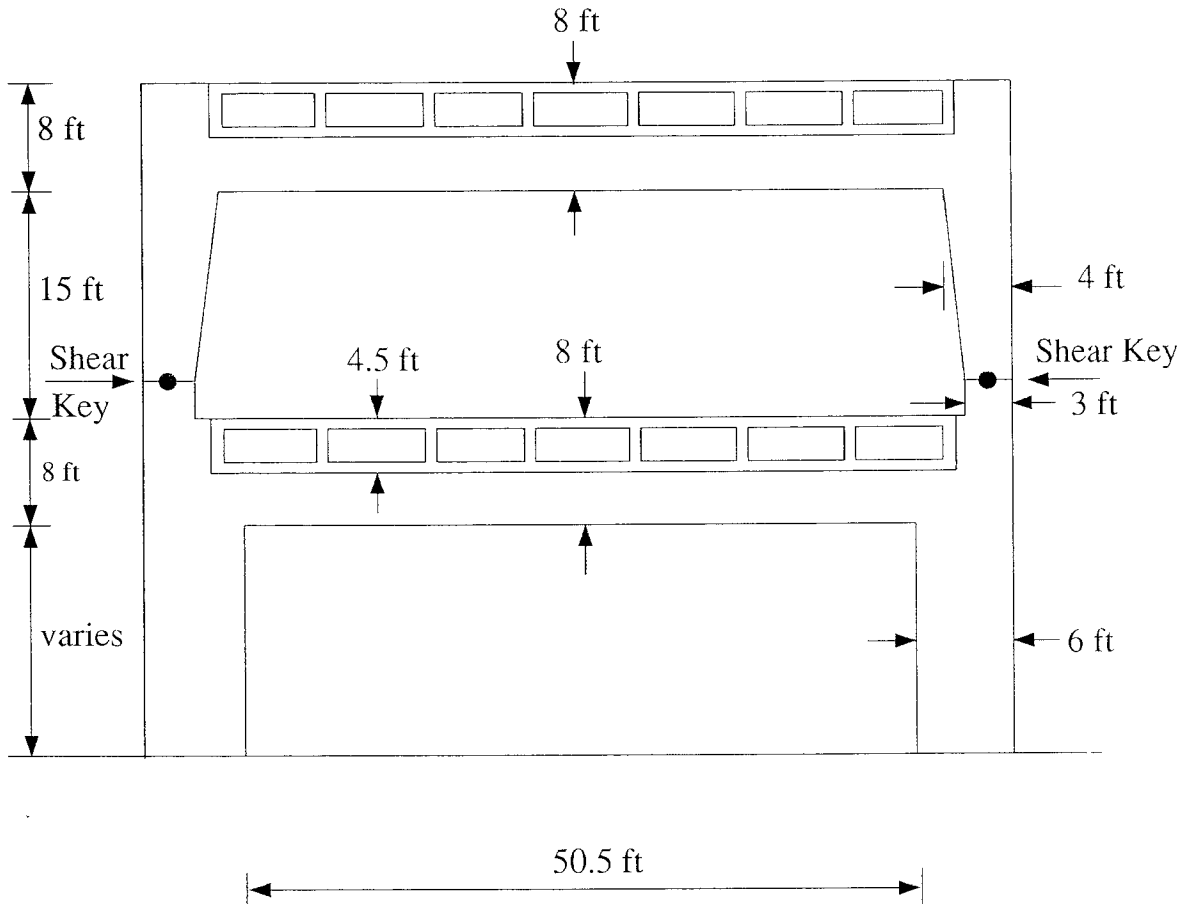


Figure 1.2 Typical Dimensions of Type B1 Bent.

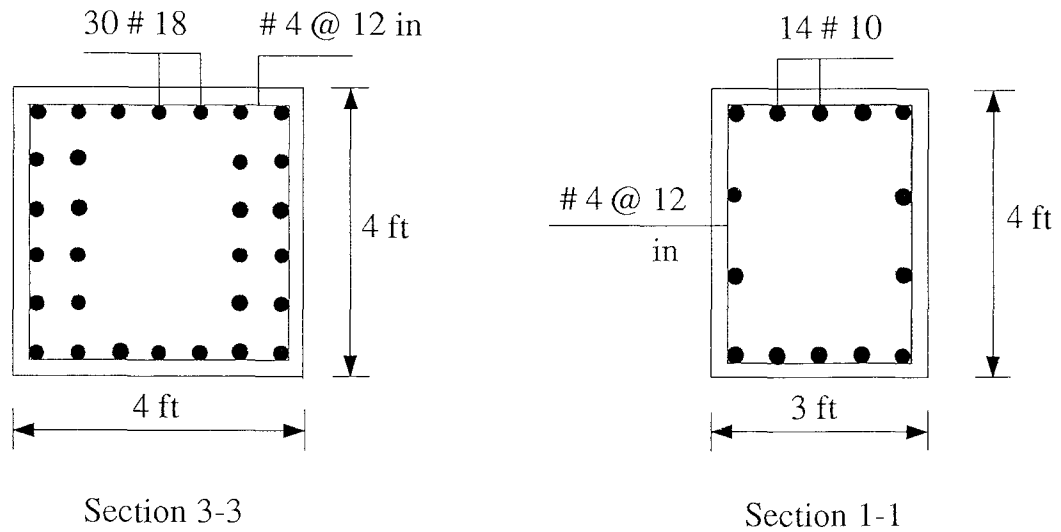
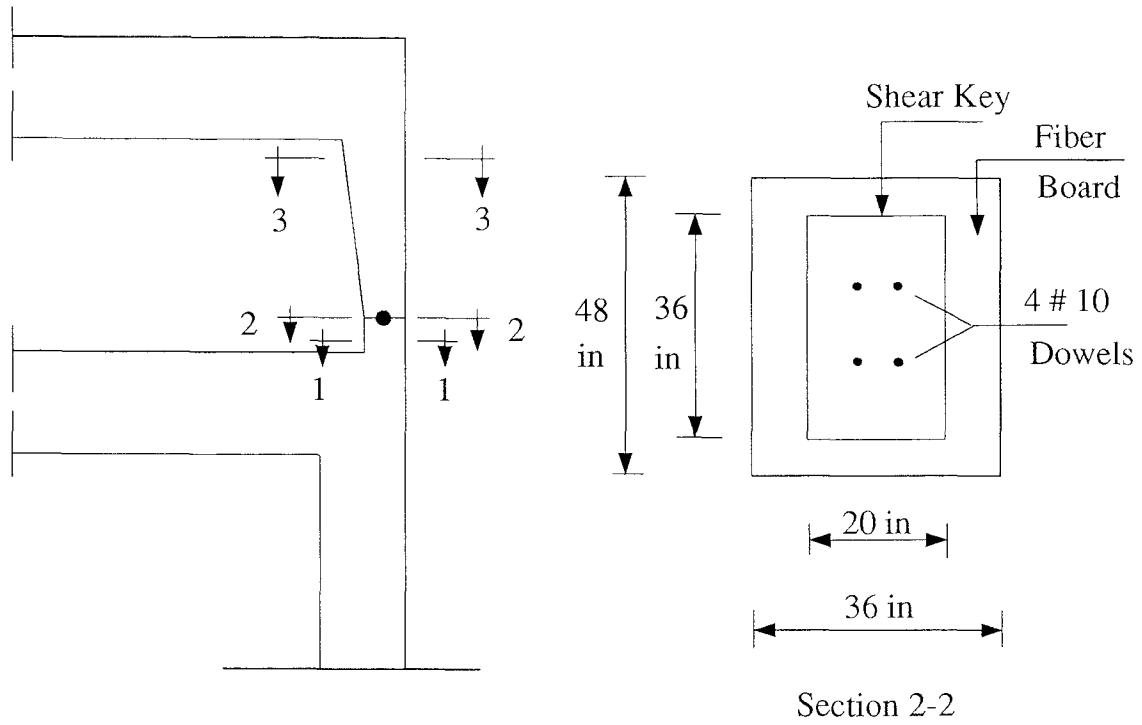


Figure 1.3 Reinforcement Details of Type B1 Bent.

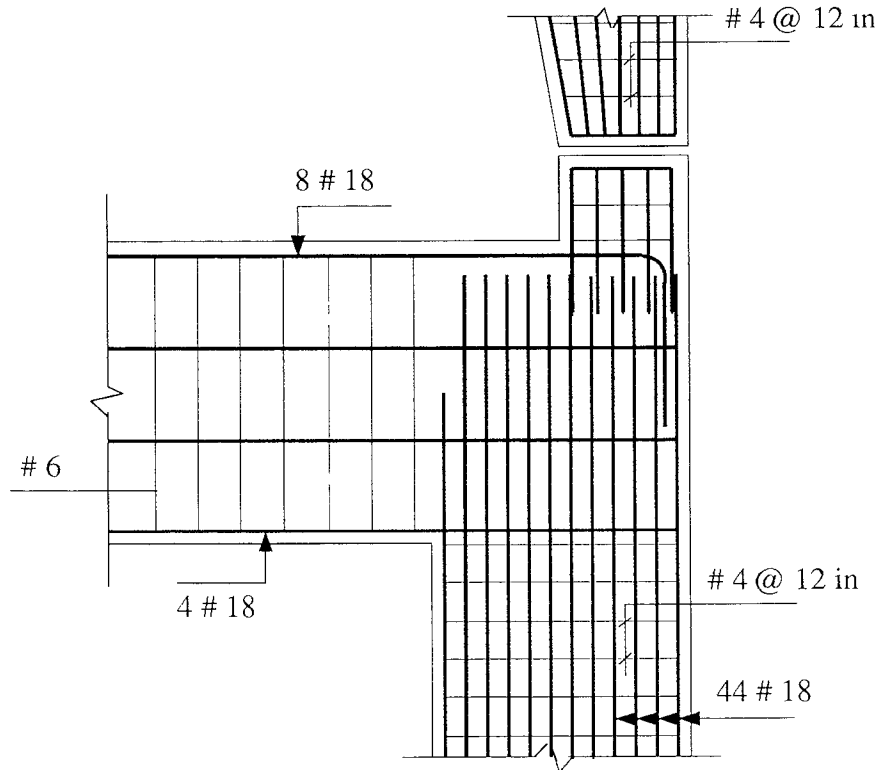


Figure 1.4 Lower Level Joint Detail of Type B1 Bent.

1.3.2 B2 Bents

The B2 bent type is the second most common bent type of which 8 bents collapsed. Figure 1.5 shows the typical dimensions and reinforcement details of the bent and the three shear keys in the upper frame. The east column of these bents is continuous from the ground level to the shear key beneath the upper girder. The west columns have two shear keys: one above the lower girder and the other is similar to the east column. Therefore, resistance to lateral loads in the upper deck is provided by the east column only [4].

1.3.3 B3 Bents

B3 bent type was used for Bents 95–98 only. Figure 1.6 shows the typical dimensions of the bent and cross sectional reinforcement details of the upper

columns, and the two shear keys beneath the upper girder and the additional column in the lower level.

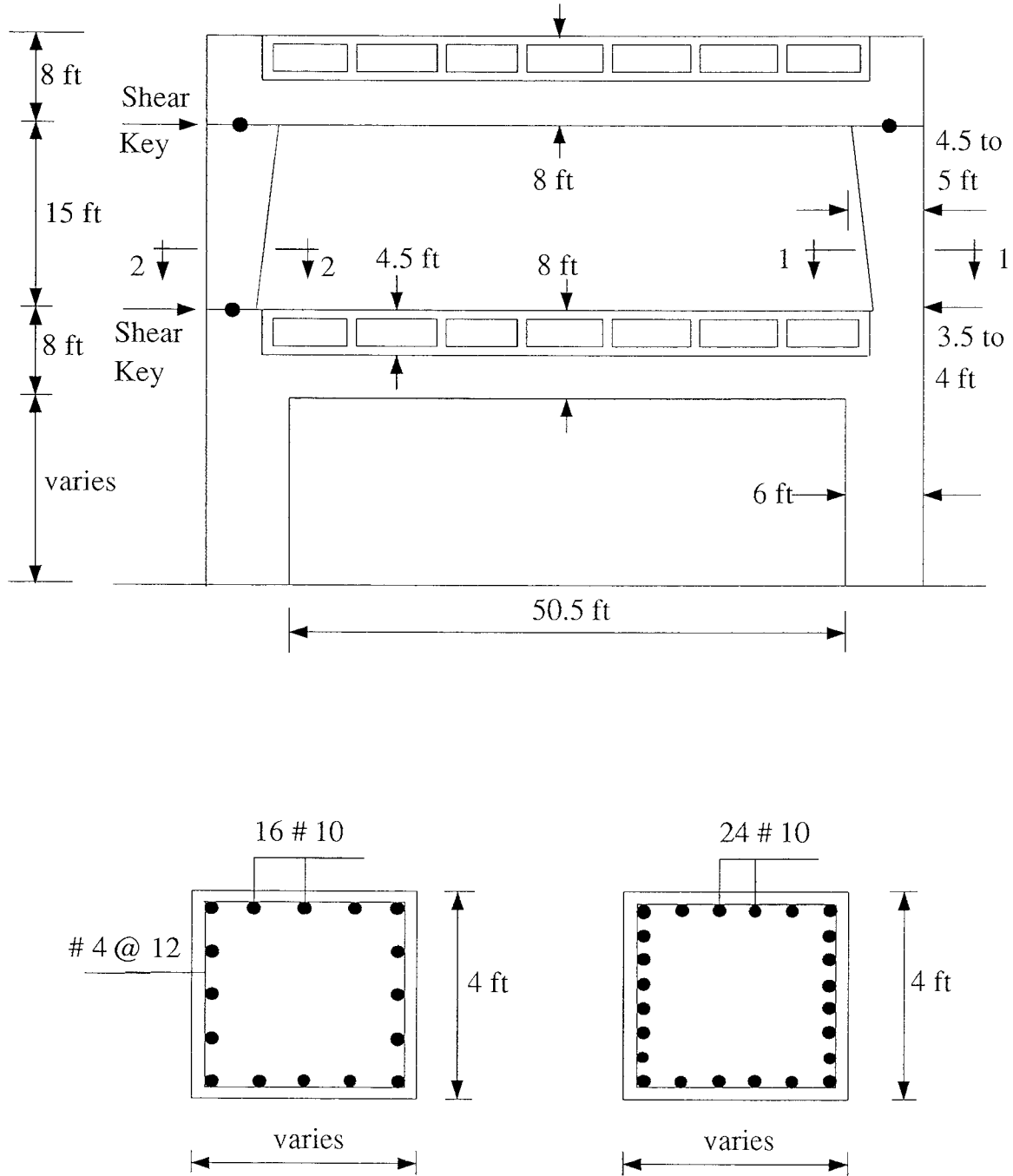


Figure 1.5 Typical Dimensions and Rfts of Type B2 Bent.

Both columns of the bent are continuous from ground level to the shear keys. Therefore, the resistance to lateral loads are provided by both columns[4]. This bent type is of particular significance because Bents 96 and 97 remained standing after the earthquake. The 96–97 span was the only span along the collapsed section that did not collapse.

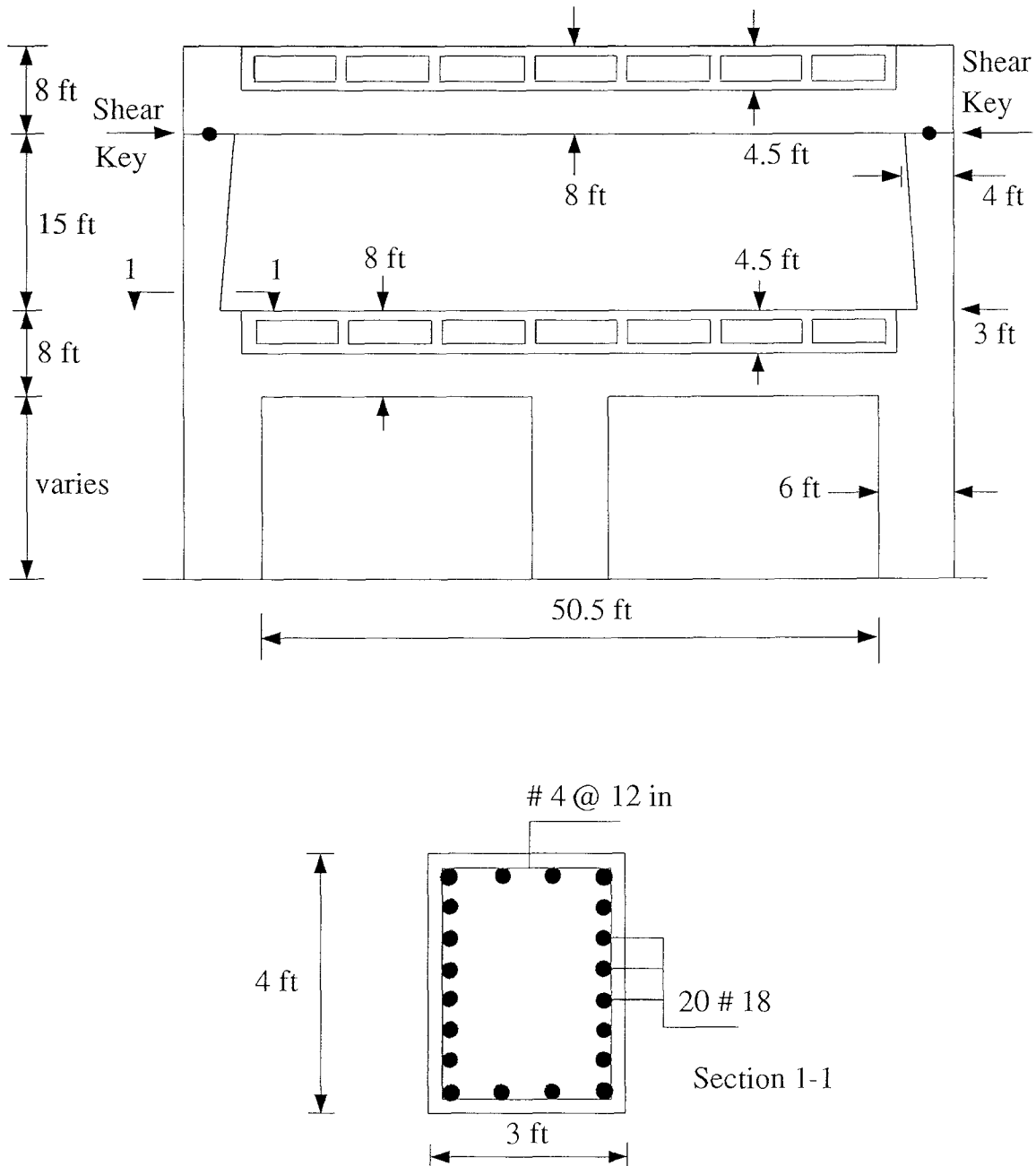


Figure 1.6 Typical Dimension and Rfts. of B3 Bents.

1.4 Site Conditions

Within the epicentral source region, peak accelerations are relatively independent of surface geology. However, outside of this region (especially beyond distances of 30 miles or so), surface geology appears to influence strongly the amplitude of ground motion: sites located on crystalline rock and rocks have the lowest accelerations, sites located on soft rock and alluvium have intermediate accelerations, and sites located on artificial fill and bay mud have the highest accelerations. The observed differences in horizontal acceleration between sites on hard rock, bay mud, and artificial fill were best demonstrated in the San Francisco and Oakland areas, where there were differences of 100% to 200%. These large differences in peak horizontal accelerations are consistent with the large differences observed in the Modified Mercalli scale (MM) intensity [3].

Figure 1.7 is a map of Oakland showing near-surface geology. Section AC indicates the extent of the effected portion of the Cypress Viaduct by the earthquake. AB indicates the segment that collapsed, and BC indicates the segment that was damaged but did not collapse.

The previous figure also shows that the highest three peak accelerations (0.29g, 0.26g, and 0.26g) measured at stations in areas located on bay mud were next to the San Francisco Bay. Sites located on alluvium, as in Berkeley, the peak accelerations were 0.1g, 0.06g, and 0.08g.

Section AB (Bents 63–112) was constructed on the border between bay mud and alluvium. The author's prediction is that the peak acceleration was less than 0.26g.

Section BC (Bents 27–62) was constructed on alluvium, the peak acceleration

would be less than section AB, and that explains why section BC was damaged while section AB collapsed.

1.5 Damage and Collapse of The Cypress Viaduct

The section of the Cypress Viaduct from bent 27 through bent 62 remained standing and suffered little damage manifested by shear cracks at critical sections of the structure [5].

The section between Bent 63 and Bent 112 collapsed, mainly with the upper deck on top of the lower deck, except Bents 96 and 97 which remained standing.

The following general description proceeds from south to north along the viaduct, the southern most damage observed were substantial cracking in the lower girder to column joint regions of Bents 27, 28, and 29. The cracking was observed immediately below the shear key at the base of the upper columns.

Bents 32–55 were B1 bents which remained standing after the earthquake. However, some bents showed significant cracking in the lower girder-to-column joint region (Figure 1.8)

Bents 56–62 were transition bents were ramps to the upper and lower roadways joined the Viaduct. These bents remained standing, but were cracked in the lower girder-to-column joint regions as shown in Figure 1.9.

The southern extent of the collapse of the upper roadway was defined by the expansion joint between Bents 62 and 63. The upper roadway collapsed flat onto the lower roadway north of the expansion joint. Bent 62 was the final transition bent in the region of the ramps and had three lower columns and no shear keys. The first failed bent to the north was bent 63, which was a B1 bent.

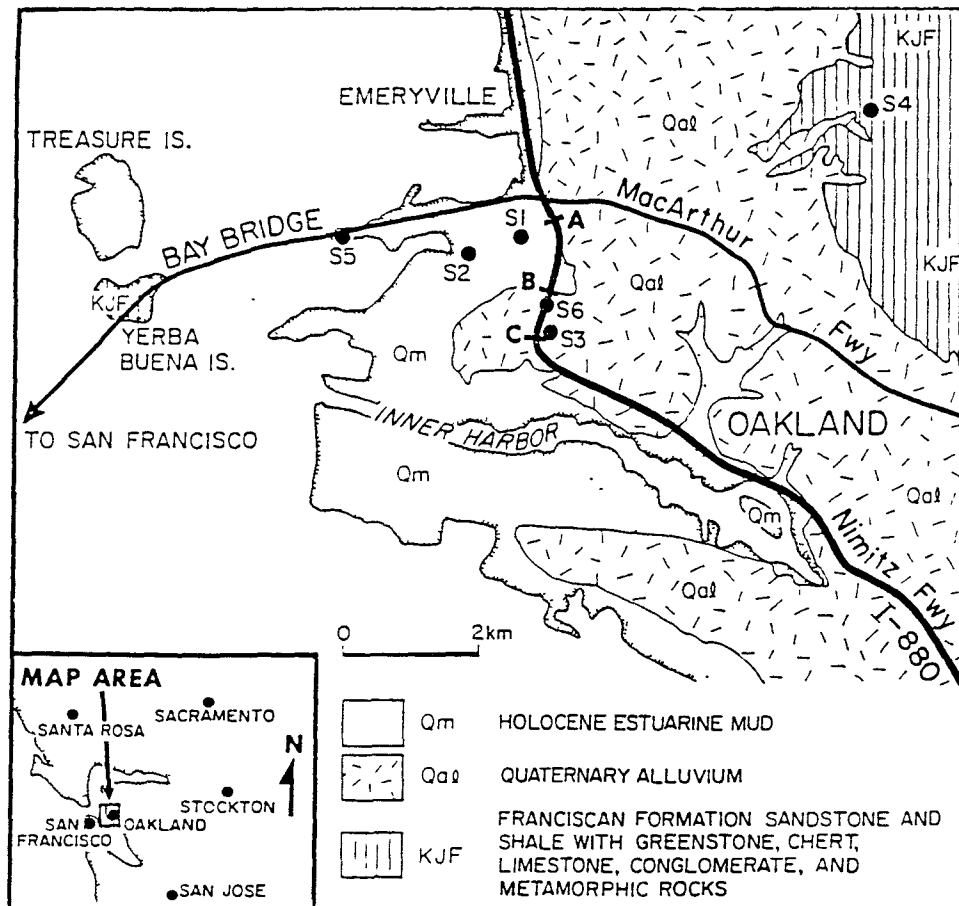


Figure 1.7 Map of Oakland Showing Near-Surface Geology. AC Indicates the Extent of the Effected Portion of the Cypress Viaduct. AB Indicates the Segment that Collapsed; BC Indicates the Segment that Was Damaged But Did Not Collapse [3].

Bents 63–69 were B1 bents. Throughout the failed portion of the viaduct, the collapsed B1 bents failed in a consistent manner. The failure of the B1 bents is described in more details in Section 1.6.1. Between these bents, the upper roadway collapsed onto the lower roadway.

Bent 70 was a transition bent between the B1 and B2 bents. Bent 70 differed from a B2 bent in that it had only two shear keys instead of three (at the upper girder-to-column joints). The upper girder of Bent 70 collapsed onto the lower roadway.

Bents 71–74 were B2 bents. The upper roadway collapsed onto the lower roadway throwing the pin-ended columns undamaged.

Bents 75–80 were B2 bents. The upper roadway did not collapse completely onto the lower roadway. The upper roadway was tilted, with the east side resting on the lower roadway. The continuous (east) column supporting the upper roadway failed. On the west side the pin-ended columns (with 2 shear keys) remained in position, but with significant rotations having occurred in both shear keys.

Bents 81–94 were B1 bents. The upper roadway collapsed onto the lower roadway (typical B1 bent failure).

Bents 95–98 were B3 bents. These bents were skewed to the longitudinal axis of the Viaduct. The upper level of Bent 95 failed and the failure on both sides of the roadway was similar to that of the continuous (east) column of B2 bents. The failure of the upper roadway deck between Bents 95 and 96, and between Bents 97 and 98 did not occur at the expansion joints but rather as a result of the shear failure of the deck. Bents 96 and 97 were still standing after the earthquake and the upper roadway remained intact between these bents.



Figure 1.8 Cracking Below the West Shear Key, Bent 55



Figure 1.9 Cracking Below the East Shear Key, Bent 56

The significant cracking in the lower girder-to-column joint of Bent 97 was evidence of severe cyclic loadings. The upper level of Bent 98 failed in a manner similar to that of Bent 95.

Bents 99–103 were B1 bents. The failure was typical B1 failure.

Bents 104–106 were B1 bents. These bents were the only locations where the lower girder failed and the lower roadway collapsed. The lower girders of Bents 104 and 106 failed adjacent to the girder-to-column joint region and the girder dropped to the ground. The lower girder of Bent 105 failed completely and the lower roadway dropped to the ground.

Bents 107–111 were transition bents. These bents were similar to B1 bents. The failure of these bents followed the general failure pattern of B1 bents.

Bent 112 was the northmost failed bents. At this location, the lower roadway was supported from the ground and Bent 112 supported only the upper roadway. The upper roadway failed in shear just to the south of Bent 113.

1.5.1 Damage to B1 Bents

Throughout the collapsed portion of the Viaduct, the B1 bents failed in a consistent manner. In all of these bents, the upper roadway collapsed completely onto the lower roadway. Typically, the lower columns were still standing and supporting the lower roadway in approximately its original position, with the only exceptions being at Bents 104–106. The collapsed upper roadway was relatively intact between B1 bents and rested flat on the lower roadway. The final resting position of the upper roadway varied: at some bents on the northern portion of the Viaduct, the roadway was displaced laterally up to 1 ft to the east, while for most of the bents no appreciable lateral movement was evident [5].

The lower girder-to-column joints on both sides of the B1 bents failed. The collapse seems to have initiated by the failure of the pedestal (the part of the upper column just below the shear key). The failure surface is basically coincident with the curved surface defined by the lower girder negative reinforcement that is bent down into the lower girder-to-column joint (see Figure 1.4).

The shear keys did not fail in pure shear. A cone of concrete remained attached to the 4#10 bars that extended through the shear key (Figure 1.13).

The upper girder-to-column joints suffered varying amount of damage. In some instance, the joint region failed completely and the column was lying on the ground. In other cases, the column hung from remnants of the nearly destroyed upper joints (Figures 1.10–1.12).

The extent of the damage to the upper columns varied. Some columns were completely destroyed, many suffered some damage. The only column that clearly failed in shear was the lower east column of Bent 108.

No evidence of buckled longitudinal reinforcing bars was seen in either the upper or the lower columns, indicating that the lack of adequate restraining of the column longitudinal bars was not the primary cause of collapse.

1.5.2 Damage to B2 Bents

The continuous (east) columns of all B2 bents failed in a consistent manner over the collapsed portion of the Viaduct [5]. The west columns failed in two ways:

- A. The columns did not collapse but the upper roadway tilted onto the lower roadway (Bents 75–80) (Figures 1.14 and 1.15).
- B. The columns failed at the shear keys and fell to the ground with the upper roadway collapsing completely onto the lower roadway (Figures

1.16 and 1.17).

In all of these bents, the lower columns remained standing, supporting the lower roadway in approximately its original positions. The lower girder-to-column on the east side of the Viaduct, failed completely. The failure surface was very similar to the failure surface that formed in the B1 lower joints. The difference between the B2 joints and the B1 joints was that in the B2 joints the outer layer of column reinforcement was continuous through the joint region. The shear key between the upper girder and the upper east column failed in the plane of the shear key after the anchorage of 4#10 dowel bars was lost.

On the west side of Bents 71 and 72, the shear keys at both ends of the upper columns failed completely. The upper column of Bent 71 was thrown nearly intact to the ground.

On the west side of Bents 75–80, large rotations occurred at the shear keys. Although the shear key did not fail, the upper roadway was tilted to the east onto the lower roadway.

1.5.3 Damage to B3 bents

Of the four B3 Bents (95–98), Bents 95 and 98 collapsed. Bents 96 and 97 were the only bents between Bent 63 and Bent 112 that remained standing. Bents 95 and 98 failed in a manner similar to the failure of B2 bents. Bents 96 and 97 were both very skewed and remained standing, suffering severe cracks in the lower girder-to-column joint region (Figures 1.18 and 1.19) [5].

1.6 Damage to Expansion Joints

The upper deck expansion joints in the collapsed region were typically heavily damaged, but it was secondary damage, resulting from the collapse, rather than



Figure 1.10 The Collapse Between Bents 84 and 90



Figure 1.11 Failure of the West Side of Bent 90



Figure 1.12 Close-up of the West Side of Bent 90



Figure 1.13 East Shear Key of Bent 108 After the Collapse

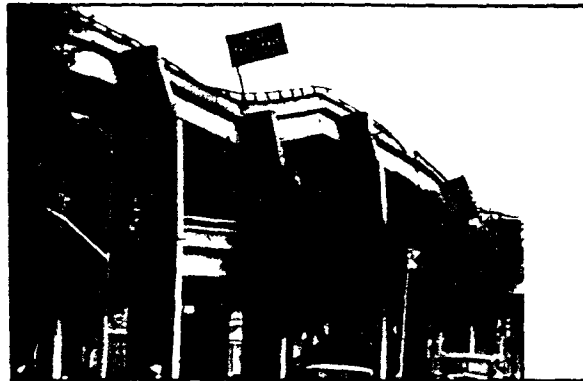


Figure 1.14 Collapse of Bents 72-76



Figure 1.15 Rotation at the Upper Part of Bent 80

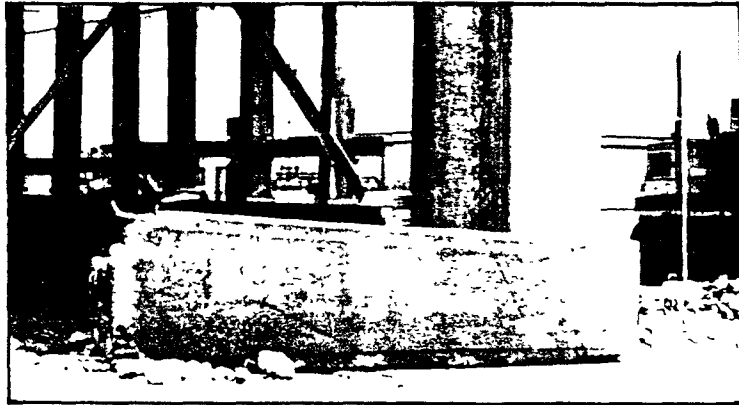


Figure 1 16 Nearly Undamaged Upper West Column of Bent 71 on the Ground



Figure 1 17 Lower Shear Key of the Upper West Column of Bent 71



Figure 1.18 Upper Part of Bent 97 (West Side)

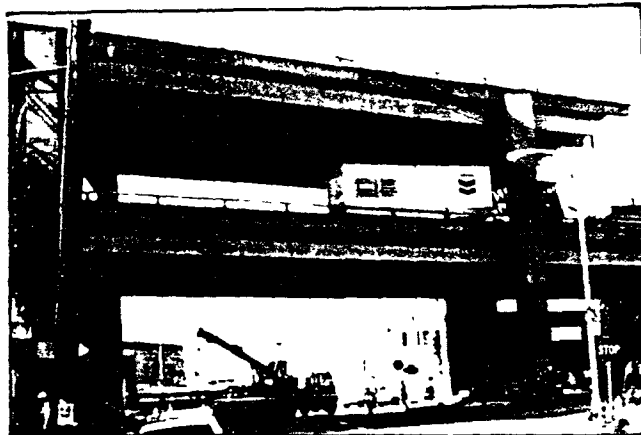


Figure 1.19 View of the Standing Bents 96 and 97

primary damage leading to the collapse [5].

1.7 Damage to Foundations

There was no relative motion between the ground and the base of the columns, no indication of pile cap rocking (no crack around each bent's pile caps), and no evidence of significant ground disturbance around the base of the columns [5].

CHAPTER 2
INVESTIGATIONS REPORTED BY CALIFORNIA
GOVERNOR'S BOARD OF INQUIRY AND NATIONAL
INSTITUTE OF STANDARDS AND TECHNOLOGY

2.1 Report by California Governor's Board of Inquiry [4]

This report included summary of investigations conducted by individuals and organizations from state and local government, universities, and professional associates.

2.1.1 Static Analyses

Static analyses of B1 bent and B2 bent were performed by different investigators for two cases:

- A. Dead load W.
- B. Seismic forces.

The seismic forces were determined using the Equivalent Static Analysis of the Uniform Building Codes (UBC) as an approximation of the first mode response. Figure 2.1 shows the seismic forces and the gravity loads acting on B1 bent.

Assumptions:

The compressive strength of concrete = 4.0 ksi.

Yield stress of the reinforcing steel = 45.0 ksi.

Spacing between bents = 80 ft.

The total dead load of one bent = 2800 kips (divided equally on both decks).

Results:

For bent B1, the horizontal shear force at the shear key due to dead load only was found to be (130–145) kips by Priestly et al., and (100–200) kips by Krawinkler.

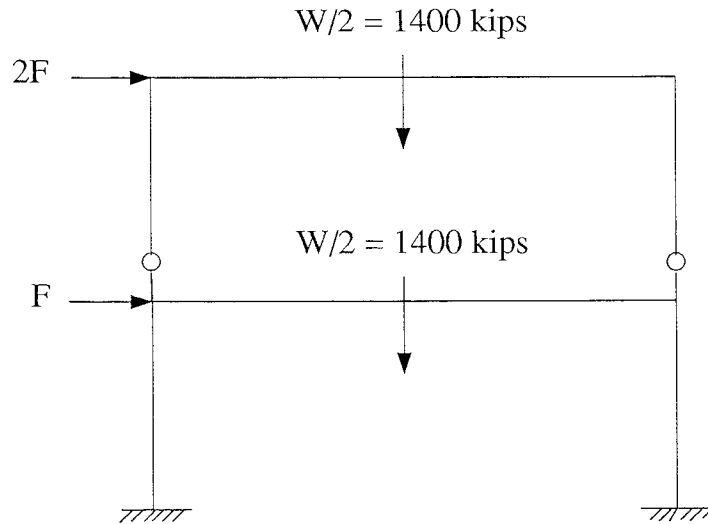


Figure 2.1 Gravity and Seismic Forces.

It was assumed that the horizontal shear force at the shear key due to seismic forces only is equal to F . The calculated horizontal shear capacity (at shear key) was equal to 272, 270 and 280 kips (by Priestly et al., Moehle and Krawinkler, respectively). The bending moment capacity of the top girder at the face of the top girder-to-column joint was found to be 3,580 and 3,800 ft-kips (by Priestly et al. and Krawinkler).

According to the above, the force F was found to be 127 kips and 140 kips (by Priestly et al. and Krawinkler), giving a base shear force of 381 kips = 14% of the total weight of one bent ($0.14W$) and 420 kips = $0.15W$. Krawinkler calculated F to be 80–180 kips, giving a base shear force (0.09 - 0.19) W .

It should be mentioned here that the experimental value of F was 233 kips (see Section 2.1.2).

For bent B2, the analysis showed that failure occurred due to developing flexural plastic hinges at both negative moment ends of the bottom girder at a

base shear $0.21W$.

Priestly et al. performed an inelastic finite element analysis of a two dimensional reinforced concrete model of the shear key pedestal region which predicted shear failure at load 390 kips. Lew et al. used concrete strength 6,000 psi, the calculated values of the lateral base shear to initiate failure were $0.2W$ for B1 and $0.25W$ for B2.

They concluded that the failure of the 29 B1 bents was the primary cause of the collapse of the Cypress Viaduct.

2.1.2 Dynamic Analyses

Frequency and time history analyses were performed on different models by different investigators [4]. Table 2.1 shows the first two transverse frequencies obtained analytically and experimentally. The experimental results were obtained by performing dynamic field testing on undamaged 3-bent portion (B1 bents) of the Cypress Viaduct.

Table 21 Fundamental Frequencies.

Analysis By	1 st Transverse Frequency (Hz)	2 nd Transverse Frequency (Hz)
Wilson	2.4	6.1
Moehle	2.6	6.9
Krawinkler	2.4	-
Lew et. al.	2.5	6.4
Experimental	2.5	6.5

The results of krawinkler's dynamic analysis using the Emeryville record (1.2 miles north of the Cypress Viaduct), indicate a predominant first-mode response

with maximum total story shear demands for the cracked column model of about 730 kips in the top story and 1,300 kips in the bottom with ratio of $1,300/730 = 1.78$. Which is greater than 1.5 assumed by static analysis ($3F/2F$). The base shear of 1300 kips represents $0.46W$.

Linear dynamic analysis of the three-bent model using the response spectra at the Oakland Wharf, 1.2 miles west of the Cypress Viaduct, gave maximum total story shear per bent of about 850 kips in the top story and 1,100 kips in the bottom story, a ratio of $(1,100/850)W = 1.29$, which is less than the assumed. The base shear of 1,100 kips represents $0.39W$.

The dynamic analysis results given by both Krawinkler and Moehle indicated their maximum elastic top-story shear demands 730 and 850 kips greatly exceed the static calculation of top-story shear capacity ($2F$) by Priestly et al., Moehle, and Krawinkler to be 254, 280, and 160– 360 kips.

Experimental static load testing was performed on a 3–bent portion (B1 bents) of the undamaged section of the viaduct. The three bents were loaded equally (at the upper decks only). The test was done for two cases, unretrofitted and retrofitted structure.

For the unretrofitted structure, the test was stopped when shear cracks started to form in the upper columns just below the shear keys (the load at each bent was 465 kips), where the upper deck lateral displacement was 0.72 in. Partial unloading to about 75 kips left a displacement of 0.2 in., showing the elastic behavior of the structure.

For the retrofitted structure, the behavior was elastic up to an upper deck displacement of 1.3 in., beyond that displacement, the structure started to suffer

inelastic deformation. At a maximum displacement of nearly 10 in., large inelastic deformation took place with 80% of this occurring in the top story.

At this maximum displacement, the structure continued to maintain its lateral and vertical load capacity. The structure sustained severe damage in the top girder-to-column joints in all frames and significant damage at the lower girder-to-column joints.

2.1.3 Conclusion

- A. Analysis and design of the Cypress Viaduct were performed between 1949 and 1954, when little design information was available on dynamic effects, realistic lateral forces and ductile design and ductile detailing of reinforced concrete structures to resist earthquake effects.
- B. The three dimensional structural system contained many hinges and joints to simplify its analyses and to allow movements resulting from creep, temperature, and prestressing. Consequently, the structure lacked redundancy, which made it highly susceptible to damage or collapse in strong earthquake.
- C. The structure lacked the ductility required in present designs and detailing of ductile reinforced concrete. By today's standards, the Cypress Viaduct had inadequate and incorrectly detailed transverse reinforcement in both columns and the joints region. Therefore, the structure was brittle, non-ductile, and lacked the energy-absorbing capacity required to resist strong cyclic earthquake motions.
- D. Static and dynamic analyses performed by several investigators using different analytical models indicate that the calculated seismic demands

required to initiate failure from the earthquake to be greater than the available structural capacities. The predominant failure mechanism in most bents was the development of a critical diagonal tension crack in the lower girder to upper column pedestal or joint region produced by horizontal shear force (horizontal ground motion). The failure surface followed the plane defined by the bent down lower girder negative reinforcement in the joint region. Gravity and seismic forces then pushed the upper columns down and away from the joint, resulting in the collapse of the upper deck. Once the collapse of one or more bents was initiated, progressive collapse of the other bents along the length of the Viaduct probably ensued.

2.2 Report by National Institute of Standards and Technology [1]

2.2.1 Description of Collapse by Motorists

Eyewitnesses who were at the scene described the dynamic behavior of the structure as they observed. It was like a big giant, long ocean wave, travelling down the structure which was moving up and down. Behind the wave a portion of the freeway collapsed. And that explained the fact that the upper deck came to rest squarely on top of the lower deck implying nearly simultaneous failure of the east and the west upper bent columns.

2.2.2 Dynamic and Static Results

Dynamic analysis: Response spectra for horizontal ground motion records of the Oakland Outer Wharf site indicate peak structural accelerations of 1.0g for a structure with a natural period of vibration of 1.5 seconds at 2% damping. In order to estimate the natural period of the Cypress Structure, a series of finite element computer models were constructed for type B1 and type B2 bents. The

models included a single bent of the specified type which included the inertial mass and stiffness contributions of an 80 foot section of the deck box girders as well as those for the bent girders and columns.

The results of these analyses, based on uncracked section properties indicate first and second mode horizontal frequencies for type B1 bents of 2.5 Hz and 6.4 Hz, respectively; for type B2 bents the first and second horizontal frequencies were 2.0 Hz and 6.3 Hz, respectively. The values for type B1 bents compare extremely favorably with the experimentally obtained first and second mode frequencies of 2.5 Hz and 6.5 Hz, respectively, measured by University of California at Berkeley researchers.

On the basis of these analyses, and the response spectra they indicate that both type B1 and type B2 bents in the Cypress Structure experienced first mode equivalent accelerations of 0.35g .

Static analyses: The Uniform Building Code (UBC, 1988) assumption of an inverted triangular distribution of the effective lateral load due to the earthquake was used to determine the forces at both decks. The force at the upper level is twice that at the lower level. Thus two-thirds of the total base shear is applied to the upper level bents and one third to the lower bent. These forces were used as input for static finite element analyses of bent type B1 and B2. Vertical loads were applied as a uniform acceleration of 1.06g (including gravity load), based on the peak vertical acceleration components at the seismic station previously mentioned. The contours of maximum principal tensile stress indicate that the column support pedestal for the upper columns in type 1 bents is highly stressed and that crack initiation will occur beneath the shear key with the crack pattern as shown in Figure 2.2.

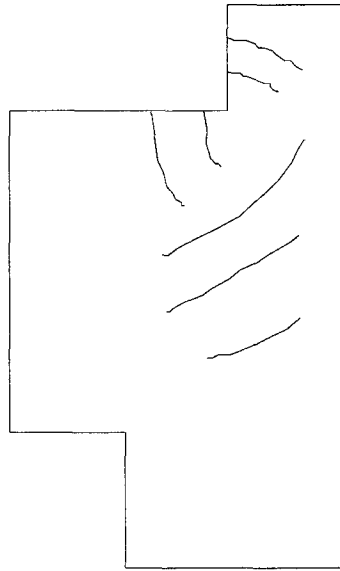


Figure 2.2 Lower Column-to-Girder Joint.

Crack initiation in the concrete was assumed to occur at a tensile stress of 460 psi, based upon the ACI tensile strength formula (ACI, 1989) for a compressive strength of 6,000 psi.

The reactions at the shear keys are due to both the lateral seismic load as well as outward shearing forces of the portal frame reactions due to vertical loads on the upper bent. This later contribution accounts for more than half the load required to shear the column support pedestal for a type B1 bent, which is determined to be 333 kips.

The calculated lateral base acceleration required to achieve a shearing load of 333 kips at the pedestal is 0.2g. With the cracking of the right column support pedestal, it can be seen that the upper left-hand beam-column joint is subjected to large tensile stresses due to bending which would lead to crack initiation. The lack of transverse reinforcement could be expected to contribute to a brittle failure

mechanism following shearing of the left lower pedestal as the bent was rocked in the opposite direction on the reverse cycle.

For bent type B2, seismic forces needed to cause failure were found to be higher than the forces required for bent type B1, and the calculated collapse acceleration for type B2 column is 0.25g.

2.2.3 Conclusion

Two pieces of evidence are worth considering:

- A. The failure was essentially vertical. It is unlikely that such uniform vertical collapse would have resulted solely from the effects of lateral loading.
- B. Eyewitness reports indicated the presence of “giant waves” rolling down the length of the elevated structure.

Taking these two points into account, dynamic modal analysis of a 9–span segment of the Cypress Structure were carried out. The results indicate that the 9–span long structure had a lateral vibrational period of 9 seconds (0.11 Hz), well beyond the period of peak lateral accelerations based upon the response spectra of the record from the Oakland Outer Harbor Wharf site. However, the vertical mode of vibration had a period of 0.16 seconds (6.2 Hz) which is remarkably close to the predominant period of the vertical acceleration of the record for the area. Structural amplification in this mode could account for three aspects of the I-880 collapse:

- A. It accounts for the observations made by witnesses.
- B. Structural amplification in this mode would lead to large vertical forces acting upon the bents. A significant increase in the vertical reaction

forces, as a result of resonance in the vertical mode (period = 0.16 seconds (6.2 Hz)), would lead to failure of the bents, but with the important exception that the failure would necessarily be symmetric.

- C. The lower and upper road decks do not necessarily vibrate in phase, nor with the same amplitude. For those places where the decks vibrate in phase, the reaction forces could be much greater.

2.3 Summary

In the first investigation, investigators concluded that the collapse of the Cypress Viaduct was predominantly due to the horizontal ground motion. While in the second one, they concluded that it was predominantly due to the vertical ground motion.

A detailed static and dynamic analyses are presented in the following two chapters (3 and 4) to investigate the effect of both the vertical and the horizontal ground motion on the Cypress Viaduct.

The fact that the collapse appeared to be perfectly vertical, will lead us to emphasize on the vertical motion. Analyses are performed to determine the net axial forces exerted on columns, and to study the effect of the axial and the shear forces combined on the structure.

CHAPTER 3

STATIC ANALYSES

3.1 General

Throughout most of the collapsed section of the Cypress Structure, the lower frame remained standing (except for Bents 104–106), and almost undamaged while the upper frame failed and collapsed with the upper deck on top of the lower one, almost intact, indicating that the collapse was caused by the failure of the upper columns.

In this chapter, cross-sectional static analyses are performed on bents B1, B2, and B3 to determine the moment and shear capacities of the critical sections of the upper columns, and to determine the seismic forces required to reach these capacities.

Dynamic analyses (see Chapter 4) are also performed on the three bent types employing the finite element software ADINA. Analyses included frequency and linear time history analyses using the ground motion records of the Oakland Outer Wharf site.

In Chapter 5, a limited nonlinear static analyses of the structure is performed to evaluate stress distribution below the shear key. Finally, a comparison between static and dynamic analyses is discussed.

3.2 General Assumptions

According to the experimental tests done on concrete and reinforcing steel of the structure (from the uncollapsed portion) after the earthquake, the compressive strength of concrete was found to be 6.0–7.0 ksi, and the yield strength of

reinforcing steel was 42.0–50.0 ksi. Therefore, the following properties are used in analyses.

The compressive strength of concrete = 6.0 ksi.

The concrete modulus of elasticity (E_c) = 4696 ksi.

Where,

$$E_c = 33 (w)^{1.5} \sqrt{f_c}$$

The yield stress of reinforcing steel = 45.0 ksi.

3.3 Analyses of B1 Bent

3.3.1 Gravity Loads

The gravity loads are equally distributed on both decks and are equal to 24 k/ft (based on 80 ft spacing between bents). Accordingly, the weight of each deck is 1,415 kips giving 2,830 kips total weight of one bent. The total mass of each deck is 44 k-sec²/ft.

To take into consideration the effect of the vertical component of the earthquake (peak acceleration = 0.06g), the gravity loads were reduced by a factor 0.06. The reason for reducing the gravity load, rather than increasing it, is that the reduction in the compressive force will result in decrease in the moment and shear capacities of the sections. Therefore, this case is more critical than the case of increasing the gravity loads.

3.3.2 Seismic Loads

The seismic base shear, V_{cq} , is distributed, as in the Uniform Building Code (UBC), at the deck-level of the bent according to the following formula:

$$F_x = \frac{V_{eq} W_x h_x}{\sum_{i=1}^n W_i h_i} \quad (3.1)$$

Where,

F_x = Lateral seismic force at level x .

W_x = Total weight at level x .

h_x = Height of level x .

n = Number of floors.

According to that, the distribution of lateral forces were found as seen in Figure 3.1.

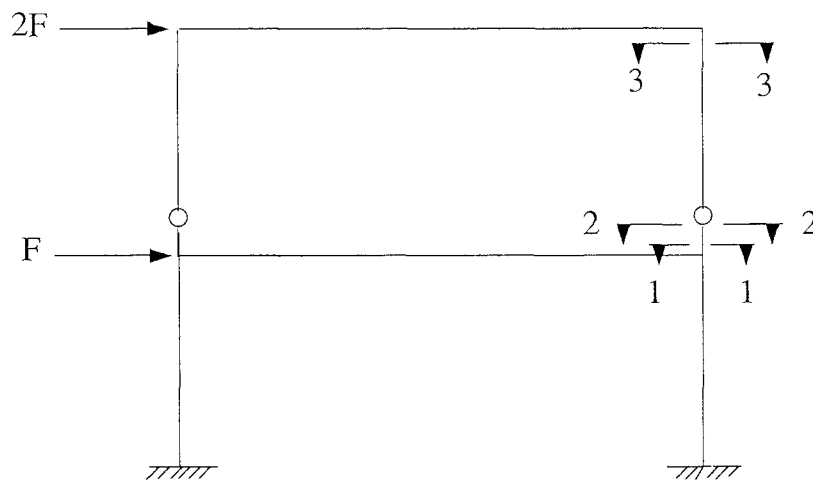


Figure 3.1 Seismic Forces for Type B1 Bent

In this case the base shear is equal to 3F.

3.3.3 Analyses at Critical Sections

Sections 1–1, 2–2, and 3–3 shown in Figure 3.1 are the critical sections to be investigated. The failure mode expected for section 1–1 is either flexural failure or shear transfer failure. For section 2–2, the expected mode of failure is shear failure. While for section 3–3, it is a flexural failure

To be able to determine the flexural capacities of section 1–1 and section 3–3 seen in Figure 3.1, the P-M interaction diagrams were calculated and are shown in Figures 3.2 and 3.3.

Starting with the frame above the shear keys, the horizontal and the vertical reactions due to gravity and seismic loads combined are determined as shown in Figure 3.4.

It is apparent that the reaction at the shear keys due to seismic forces are added to the reaction due to gravity loads on one side of the frame (additive side) and subtracted on the other side (subtractive side).

For the part of the upper columns below the shear keys, shown in Figure 3.5, the ratio $a/d < 1.0$. Therefore, it will be treated as a corbel according to ACI code. The failure modes of the corbel are:

- A. Shear Failure at Section 2–2.
- B. Flexural Failure at Section 1–1.
- C. Shear Transfer Failure at Section 1–1.

3.3.4 Analyses at Section 1–1

The reactions obtained from the top frame are reversed on the lower one as shown in Figure 3.6.

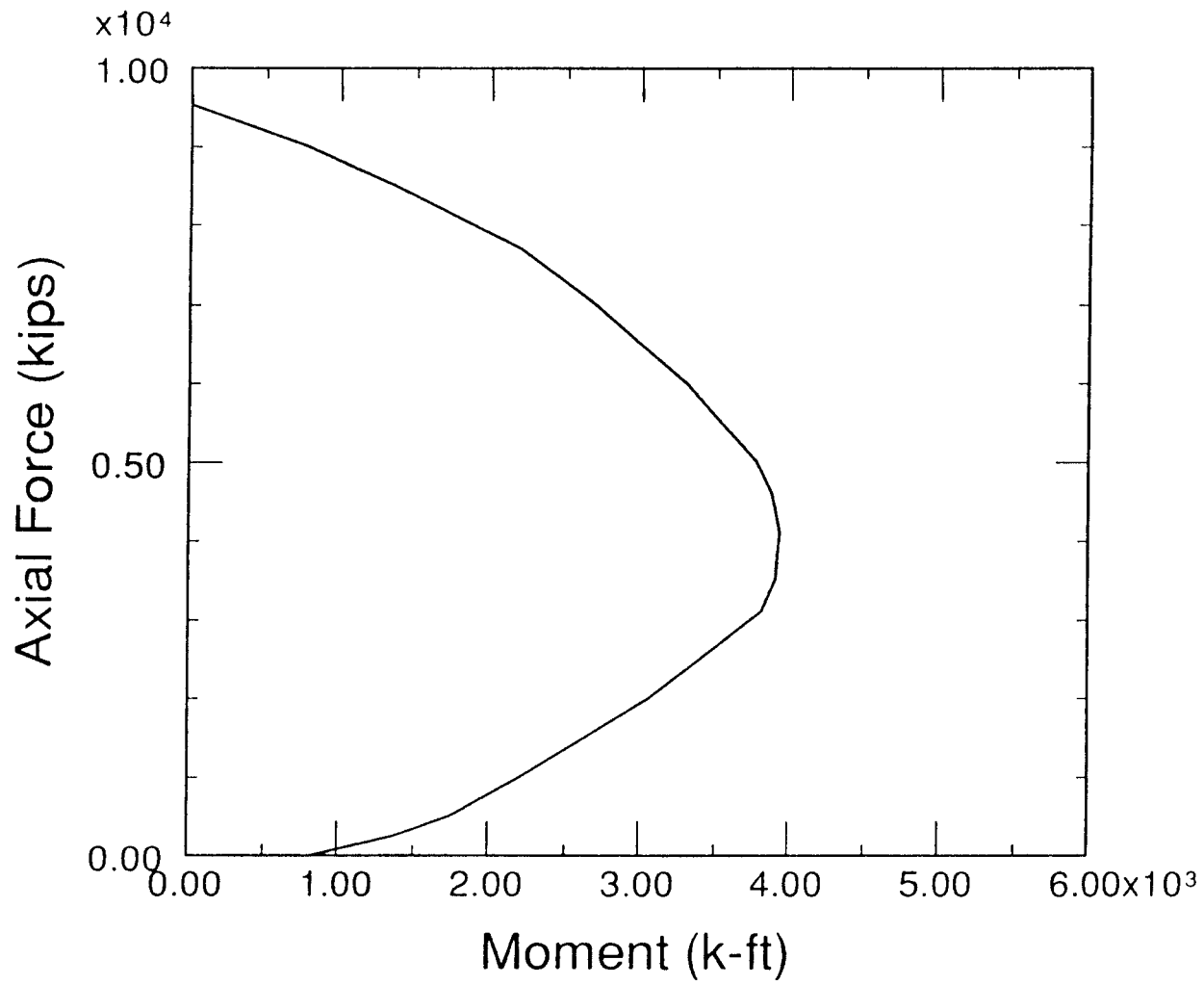


Figure 3.2 P-M Interaction Diagram (Section 1-1)

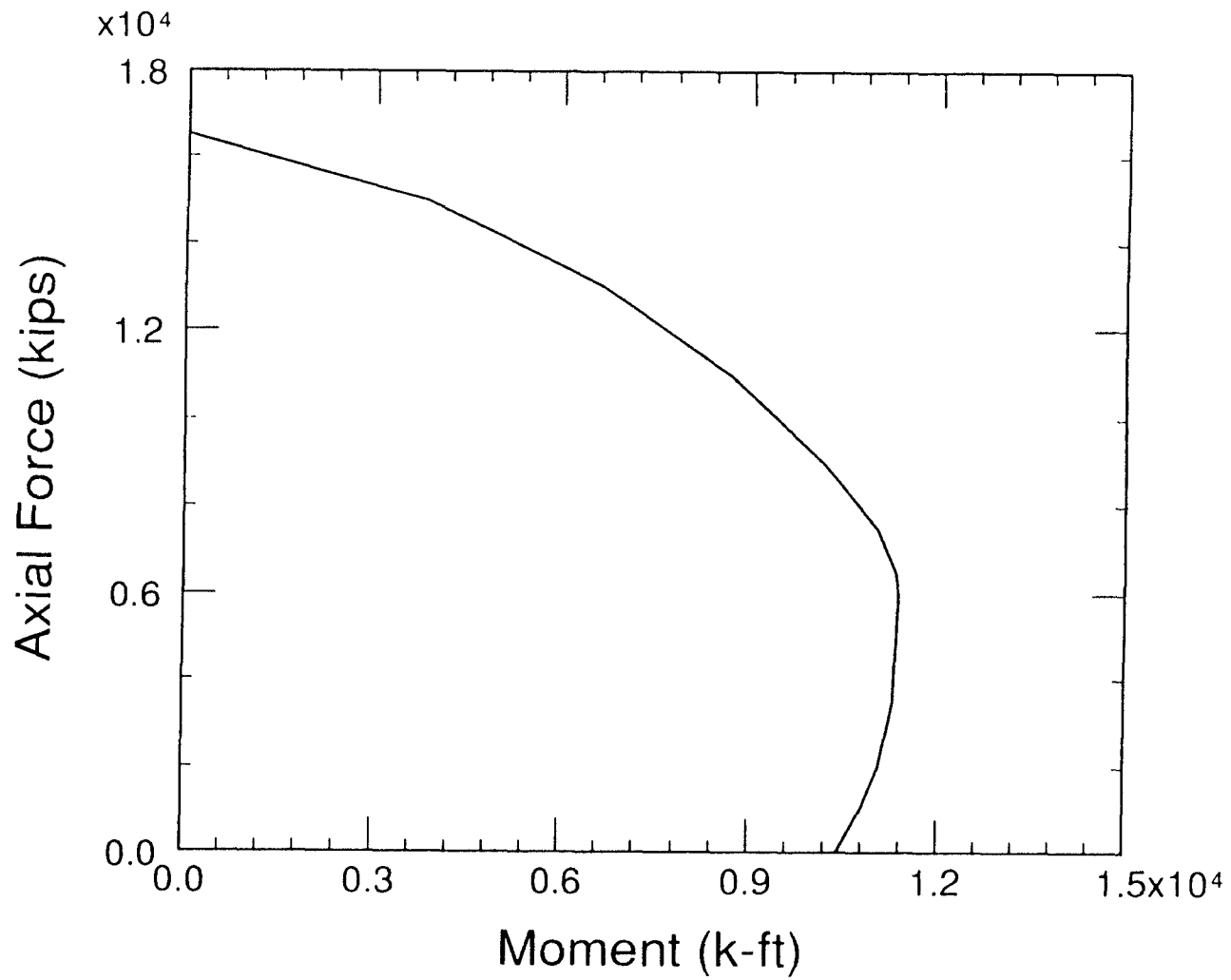


Figure 3.3 P-M Interaction Diagram (Section 3-3)

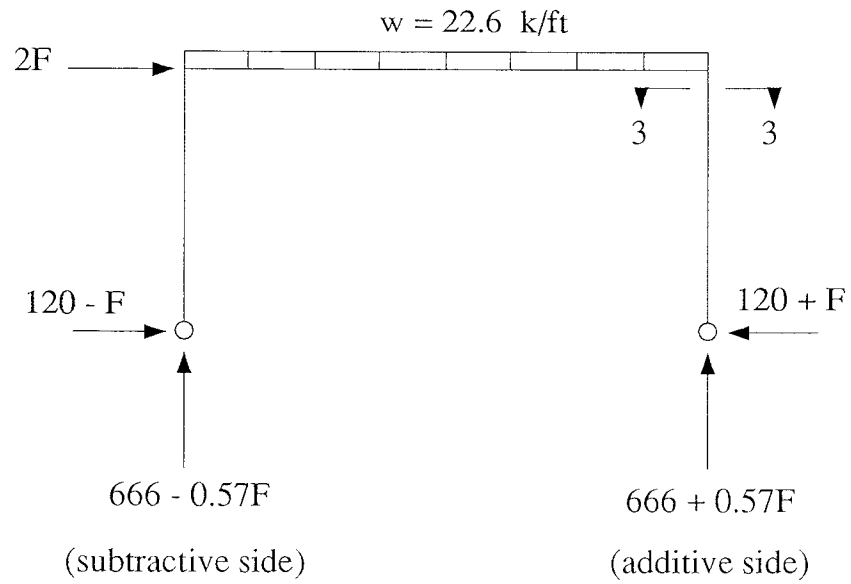


Figure 3.4 Analysis of the Upper Frame.

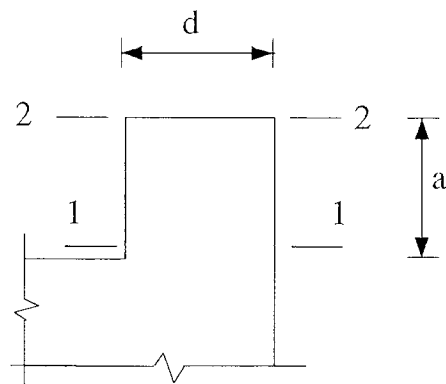


Figure 3.5 Upper Column Just Below the Shear Key.

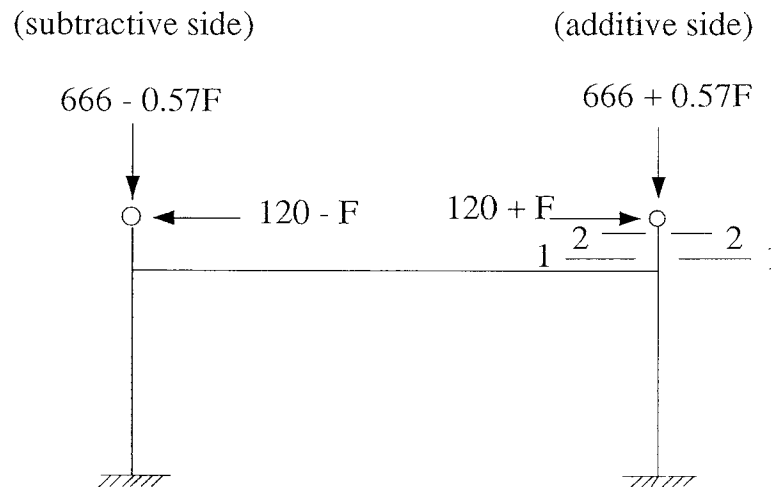


Figure 3.6 Analysis of the Lower Frame.

It is necessary to determine the seismic forces, for section 1-1 shown in Figure 3.5, required to initiate the following modes of failure:

- A. Cracking (tension side).
- B. First Yield of Steel (after concrete cracking).
- C. Flexural Failure.
- D. Shear Transfer Failure.

A. Cracking

At this stage, the section is treated as an uncracked section, utilizing the moment of inertia of the whole cross section. The stress distribution is linear according to the following formula:

$$F_{cr} = M_{cr} \frac{c}{I} \pm \frac{N}{A} \quad (3.2)$$

Where,

$$F_{cr} = 7.5 \sqrt{f_c} = 83.7 \text{ k/ft}^2 \quad (3.3)$$

And,

F_{cr} = modulus of rupture.

The bending moment at section 1–1 is determined by the following equation:

$$M_{cr} = (120 + F) \times (2.25) \text{ k-ft} \quad (3.4)$$

By solving Equations 5.2 and 5.3, we determine the value of F. Then, we determine the seismic forces at lower and upper girders (F and 2F), and the base shear force (3F). The results are listed in Table 3.1.

B. At First Yield of Steel (after concrete cracking)

At this stage, the section is treated as a cracked section (tension side). Tensile stresses and forces are resisted merely by reinforcing steel.

Figure 3.7 shows the forces acting on the section along with the stress and the strain distribution diagrams.

First, we have to determine the value of the distance x shown in Figure 3.7. To do so, we have to solve the following equation:

$$\sum \text{Axial forces on section 1 - 1} = 0 \quad (3.5)$$

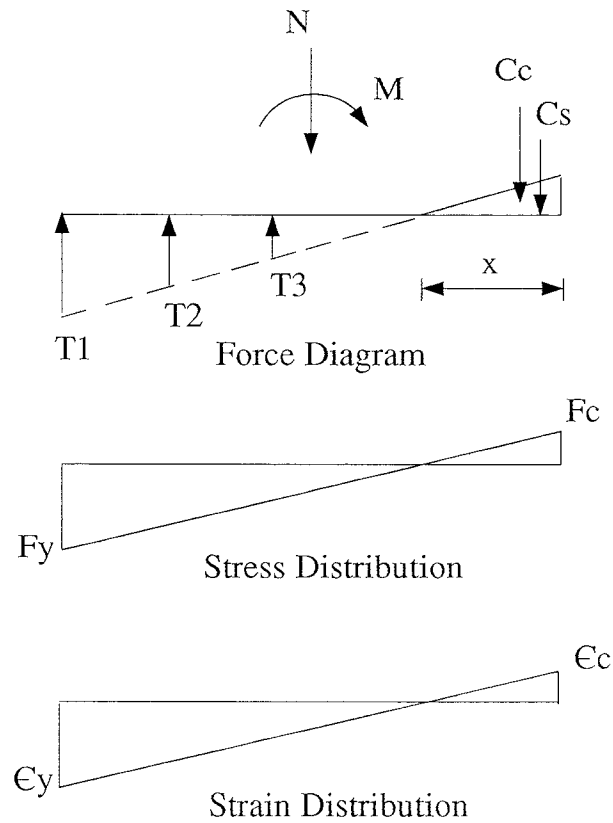


Figure 3.7 Forces Acting on Section 1–1.

In order to solve Equation 5.5, we have to determine the value of the axial force, N , knowing that the axial force is determined from the following equation:

$$N = 666 + 0.57F \quad \text{kips} \quad (3.6)$$

First, we assume a value for F (to be checked later), substitute it in Equation 5.6, get N , and then substitute it in Equation 5.5. After solving equation 5.5 and determining the value of x , we can determine the corresponding moment M acting on the section. Since the bending moment M at section 1–1 is determined by the following equation:

$$M = (120 + F) \times (2.25) \quad \text{k - ft} \quad (3.7)$$

We substitute the obtained M in Equation 5.7, determine F , and then compare this value of F with the assumed one. By using an iterative method, we can determine the exact value of F that would initiate the first yield of reinforcing steel. The value of F is determined by examining both sides of the frame, the additive and the subtractive. The above calculations can be summarized as:

Equation 5.5 has two unknowns, x and N . N is a function of F (as seen in Equation 3.6). We assume a value for F (to begin with) to be able to determine x . And then Equation 5.7 is used as a check for the assumed F .

Lower and upper girder seismic forces (F and $2F$), and the base shear force ($3F$) are listed in Table 3.1.

C. Flexural Failure

For the additive side we have the following equations for bending moment and normal force:

$$M = (120 + F) \times (2.25) \quad (3.8)$$

And,

$$N = 666 + 0.57F \quad (3.9)$$

For the subtractive side we have:

$$M = (120 - F) \times (2.25) \quad (3.10)$$

And,

$$N = 666 - 0.57F \quad (3.11)$$

These equations for both sides of the frame along with the P-M interaction diagram are used in an iterative method to determine the seismic force F . Then, the seismic forces at lower and upper girders (F and $2F$), and the base shear force ($3F$) are determined as seen in Table 3.1.

Table 3.1 Seismic Forces Causing Flexural Damage at Section 1-1

B1 Bent	Cracking (kips)	First Yield of Steel (kips)	Flexural Failure (kips)
Lower Girder Force (F)	310	715	730
Upper Girder Force (2F)	620	1,430	1,460
Base Shear Force (3F)	930 (0.33W)	2,145 (0.76W)	2,190 (0.77W)

D. Shear Transfer

The forces required to cause shear transfer failure are determined according to ACI code by the following equation:

$$\max V_n \leq 0.2f_c b_w d \leq (800 \text{ psi}) b_w d \quad (3.12)$$

Where,

f_c = concrete compressive strength.

b_w = width of the concrete section.

d = depth of the concrete section.

In this case we have:

$$0.2 f_c b_w d = 1,900 \text{ kips.}$$

$$(800) b_w d = 1,267 \text{ kips.}$$

Therefore, the maximum $V_n = 1,267$ kips.

It must be mentioned that the shear strength of section 1–1 is significantly higher than the shear strength of the concrete (due to the steel contribution) as shown in the following two equations:

$$800 \text{ psi} = 10 \sqrt{f_c}$$

$$v_c = (2 - 3.5) \sqrt{f_c}$$

3.3.5 Analysis at Section 2-2

The following two formulas for the shear stress and the shear force are used in analysis to determine the shear capacity of section 2-2:

$$v_c = 2 \left(1 + \frac{N_u}{2000 A_g} \right) \sqrt{f_c} \quad (3.15)$$

And,

$$V_c = v_c b d \quad (3.16)$$

Where,

N_u = factored normal force (positive for compression force and negative for tension force).

A_g = gross sectional area.

For the additive side of the frame we have the following equations:

$$N = 666 + 0.57F \quad (3.17)$$

And,

$$V_c = 120 + F \quad (3.18)$$

For the subtractive side we have the following equations:

$$N = 666 - 0.57F \quad (3.19)$$

And,

$$V_c = 120 - F \quad (3.20)$$

By assuming a value for F , using an iterative method and solving the two equations of each side of the frame in conjunction with Equations 5.13 and 5.14, we determine the value of F .

The seismic forces at lower and upper girders (F and $2F$), and the base shear force ($3F$) are listed in Table 3.2.

Table 3.2 Seismic Forces Causing Shear Failure at Section 2-2

B1 Bent	Shear Failure (kips)
Lower Girder Force (F)	185
Upper Girder Force ($2F$)	370
Base Shear Force ($3F$)	555 ($0.20W$)

3.3.6 Analysis at Section 3-3

As seen in Figure 3.8, the critical bending moment and axial force are determined from the additive side.

We have the following Equations for the bending moment and the axial force:

$$M = (120 + F) \times (12.75) \quad (3.21)$$

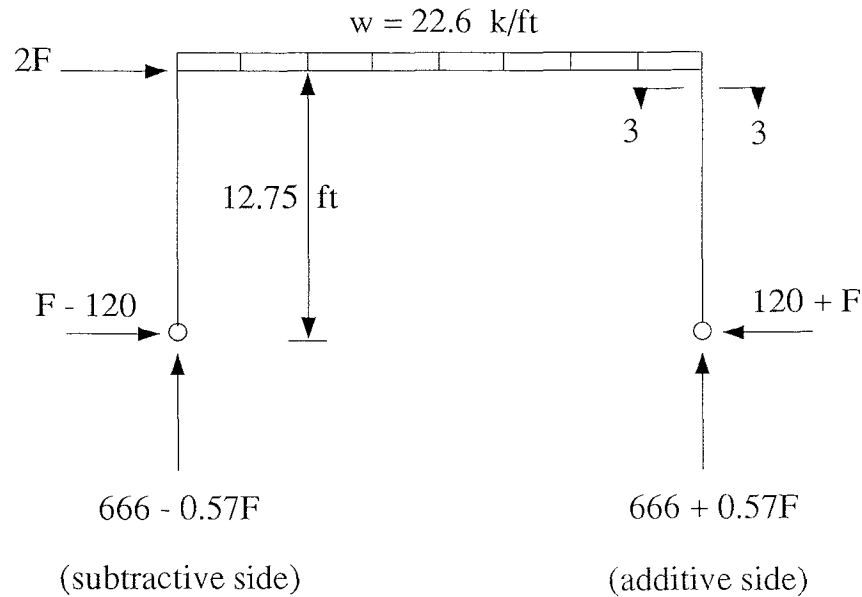


Figure 3.8 Analysis at Section 3-3.

And,

$$N = 666 + 0.57F \quad (3.22)$$

Analyses are performed on section 3-3 in the same manner as done before on section 1-1 to determine the seismic forces at both girders and the base shear force for the following cases:

- A. Cracking (tension side).
- B. First Yield of Steel (after concrete cracking).
- C. Flexural Failure.

The results of the analysis are listed in Table 3.3.

Table 3.3 Seismic Forces Causing Flexural Damage at Section 3–3

B1 Bent	Cracking (kips)	First Yield of Steel (kips)	Flexural Failure (kips)
Lower Girder Force (F)	0.0	470	730
Upper Girder Force (2F)	0.0	940	1,460
Base Shear Force (3F)	0.0 (0.0W)	1,410 (0.50W)	2,190 (0.77W)

It has to be mentioned that according to ACI code, section 3–3 is already cracked due to the gravity loads only.

From Tables 3.1, 3.2, and 3.3, it is apparent that section 1–1 is the strongest among the three sections. Where, the seismic forces required to initiate damage are higher than the forces required for the other two sections. Extensive flexural cracking at section 3–3 (already cracked) and extensive shear cracking at section 2–2 (initiates at upper girder force $(2F) = 370$ kips) would take place before the flexural cracking of section 1–1 (initiates at 620 kips). After cracking, the first yield of reinforcing steel at section 3–3 (at $2F = 940$ kips) takes place before the first yield of reinforcing steel at section 1–1 (at $2F = 1,430$ kips). Finally a flexural failure is expected to occur simultaneously at section 1–1 and section 3–3 (at $2F = 1,460$ kips).

It must be mentioned here that the forces required to cause cracking, first yield of steel, and flexural failure of section 3–3 are less than the forces required

for section 1–1. This is despite the fact that the cross sectional area of section 3–3 is bigger and the steel reinforcement is higher (as seen in Figure 1.3). This is due to the fact that the bending moment at section 3–3 is higher than the bending moment at section 1–1 (see Equations 5.19 and 5.7).

As seen from above, extensive cracking is expected at sections 1–1, 2–2, and 3–3 before the upper girder force ($2F$) reaches 1,267 kips = $0.45W$, where shear transfer failure occurs at section 1–1 leading to the collapse of the B1 bents. This collapse occurs before the first yield of steel and flexural failure at section 1–1. While at section 3–3, the yielding of steel takes place.

The maximum force F (730 kips) that would cause flexural failure at sections 1–1 and 3–3 yields a compressive axial force at section 2–2 (the subtractive side of the frame, Figure 3.4). This is important in studying the combined effect of the axial and the shear forces. Where, the compressive force increases the shear strength of concrete and the tensile force reduces it.

From Table 3.2, the seismic shear force (F) that would cause shear failure below shear keys is 185 kips compared to 127 kips and 140 kips calculated by Priestly et al. and Krawinkler (see Chapter 2, Section 2.1.1). Giving a base shear force of $0.2W$ compared to $0.14W$ and $0.15W$ by the previous investigators.

3.4 Analyses of B2 Bent

As shown in Figure 3.9, the lateral seismic force $2F$ at the upper girder is resisted entirely by the continuous column (with one hinge at the top). This is due to the fact that the two hinges in the upper west column of the bent allowed significant rotation as shown in Figures 1.14 and 1.15 (Chapter 1). The upper west column (with two hinges) structurally behaved as a truss member, resisting axial forces

only. Practically, the column resisted a portion of the horizontal shear force. Where some bents suffered shear cracking underneath the truss members. To be more conservative, that portion will be ignored.

Analyses are performed on section 1-1 and section 2-2 in the same manner as mentioned before in analyses of B1 bent. The calculated P-M interaction diagram of section 1-1 shown in Figure 3.10 is used in the analyses. The results are listed in Tables 3.4 and 3.5.

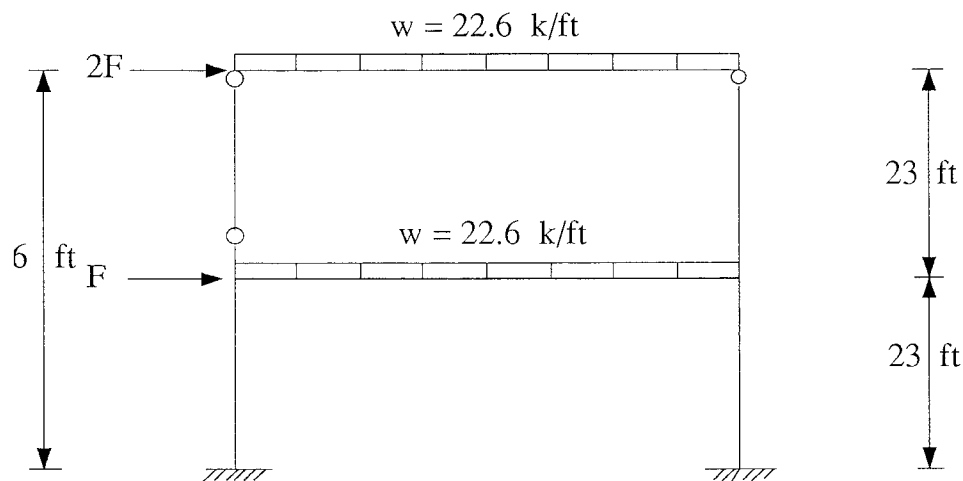


Figure 3.9 Analysis of B2 Bents

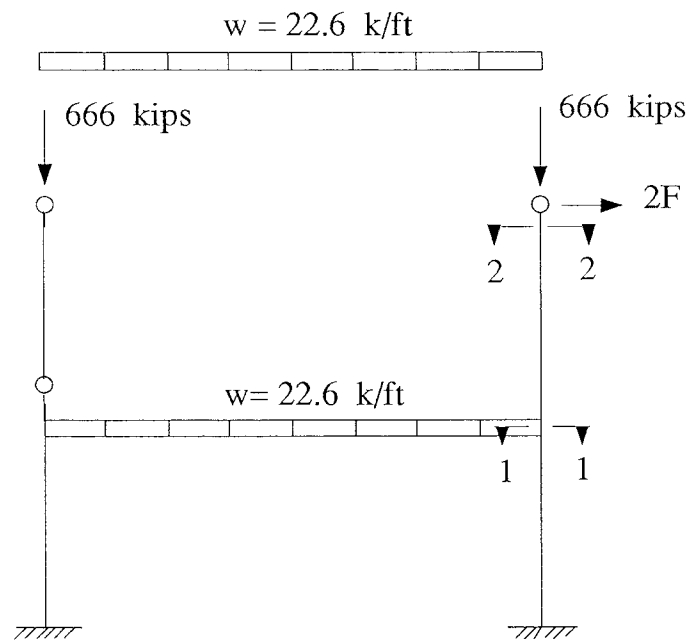


Figure 3.9 (continued) Analysis of B2 Bents

Table 3.4 Seismic Forces Causing Flexural Damage at Section 1-1

B2 Bent	Cracking (kips)	First Yield of Steel (kips)	Flexural Failure (kips)
Lower Girder Force (F)	50	100	130
Upper Girder Force (2F)	100	200	260
Base Shear Force (3F)	150 (0.05W)	300 (0.10W)	390 (0.14W)

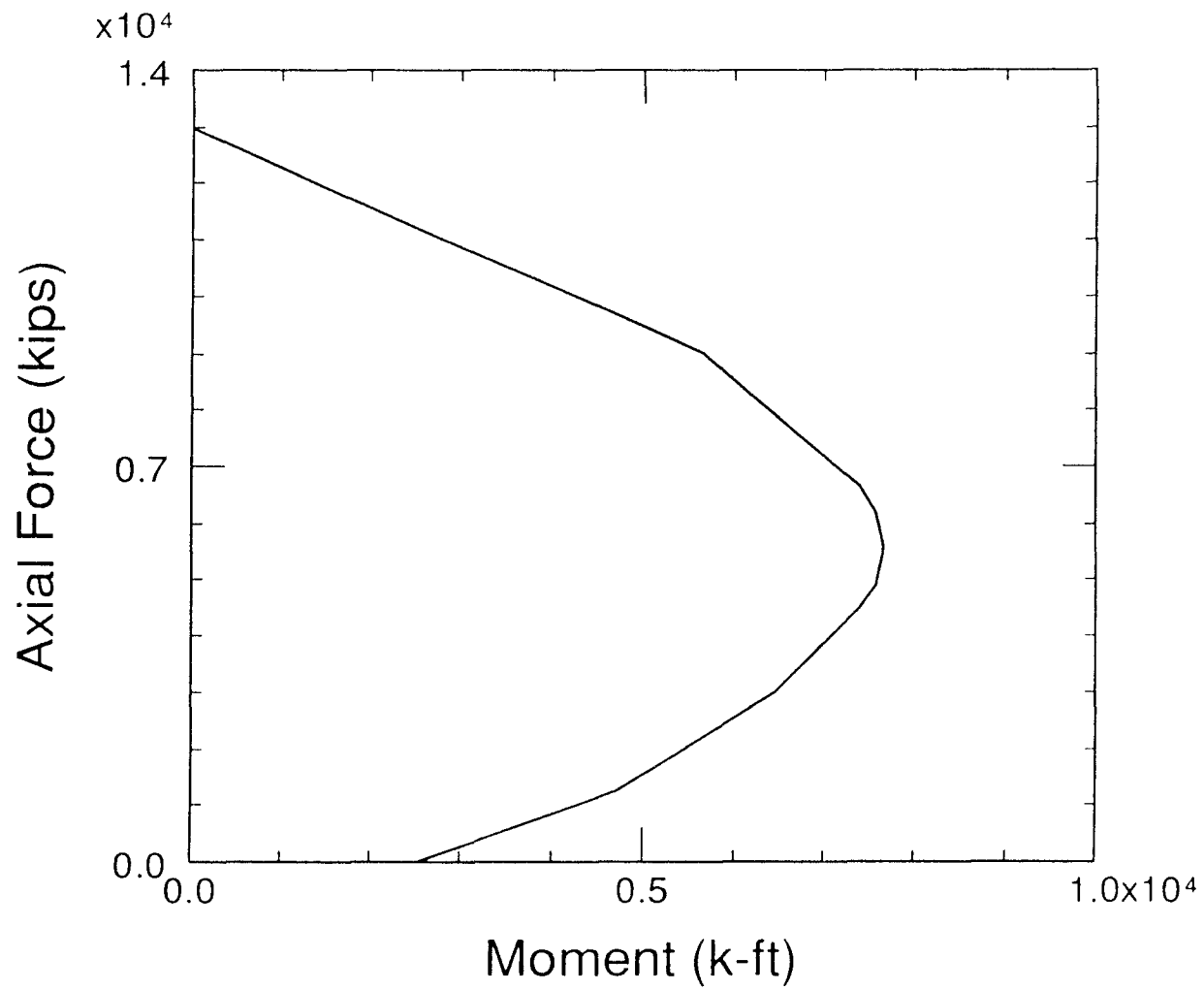


Figure 3.10 P-M Interaction Diagram (Section 1-1)

Table 3.5 Seismic Forces Causing Shear Failure at Sections 1-1 and 2-2

B2 Bent	Shear Failure (section 1-1) (kips)	Shear Failure (section 2-2) (kips)
Lower Girder Force (F)	750	190
Upper Girder Force (2F)	1500	380
Base Shear Force (3F)	2250 (0.80W)	570 (0.2W)

As seen from Tables 3.4 and 3.5, flexural failure at section 1-1 (at upper girder force $(2F) = 260$ kips) is expected to occur before shear failure at section 1-1 (at $(2F) = 1500$ kips) and shear failure at section 2-2 (at $(2F) = 380$ kips). Therefore, a base shear force $(3F)$ of 390 kips $= 0.14W$ (due to the horizontal ground motion) would cause the failure of B2 bents (flexural failure).

The shear force $(2F)$ required to cause shear failure at section 1-1 (Table 3.5) is determined using Equation 3.12.

3.5 Analyses of B3 Bents

The height of the four B3 bents is constant throughout the structure and is approximately equal to 51.4 ft. According to the Uniform Building Codes (UBC), the seismic forces at both decks are determined as shown in Figure 3.11.

As seen in Figure 3.11, the lateral seismic force at the upper deck is resisted by both columns. The P-M interaction diagram of section 1-1 was calculated as shown in Figure 3.12 and used in analyses.

Analyses are performed at section 1–1 and section 2–2 in the same manner as for B1 and B2 bents to determine the seismic forces at both girders (F and $1.82 F$) and the total base shear force ($2.82F$). The results of analyses are listed in Tables 3.6 and 3.7.

Table 3.6 Seismic Forces Causing Flexural Damage at Section 1–1

B3 Bent	Cracking (kips)	First Yield of Steel (kips)	Flexural Failure (kips)
Lower Girder Force (F)	80	310	400
Upper Girder Force ($1.82F$)	145	562	727
Base Shear Force ($2.82F$)	225 ($0.08W$)	870 ($0.31W$)	1,126 ($0.40W$)

Table 3.7 Seismic Forces for Shear Failure at Sections 1–1 and 2–2

B3 Bent	Shear Failure (section 1-1) (kips)	Shear Failure (section 2-2) (kips)
Lower Girder Force (F)	1392	290
Upper Girder Force ($1.82F$)	2534	526
Base Shear Force ($2.82F$)	3926 ($1.39W$)	815 ($0.29W$)

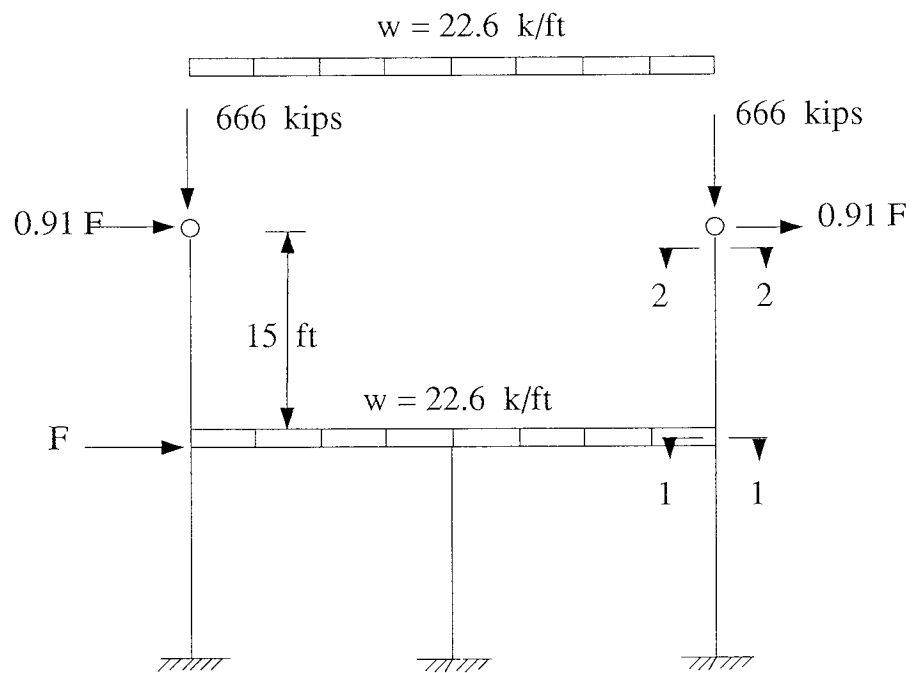
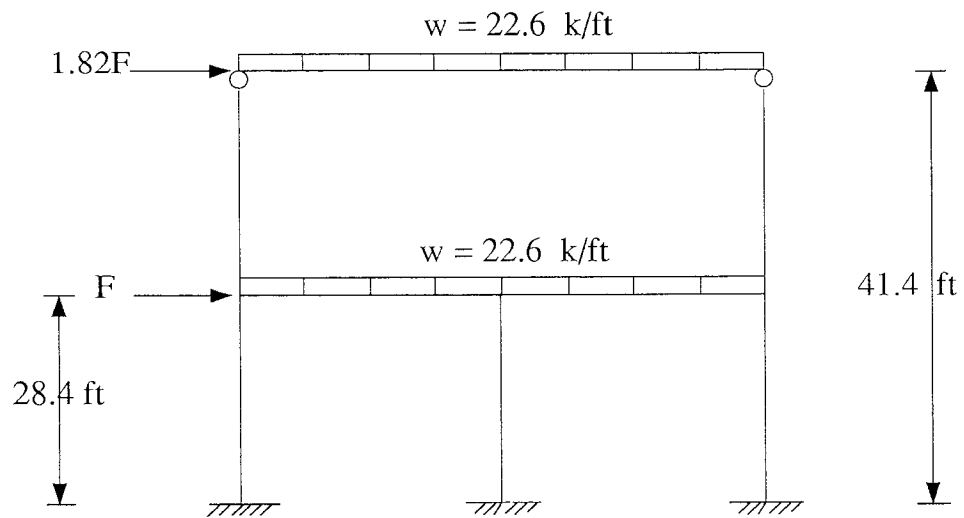


Figure 3.11 Analysis of B3 Bents.

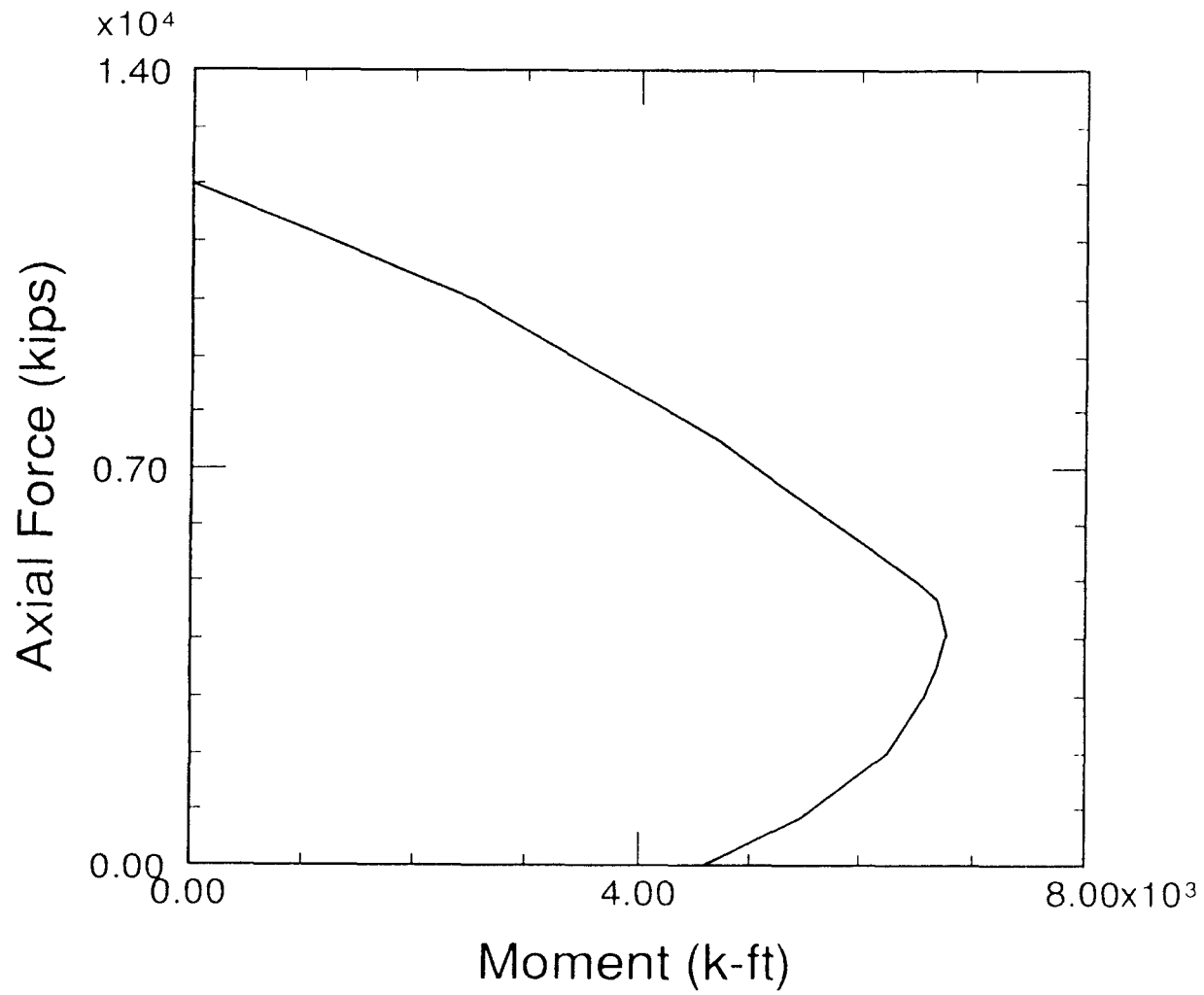


Figure 3.12 P-M Interaction Diagram (Section 1-1)

As seen from Table 3.6 and 3.7, a flexural failure at section 1–1 would occur at upper girder force $(1.82F) = 727$ kips. Where shear cracking at section 2–2 would not cause the failure of the structure. Therefore, a base shear force $= 1126$ kips $= 0.40W$ would cause the flexural collapse of B3 bents.

3.6 Conclusion

For B2 bents, a flexural failure is expected (at section 1–1) at a base shear force $= 390$ kips $= 0.14W$. Followed by the flexural failure of B3 bents (failure at section 1–1) at a base shear force $= 1,126$ kips $= 0.40W$. Finally, for B1 bent, a shear transfer failure takes place (at section 1–1) at a base shear force $= 1,900$ kips $= 0.67W$. Therefore, B2 bent is the weakest bent among the three bent types and the horizontal ground motion would be the cause for these failures.

The discontinuity of each bent of the three bent types due to the existence of the shear keys, resulted in reduction of the structural stiffness of the bents and reduction of shear capacities of the sections at these shear keys. Where, only concrete shear strength is considered without the contribution of steel.

CHAPTER 4
DYNAMIC ANALYSES
4.1 Analyses of B1 Bent

The following two models were used in the dynamic analyses:

- A. Two dimensional model.
- B. Three dimensional model (two B1 bents).

Frequency and linear time history analyses are performed on each model for two cases: (1) The maximum height of the bent throughout the structure, (2) The minimum height of the bent. This will enable us to determine the range of the frequencies and the seismic forces. The transverse record (peak acceleration = 0.29g) of the ground motion measured at the Oakland Outer Wharf site along with its vertical record (peak acceleration = 0.06g) (shown in Figures 4.1 and 4.2) are used simultaneously in linear time history analyses. A third case (for B1 only), the 3-D model is to be subjected only to the vertical component to determine the effect of this record on the structure. Models are used in analyses without the exact boundary conditions in the longitudinal direction of the Cypress Viaduct. Therefore, no ground motion record is used in that direction in all linear time history analyses. Knowing that the reported damage to the structure in that direction was minimal [5].

The foundations are assumed as a fixed boundaries to the structure, though the structure was constructed to have shear keys at the foundation as mentioned earlier. This assumption of fixity is based on the following observations:

- A. No displacements or rotations of foundations were reported.
- B. No damage to foundations was reported.

C. The lower columns were perfectly vertical and undamaged after the earthquake (no sign of rotation).

D. The lower columns were 6 ft wide (wide enough to resist rotation).

Furthermore, the first two transverse frequencies based on the previous assumption are in a good agreement with those obtained by other investigators experimentally as well as analytically (see Table 2.1).

4.1.1 Two Dimensional Model

Figure 4.3 shows the model used in analyses. The results of the linear time history analysis are presented for the nodes shown in this figure.

The analytical model for the finite element software ADINA consisted of 2–node Hermitian beam elements. The shear keys were modeled by releasing the moment at their locations. The numerical integration was performed using 4 gauss integration points for each element.

The frequencies obtained from frequency analysis are listed in the following Table:

Table 4.1 Fundamental Frequencies

Bent Height	1 st	2 nd	1 st	2 nd
	Transverse	Transverse	Vertical	Vertical
46 ft	2.18	6.70	6.42	8.52
54 ft	1.95	5.03	6.38	8.04

The mode shapes (bent height = 46 ft) are shown in Figures 4.4–4.6.

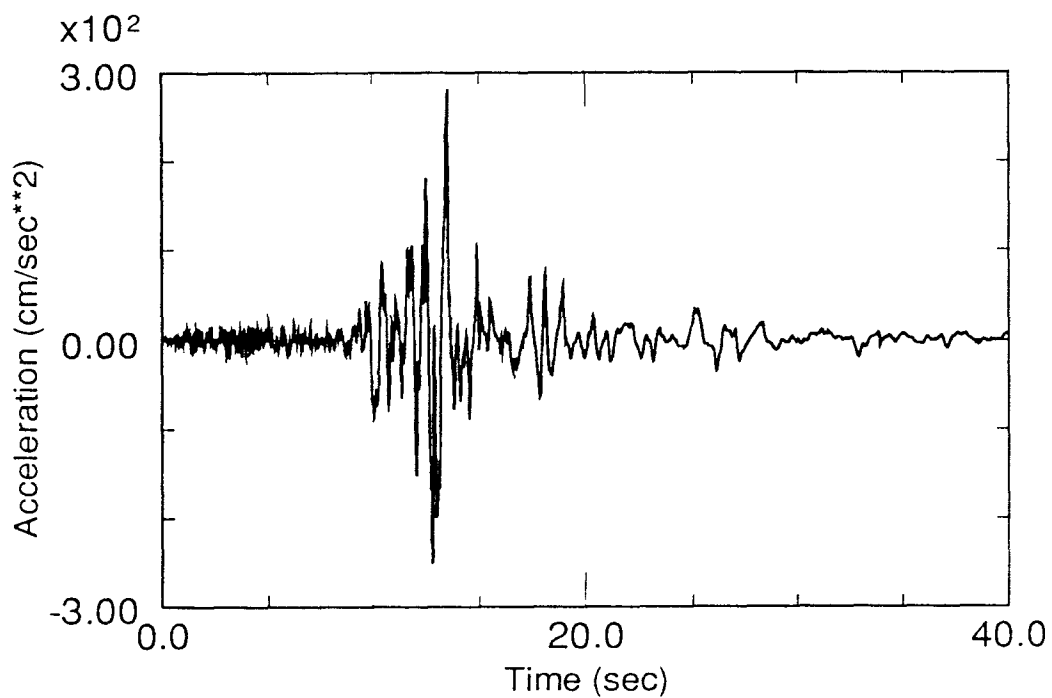


Figure 4.1 Horizontal Ground Acceleration (Peak = 0.29g)

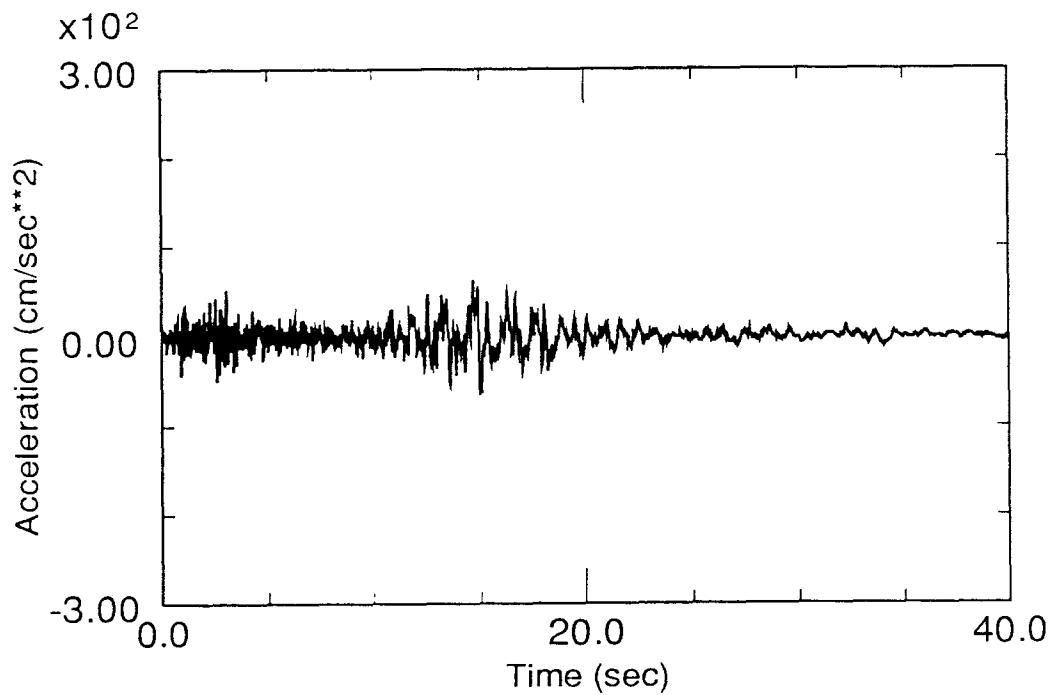


Figure 4.2 Vertical Ground Acceleration (Peak = 0.06g)

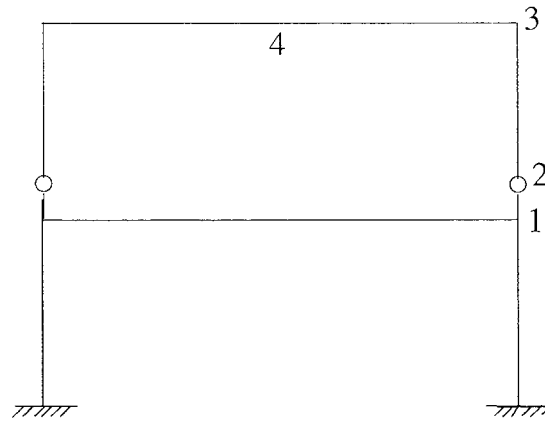


Figure 4.3 2-D Model of B1 Bent.

Linear time history analysis is performed using the transverse and the vertical records of the ground motion simultaneously as mentioned before. The modal damping of the model is taken equal to 5%. The results of time history analysis are listed in the following tables:

Table 4.2 Maximum Lateral Displacements

Bent Height	Displacement (node 3) (in)	Displacement (node 1) (in)
46 ft	1.28 (t = 13.46 sec)	0.26 (t = 13.50 sec)
54 ft	1.77 (t = 13.54 sec)	0.70 (t = 13.52 sec)

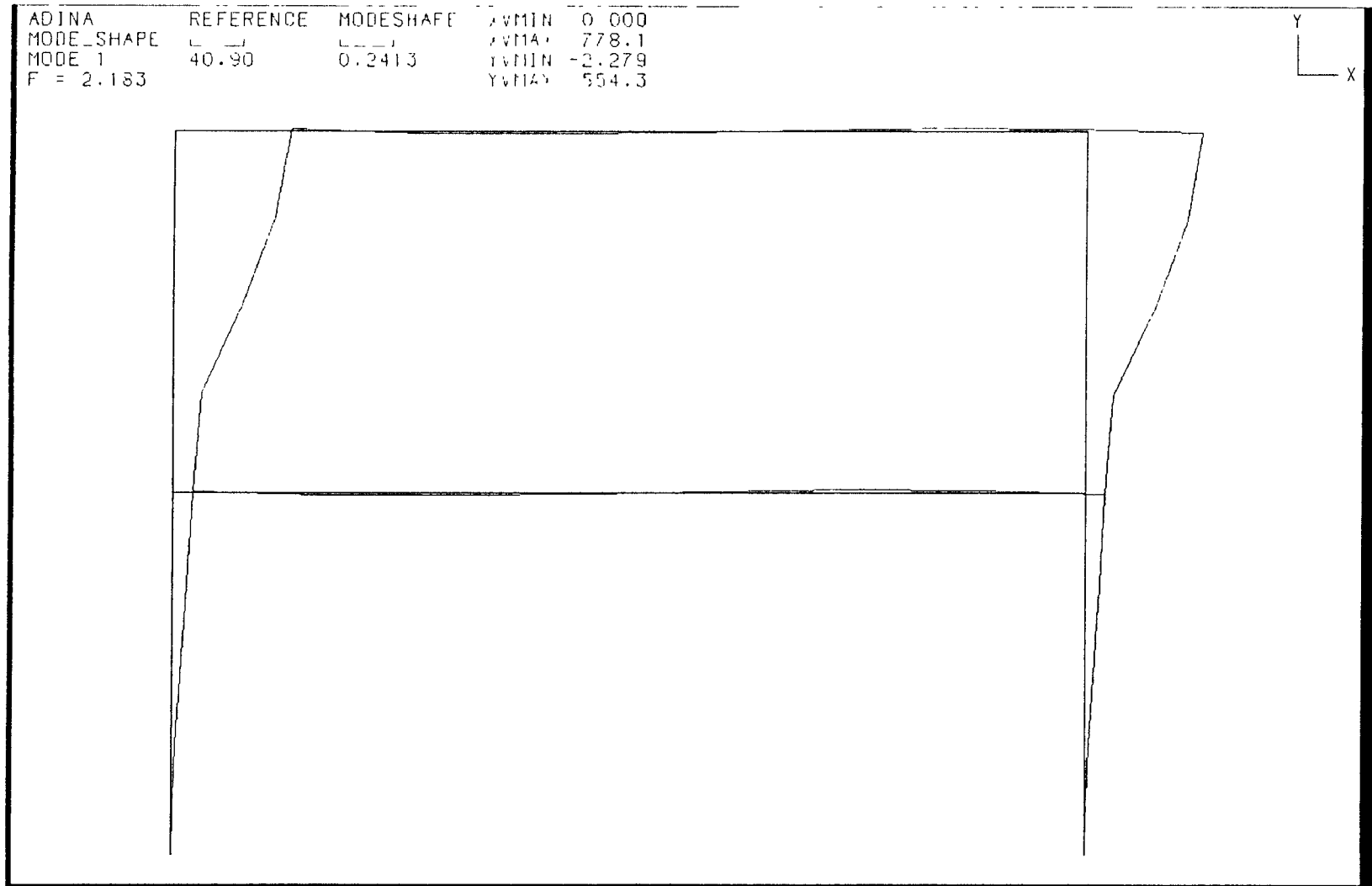


Figure 4.4 First Transverse Mode Shape

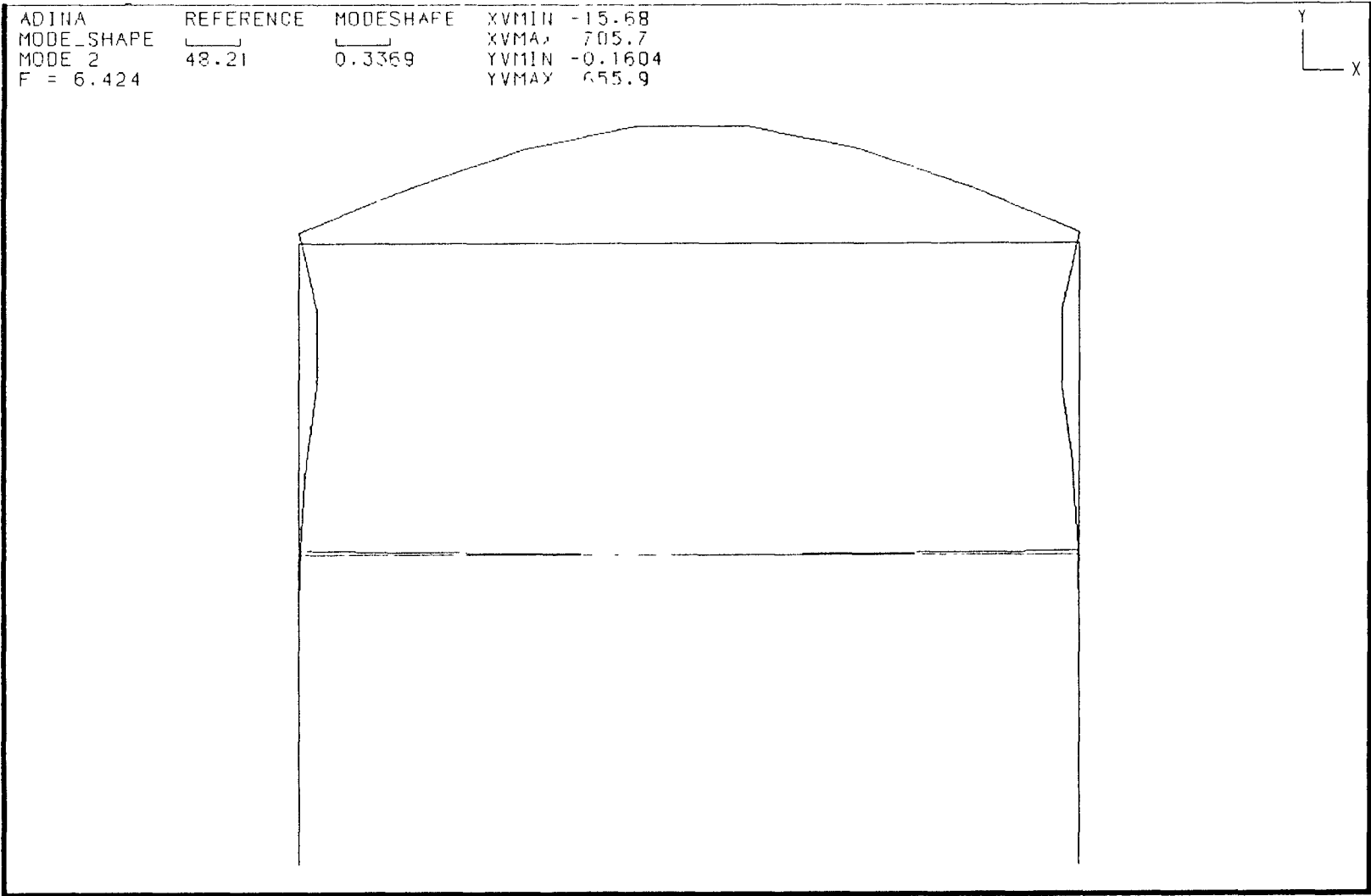


Figure 4.5 First Vertical Mode Shape

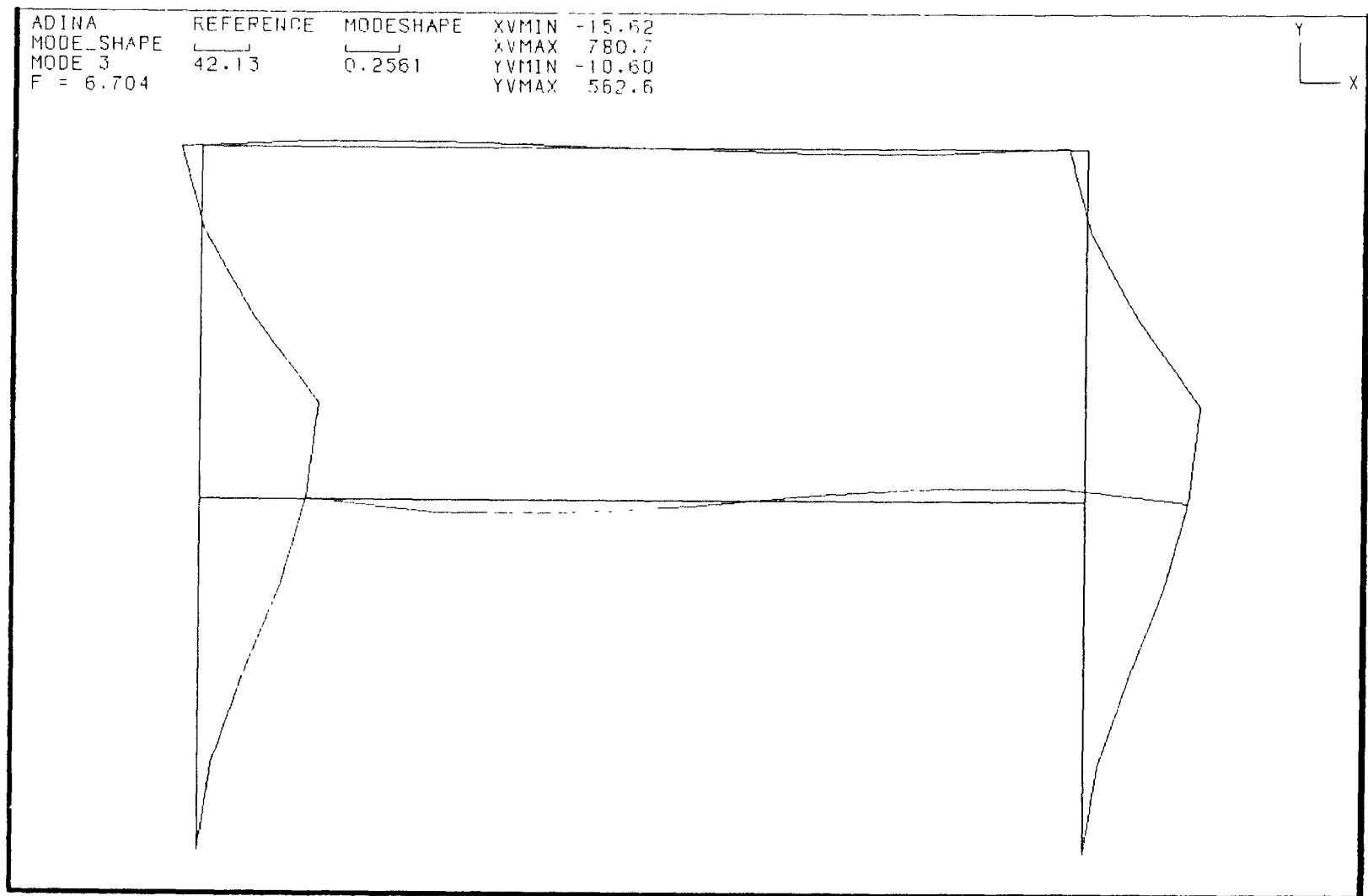


Figure 4.6 Second Transverse Mode Shape

Table 4.3 Seismic Shear and Axial Forces

Bent Height	Max. Shear (node 2) (kips)	Total Shear (node 2) (kips)	Max. Tension (node 2) (kips)	Total Axial (node 2) (kips)
46 ft	427 (t = 13.46 sec)	555	-259 (t = 13.46 sec)	449
54 ft	446 (t = 13.56 sec)	574	-289 (t = 13.56 sec)	419

Table 4.4 Seismic Forces

Bent Height	Max. Force (lower deck) (Kips)	Force (upper deck) (Kips)	Ratio
46 ft	378 (t = 13.52 sec)	520 (t = 13.52 sec)	1 : 1.38
54 ft	530 (t = 13.54 sec)	816 (t = 13.54 sec)	1 : 1.54

The time history plots of displacements and forces (bent height = 46 ft) are shown in Figures 4.7–4.12.

As seen from the previous figures, the effect of the ground motion on the structure was insignificant during the first 10 seconds of the earthquake. The structure experienced large displacements and forces within the interval (10th–16th) seconds, with maximum lateral displacements and forces precisely occurring between the 13th and the 14th second of the ground motion. The maximum lateral displacements of nodes 2 and 3, and the maximum forces at node 2 occurred simultaneously as seen in Table 4.2.

There were almost no vertical displacements throughout the bent (nodes 2 and 4) as seen in Figures 4.11 and 4.12.

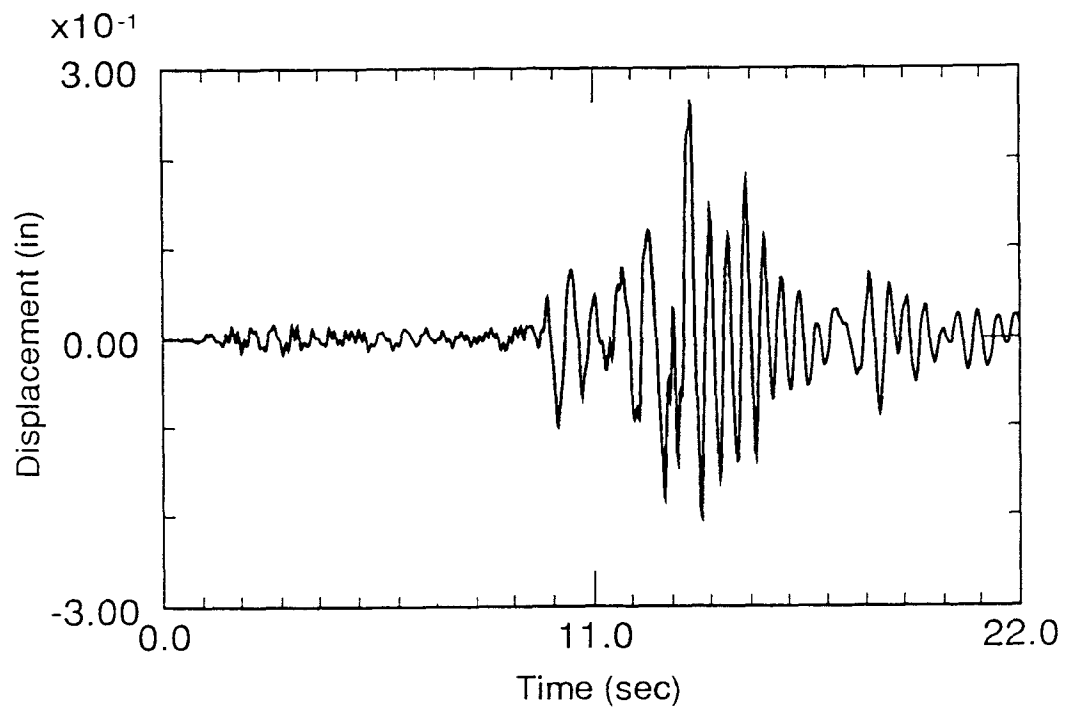


Figure 4.7 Lateral Displacement (Node 1)

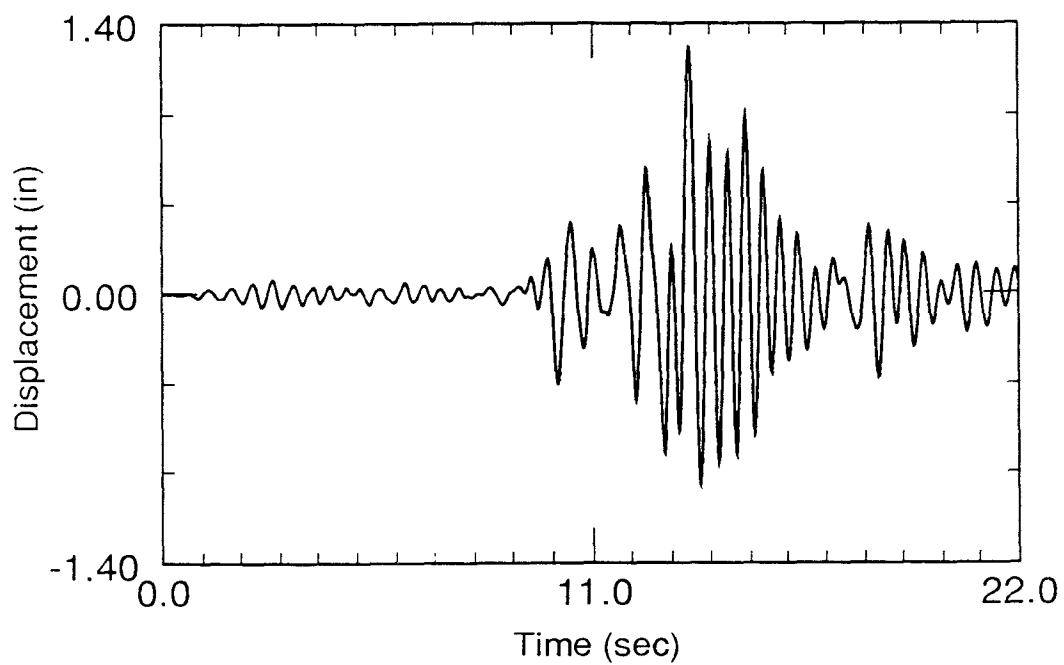


Figure 4.8 Lateral Displacement (Node 3)

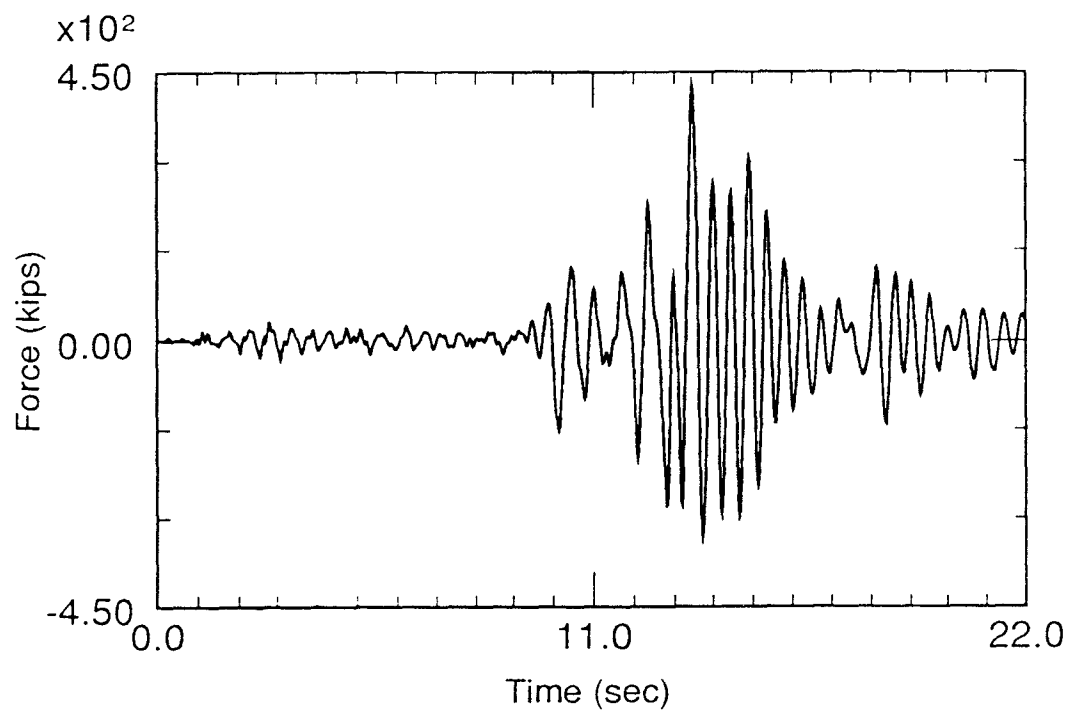


Figure 4.9 Seismic Shear Force at Shear Key (Node 2)

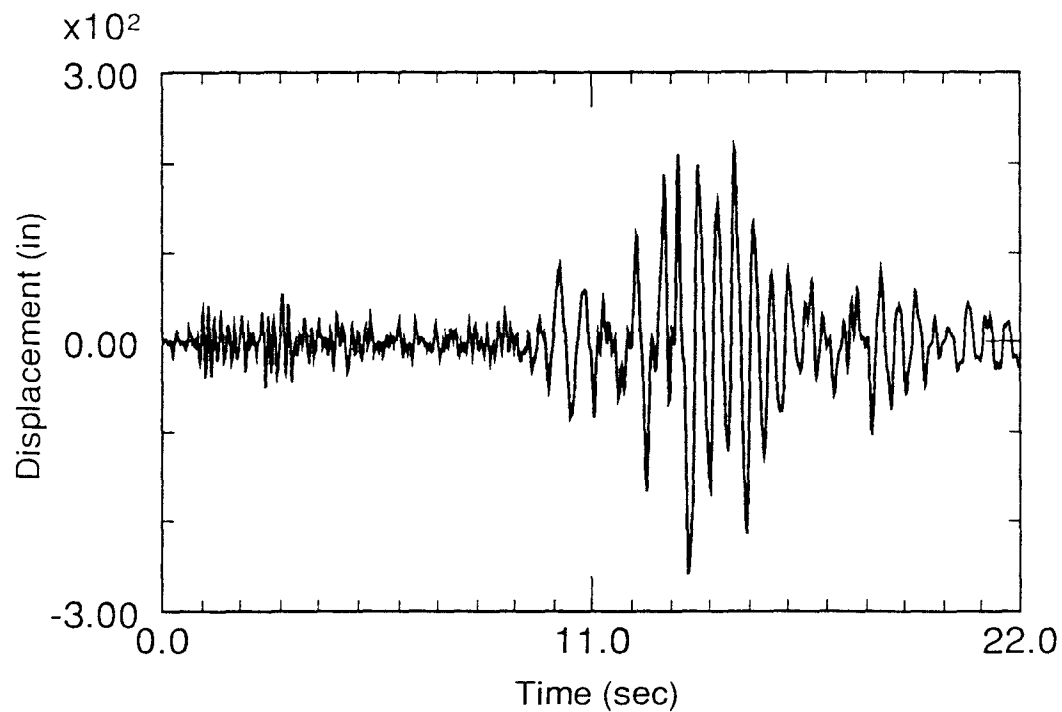


Figure 4.10 Seismic Axial Force at Shear Key (Node 2)

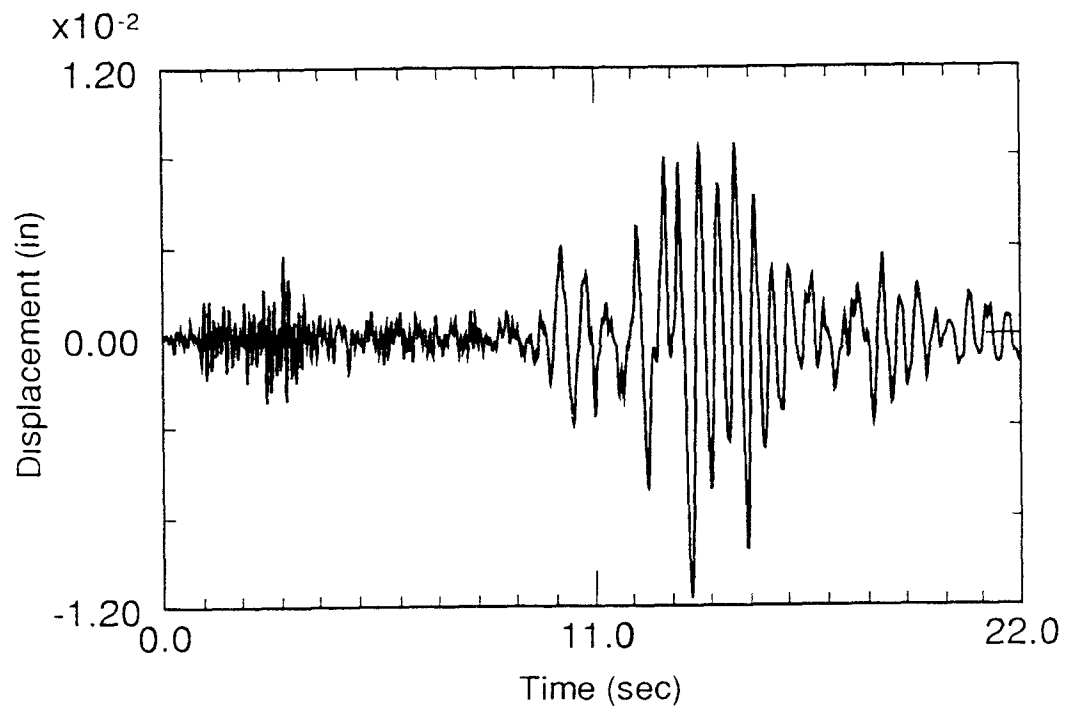


Figure 4.11 Vertical Displacement (Node 2)

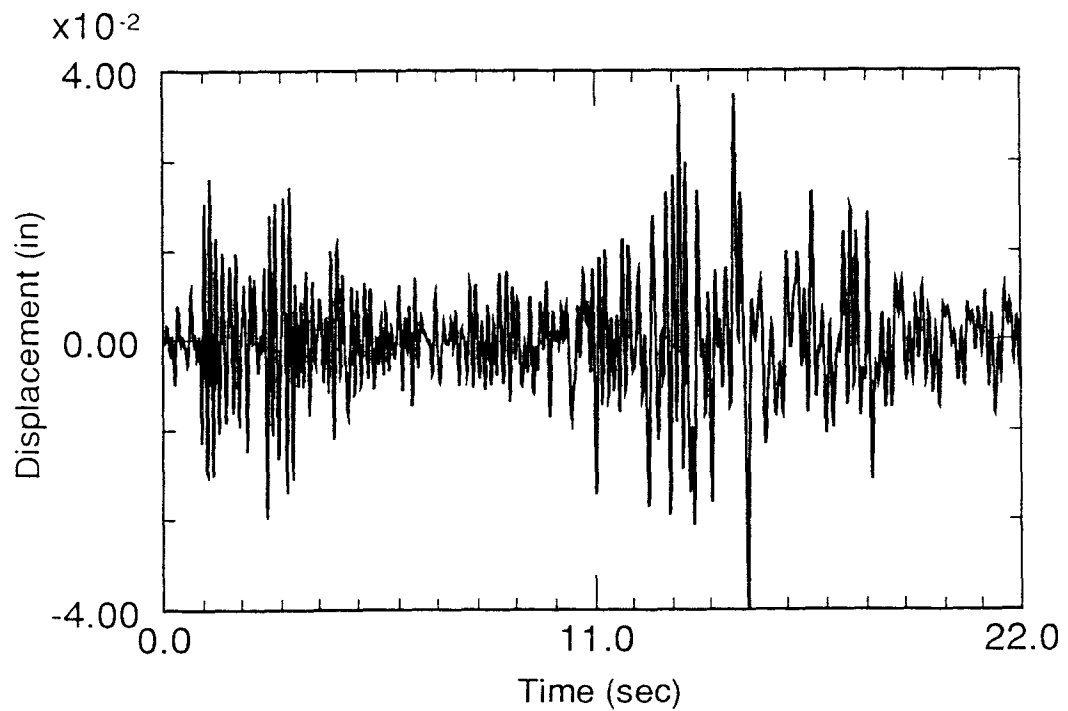


Figure 4.12 Vertical Displacement (Node 4)

Comparison between dynamic and static analyses results will be presented later.

4.1.2 Three Dimensional Model

The 3-D model is used to get more accurate results (frequencies, displacements, forces, and acceleration amplification factors) especially in the vertical direction. The reason is that the upper and lower decks are well modeled. Where the total mass of the decks are distributed horizontally.

Figure 4.13 shows the three dimensional model consisting of two B1 bents modeled with 2-node Hermitian beam elements. Figure 4.14 shows a cross section of the upper and lower decks (box section) modeled with 8-node shell elements (each element has 4 integration gauss points).

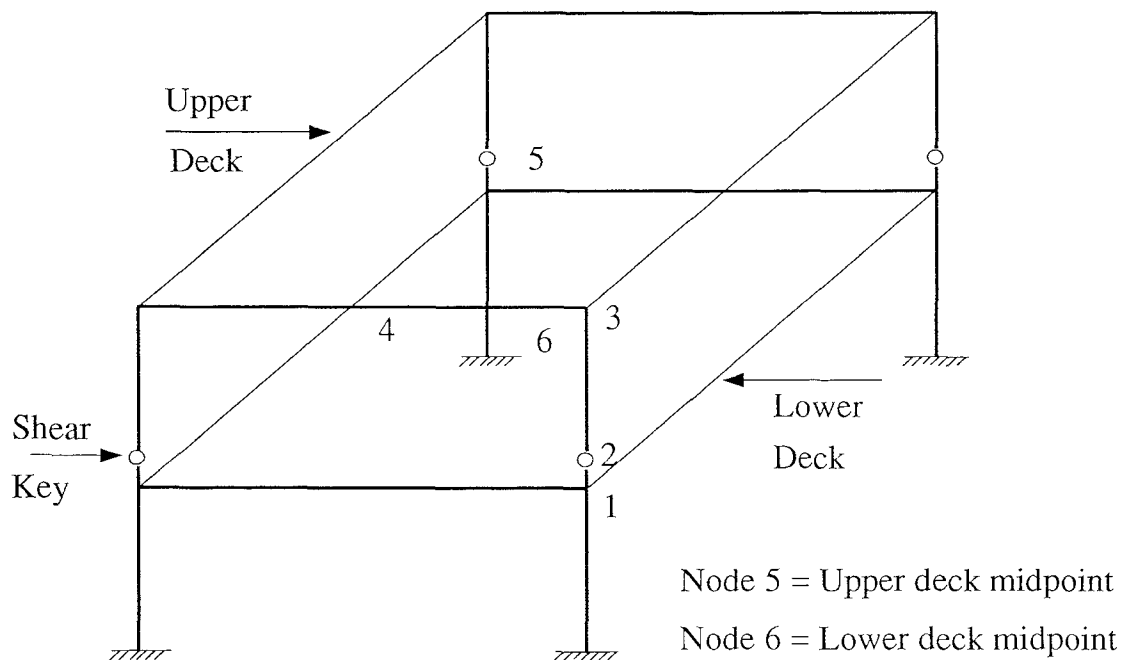


Figure 4.13 3-D Model of B1 Bent.

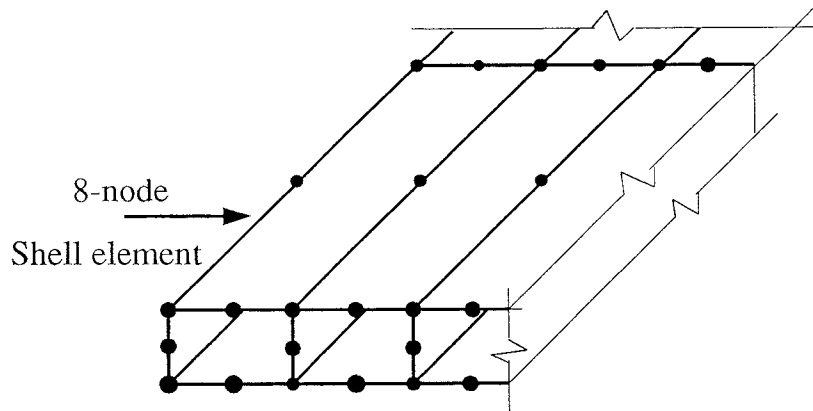


Figure 4.14 Cross Section of Upper and Lower Decks.

Results of the frequency analysis are listed in the following table:

Table 4.5 Fundamental Frequencies

Bent Height	1 st Transverse	2 nd Transverse	1 st Vertical	2 nd Vertical
46 ft	2.28	6.87	3.95	4.02
54 ft	2.00	5.21	3.94	4.01

Bent Height	1 st Longitudinal (Hz)	1 st Torsional (Hz)
46 ft	0.71	2.76
54 ft	0.58	2.35

The mode shapes (bent height = 46 ft) are shown in Figures 4.16–4.21.

The 2-D model and the 3-D model have almost the same transverse frequencies. While there was significant difference in the vertical frequencies.

Next, two different linear time histories for the 3-D model are presented. The first one is performed using the transverse and the vertical records of the ground motion simultaneously. The second one is performed using the vertical record only.

A. Linear Time History (using transverse And vertical records)

The linear time history analysis performed on the 2-D model is repeated on the 3-D model. The results of the analysis are listed in the following tables:

Table 4.6 Maximum Lateral Displacements

Bent Height	Displacement (node 3) (in)	Displacement (node 1) (in)
46 ft	1.39 (t = 13.46 sec.)	0.30 (t = 13.50 sec.)
54 ft	1.88 (t = 13.52 sec.)	0.78 (t = 13.52 sec.)

Table 4.7 Seismic Shear and Axial Forces

Bent Height	Max. Shear (node 2) (Kips)	Total Shear (node 2) (Kips)	Max.Tension (node 2) (Kips)	Total Axial (node 2) (Kips)
46 ft	458 (t = 13.46 sec)	586 (t = 13.46 sec)	-268 (t = 13.50 sec)	440 (t = 13.50 sec)
54 ft	476 (t = 13.54 sec)	604 (t = 13.54 sec)	-328 (t = 13.54 sec)	380 (t = 13.54 sec)

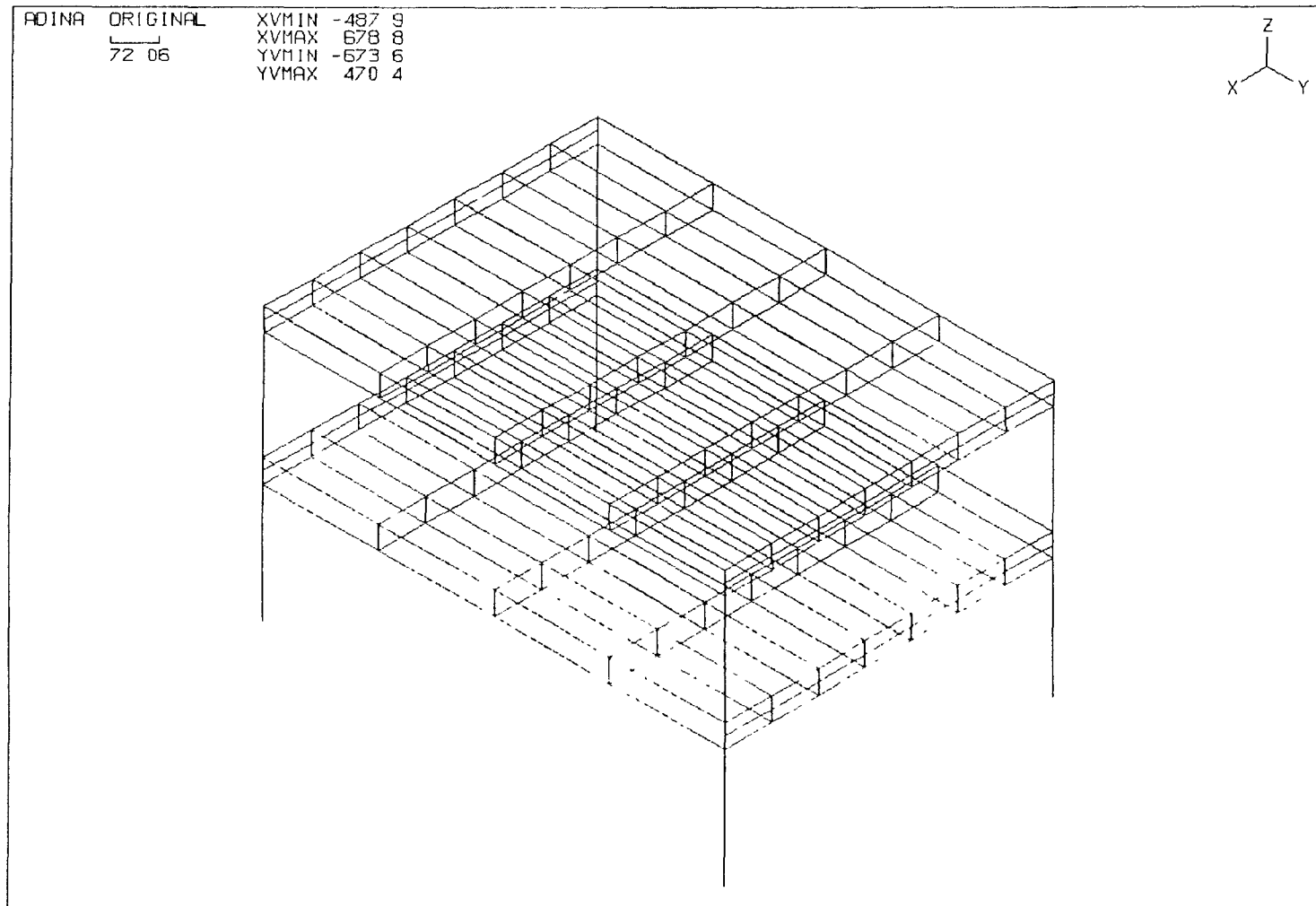


Figure 4.15 3-D Model of B1 Bents

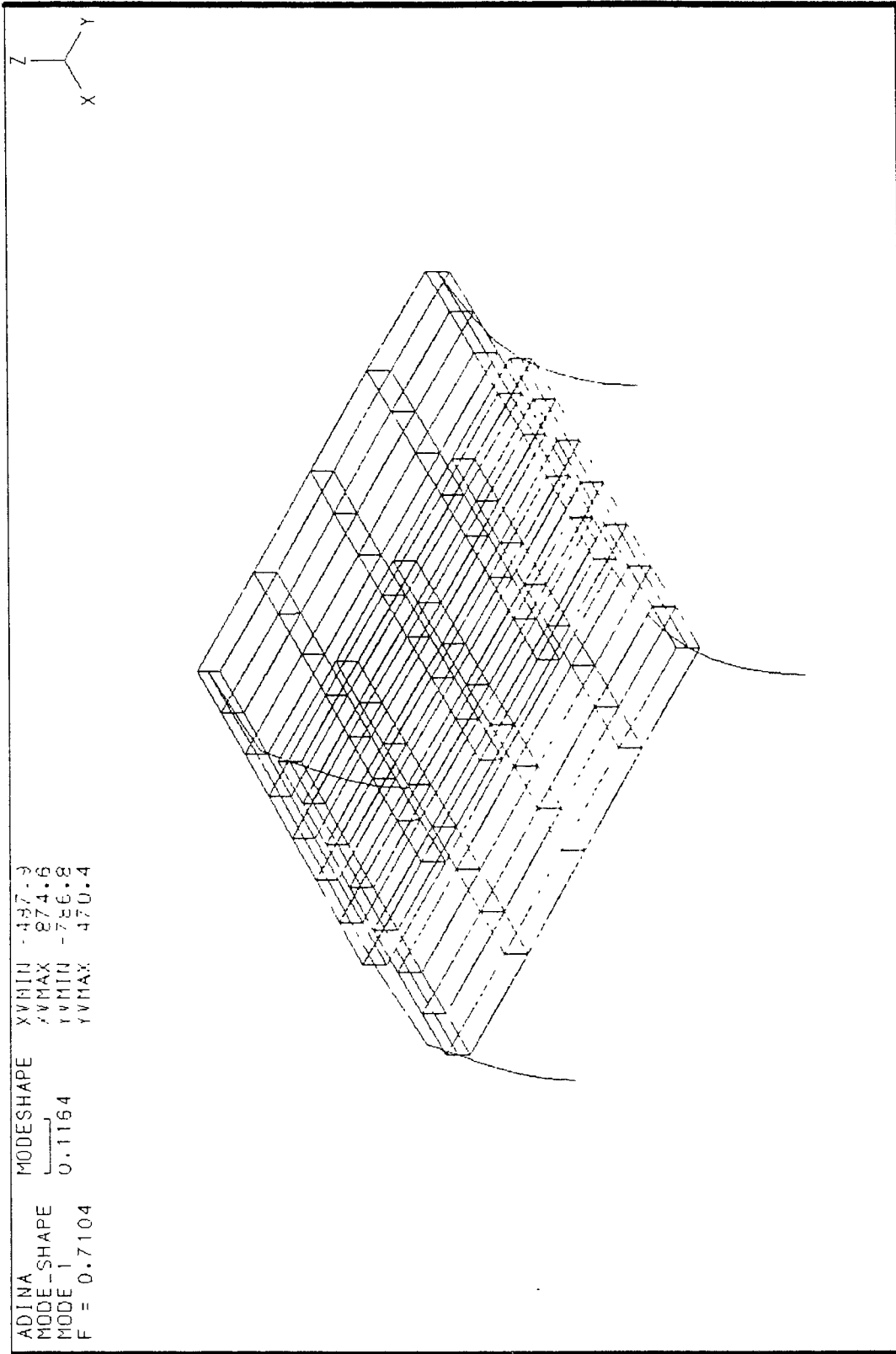


Figure 4.16 First Longitudinal Mode Shape

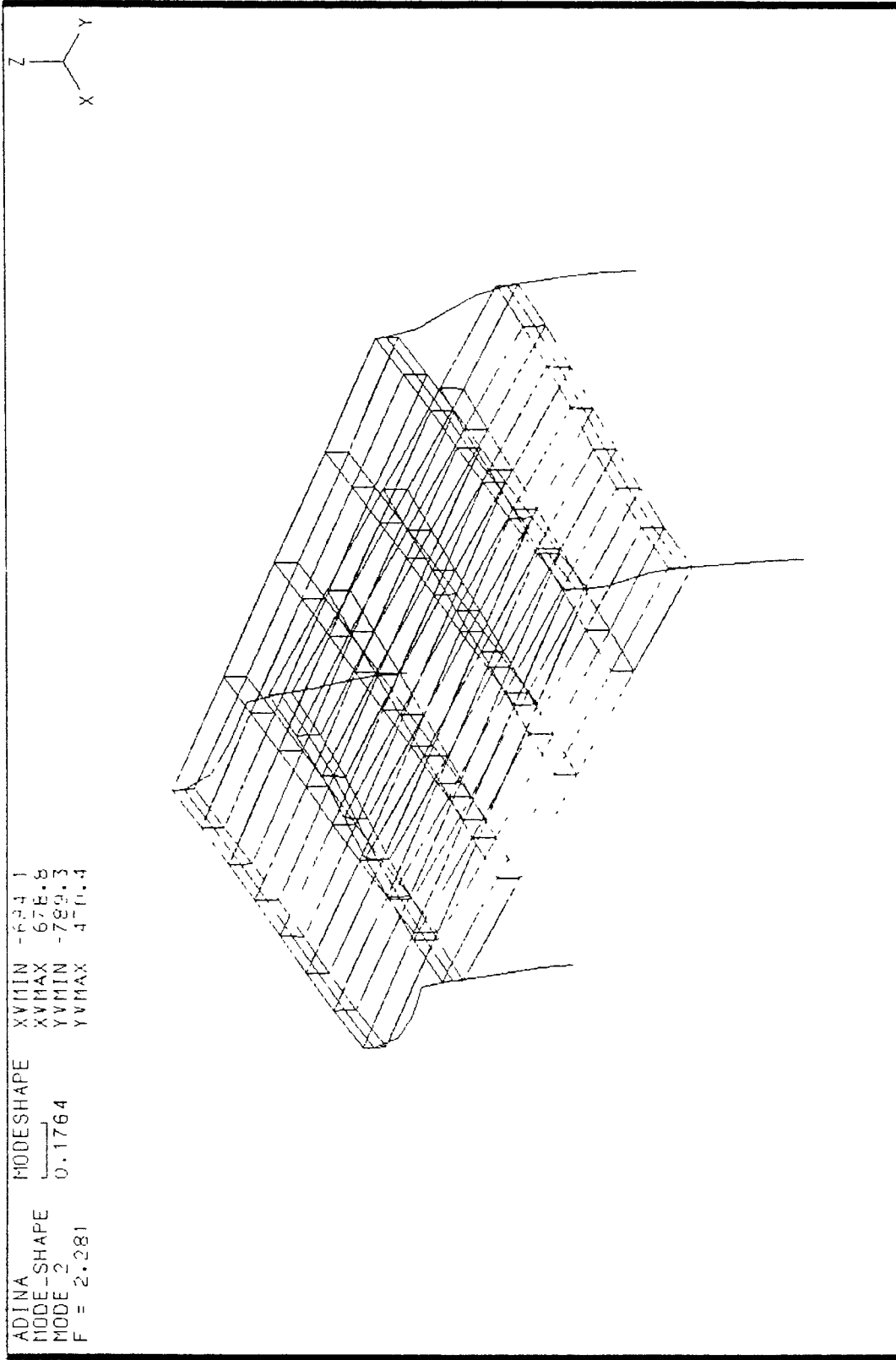


Figure 4.17 First Transverse Mode Shape

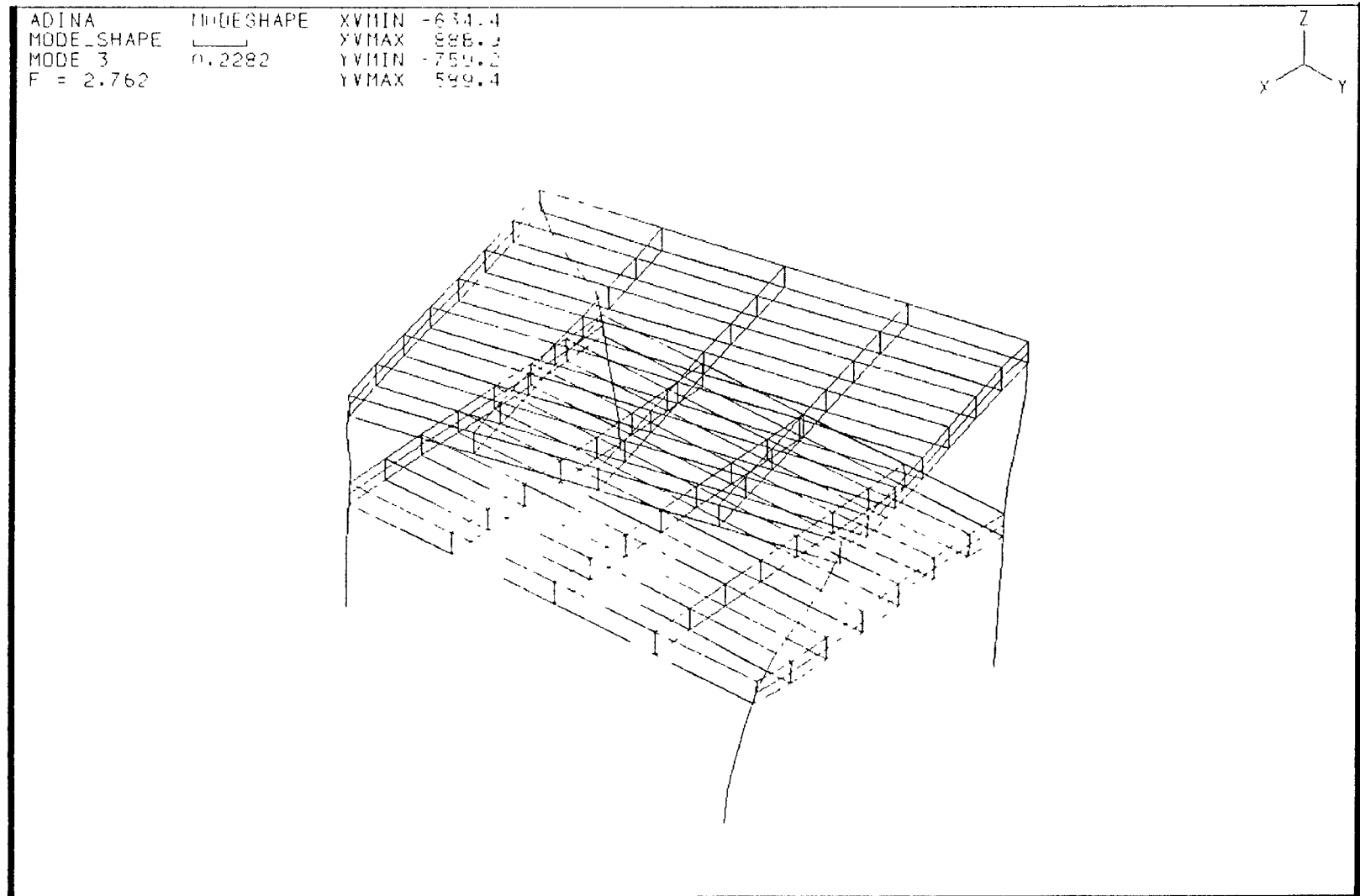


Figure 4.18 First Torsional Mode Shape

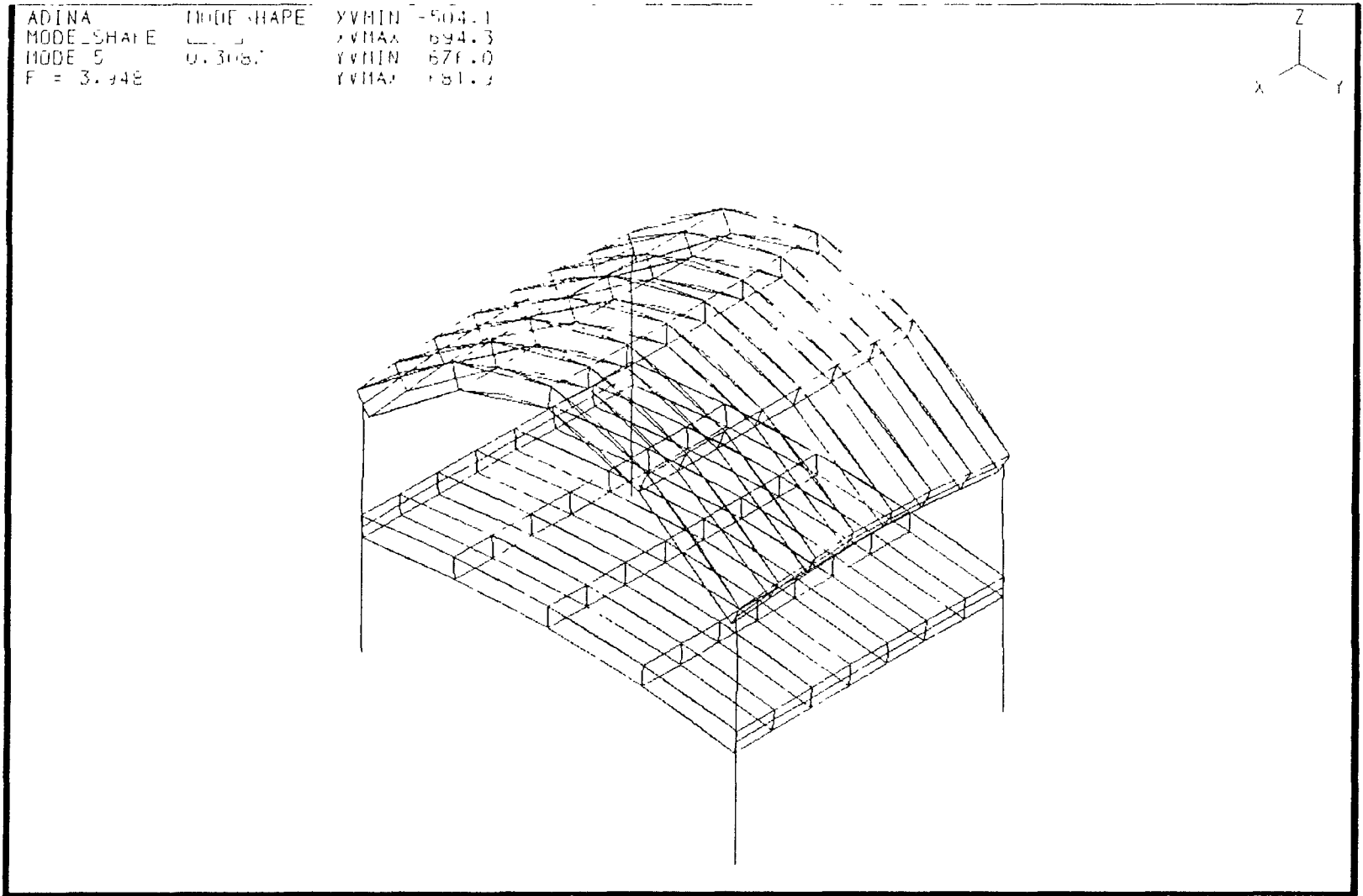


Figure 4.19 First Vertical Mode Shape

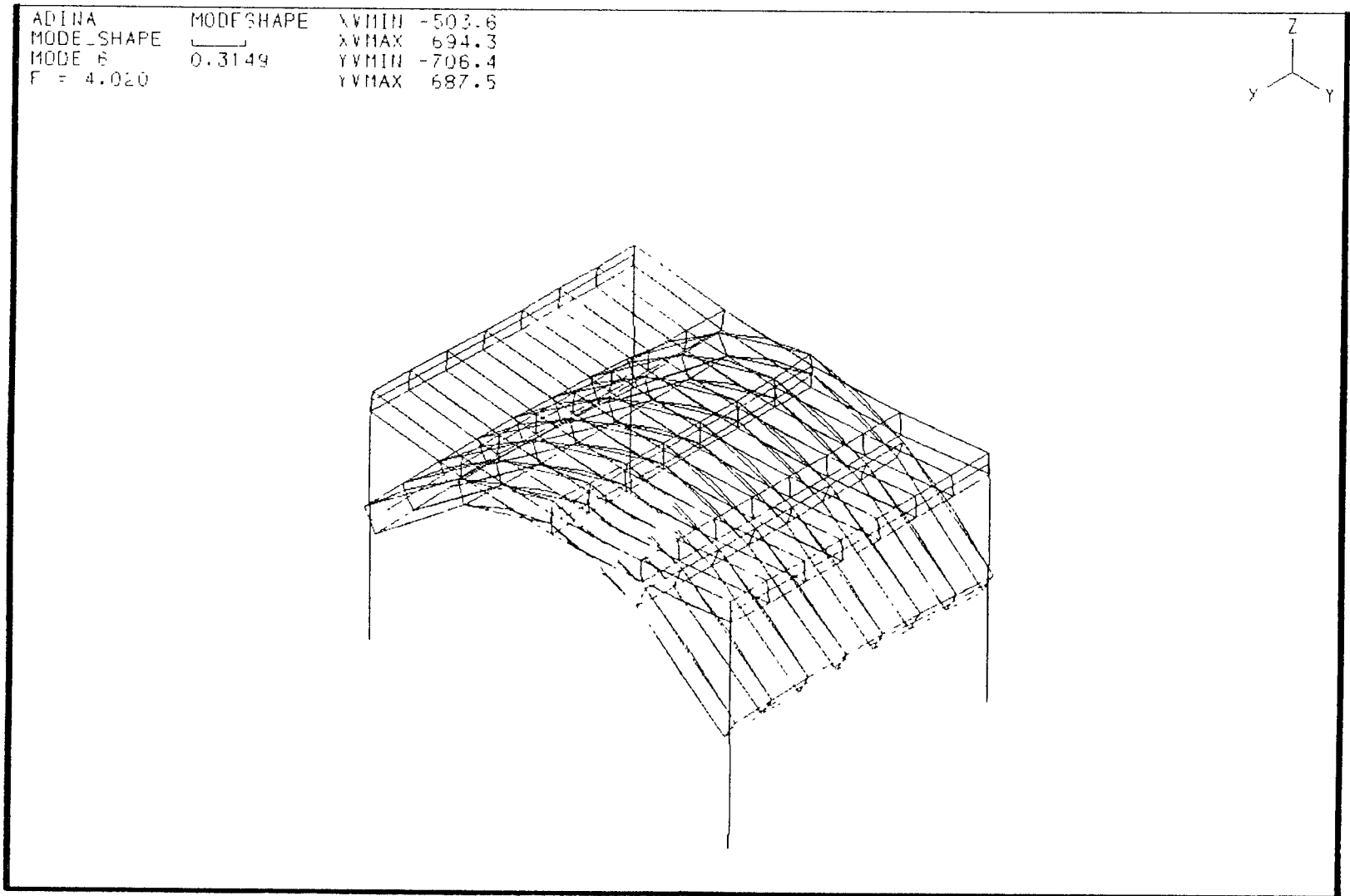


Figure 4.20 Second Vertical Mode Shape

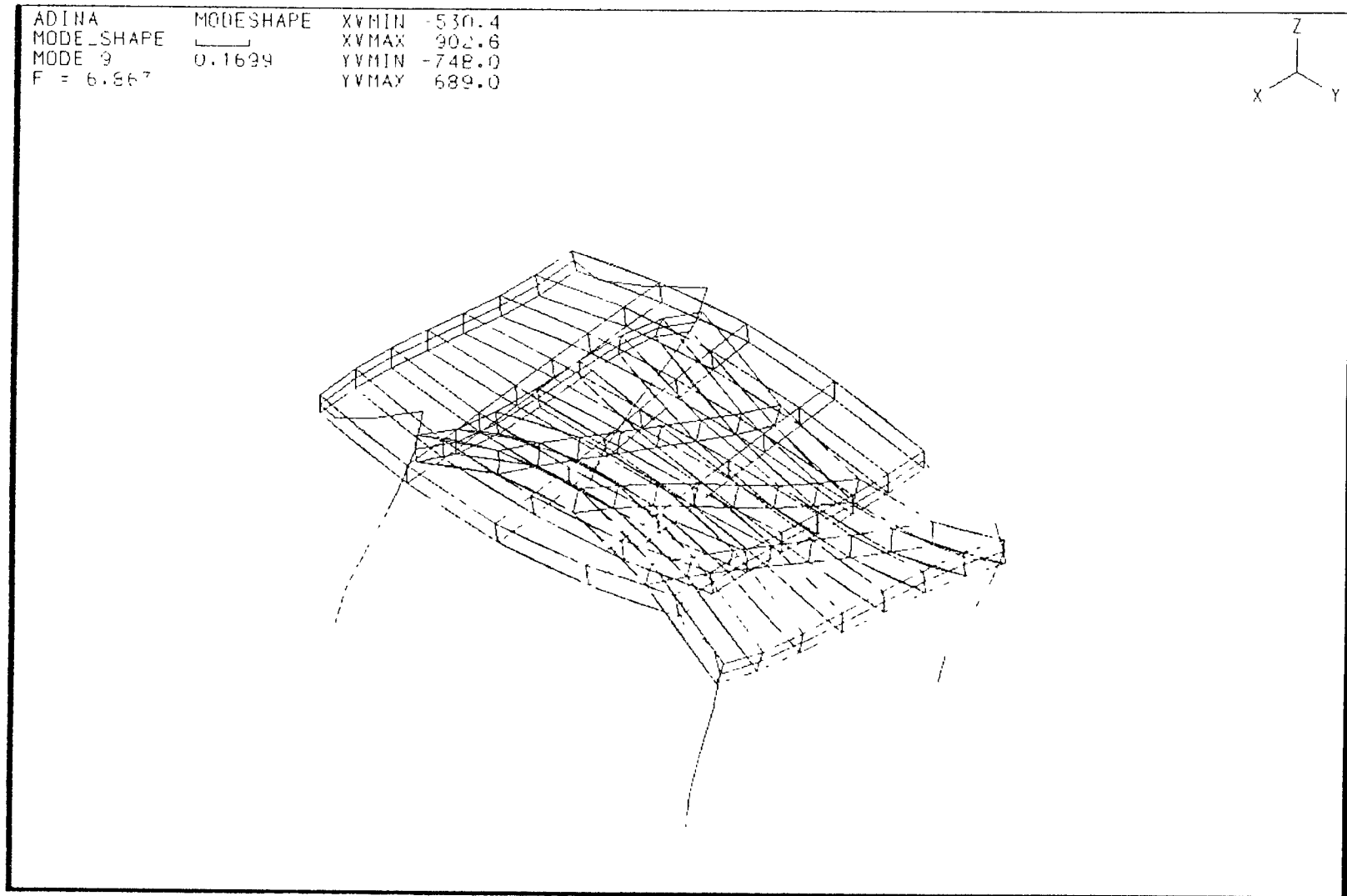


Figure 4.21 Second Transverse Mode Shape

Table 4.8 Seismic Forces

Bent Height	Max. Force (lower deck) (Kips)	Force (upper deck) (Kips)	Ratio
46 ft	433 (t = 13.52 sec)	575 (t = 13.52 sec)	1 : 1.33
54 ft	594 (t = 13.52 sec)	792 (t = 13.52 sec)	1 : 1.33

Table 4.9 Vertical Accelerations (Bent Height = 46 ft)

Location	Max. Vertical Acceleration (in/sec²)	Amplification Factor
Upper deck midpoint (node 5)	88.6 (0.23g)	3.82
Lower deck midpoint (node 6)	74.6 (0.19g)	3.22

Table 4.10 Participation Factors of Frequencies (Time = 13.52 Sec)

Bent Height	1 st Transverse	2 nd Transverse	1 st Vertical	2 nd Vertical
54 ft	1.0	0.47	1.0	0.58

Time history of displacements and forces (bent height = 46 ft) are shown in Figures 4.22–4.25.

As shown in Tables (4.2–4.4 and 4.6–4.8), the results of the analyses of the two dimensional and the three dimensional models are very close, which indicates that the two dimensional model is a good representation of the structure.

The top level lateral displacements (node 3) are 1.39 in. (Figure 4.23) and 1.88 in. for bent heights of 46 ft and 54 ft, respectively. These are significantly higher than the top level displacements of 0.72 in. and 1.3 in. for the unretrofitted and the retrofitted structures (as mentioned before in Chapter 2, Section 2.1.2), which indicates that the structure had undergone large inelastic deformations in the upper story especially in columns just below the shear keys.

The maximum input lateral ground acceleration of 0.29g is amplified to 0.42g at the lower deck, and to 0.74g at the upper deck compared to 0.44g at the lower deck and 0.70g at the upper deck obtained from dynamic analysis done by Wilson (1989) [4].

The maximum vertical acceleration of the midpoints of the upper and the lower decks (nodes 5 and 6), are amplified by factors of 3.82 and 3.22, respectively.

Table 4.10 shows the normalized participation factors of the transverse and the vertical frequencies (Table 4.5) at time equal to 13.52 second of the ground motion where we obtained maximum displacements, shear forces, and axial forces (Tables 4.6–4.8). Higher frequencies (transverse and vertical) had insignificant participation factors.

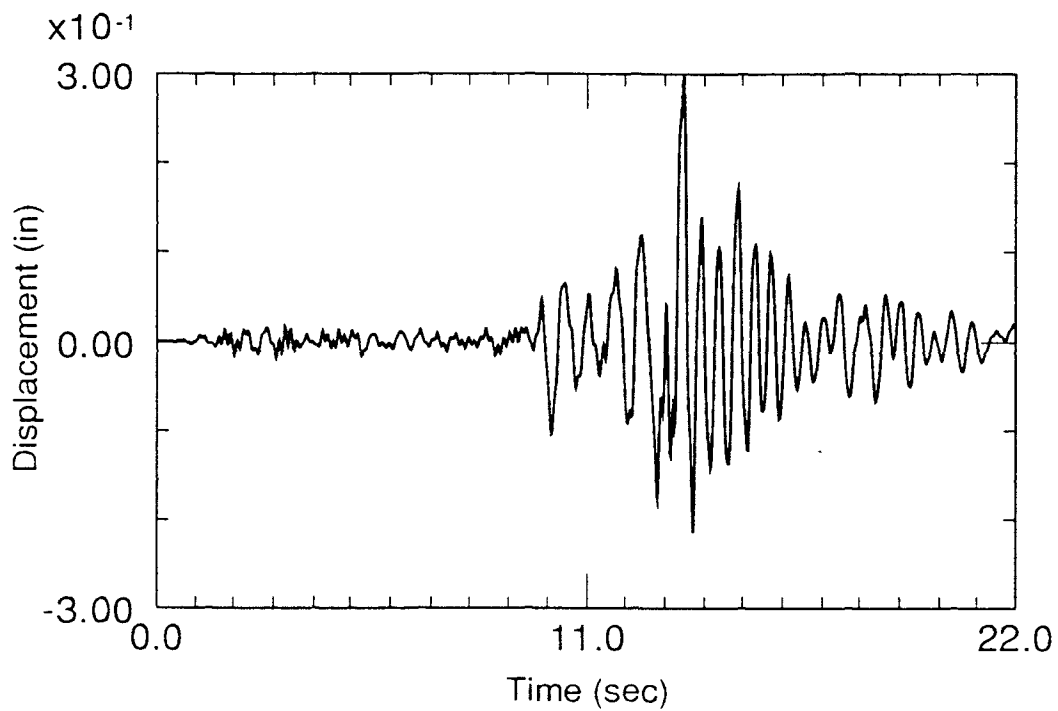


Figure 4.22 Lateral Displacement (Node 3)

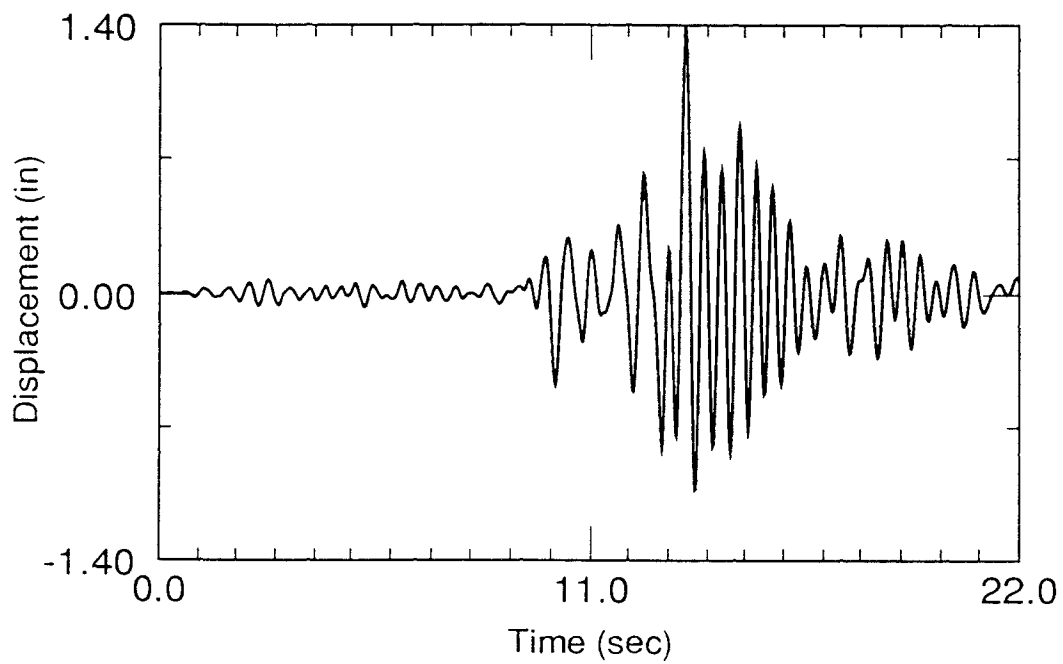


Figure 4.23 Lateral Displacement (Node 3)

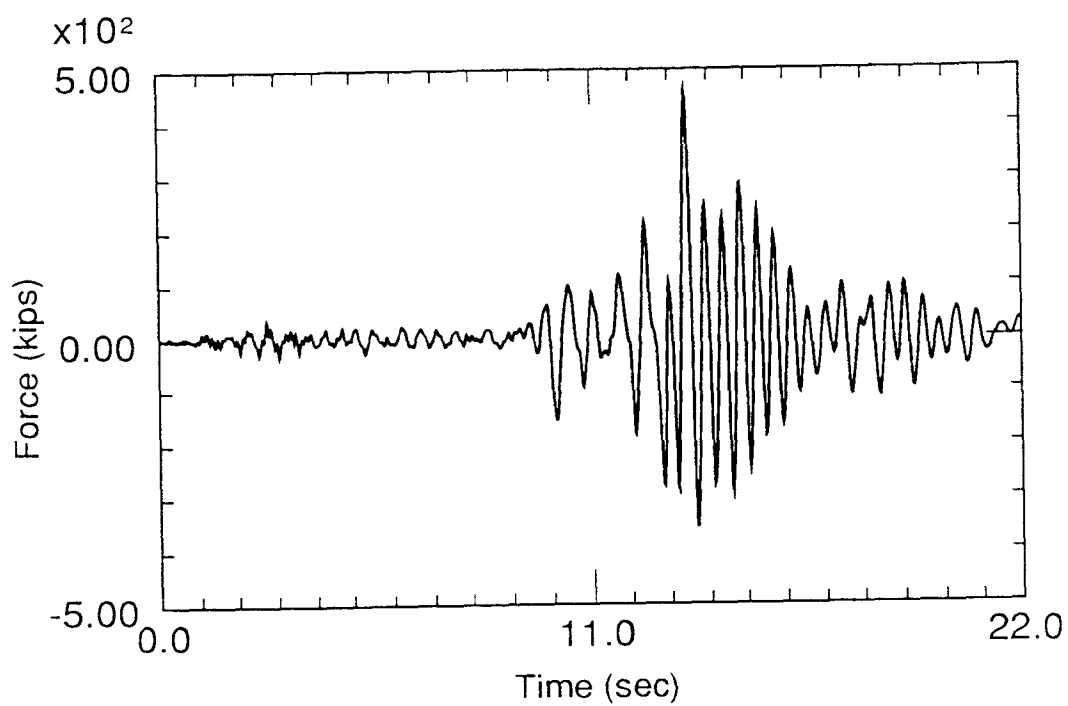


Figure 4.24 Seismic Shear Force at Shear Key (Node 2)

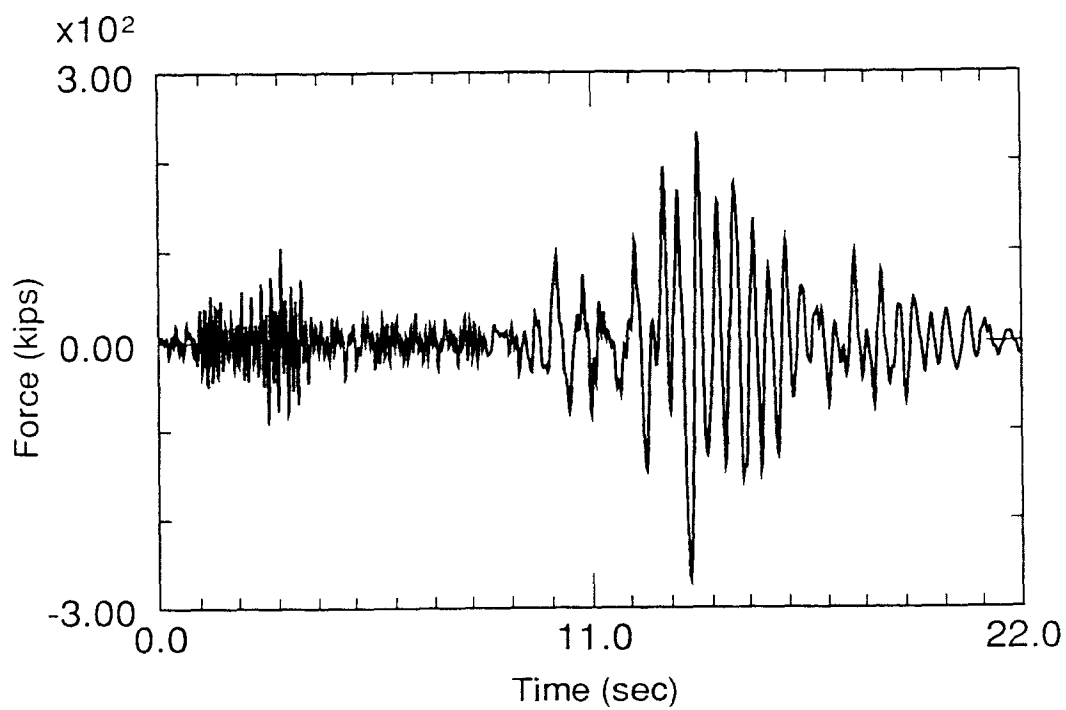


Figure 4.25 Seismic Axial Force at Shear Key (Node 2)

B. Linear Time History (using vertical record only)

Analysis is performed using the vertical record of the ground motion only to determine the contribution of this record to the collapse of the structure.

Time history of the forces and displacements (bent height = 46 ft) are shown in Figures 4.26–4.31. As seen from the previous figures, the vertical displacements throughout the bent (nodes 2, 4, and 5) are insignificant. The increase in the axial force in the upper columns did not exceed 70 kips = 0.025W during the period of time of our interest (10th-15th second), which is insignificant. Also, the seismic shear force at the shear key did not exceed 10 kips. Therefore, the effect of the vertical ground motion is negligible.

The previous force represents only 1/10 of the gravity load resisted by the upper column, which is relatively small. Despite the fact that the vertical acceleration of the upper deck was amplified by a factor of 3.82, the axial force in the upper column increased by only 10%. Also, the axial force of the balanced condition for sections 1–1, and 3–3 (from P-M diagrams) are 4,000 kips and 11,400 kips, respectively, which are significantly higher than the axial forces exerted on sections 1–1 and 3–3 due to gravity and ground motion combined.

It was mentioned earlier in Chapter 2 (Section 2.2.1) that the eyewitnesses described the movement of the structure during the earthquake as a giant wave travelling down the structure and behind the wave a portion of the structure collapsed. But from analysis above, there was almost no vertical displacements throughout the structure. Therefore, the giant wave can be explained as a mode of failure (collapse) of the different bents. Where the sequence of collapse of the bents appeared as a wave.

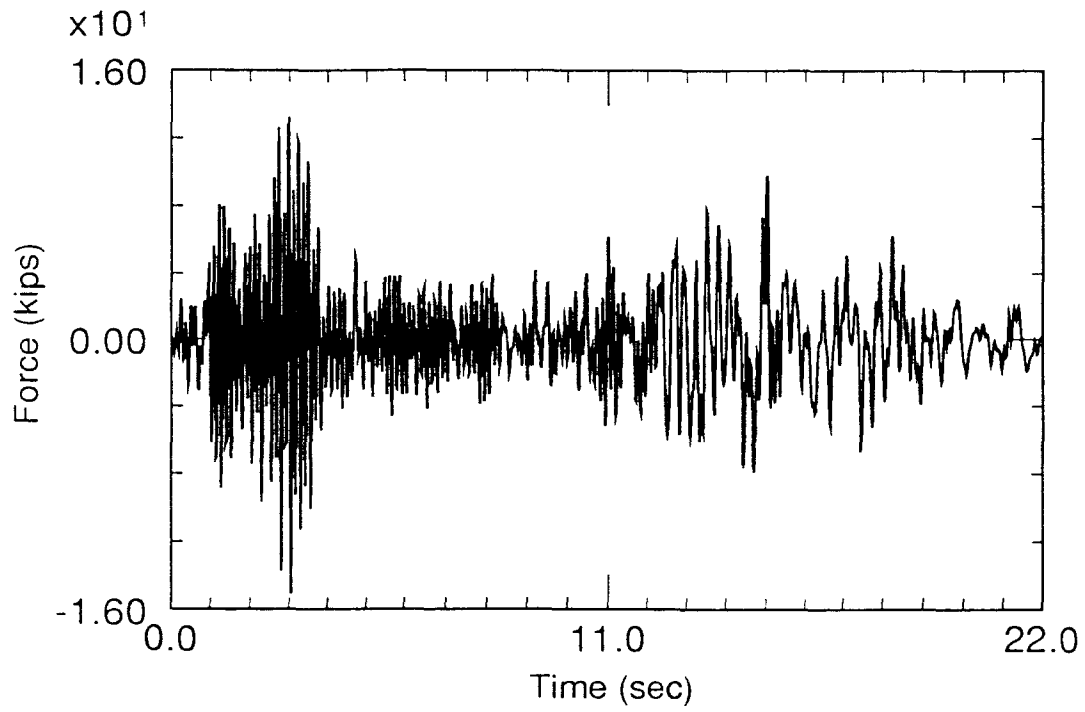


Figure 4.26a Seismic Shear Force at Shear key (Node 2)

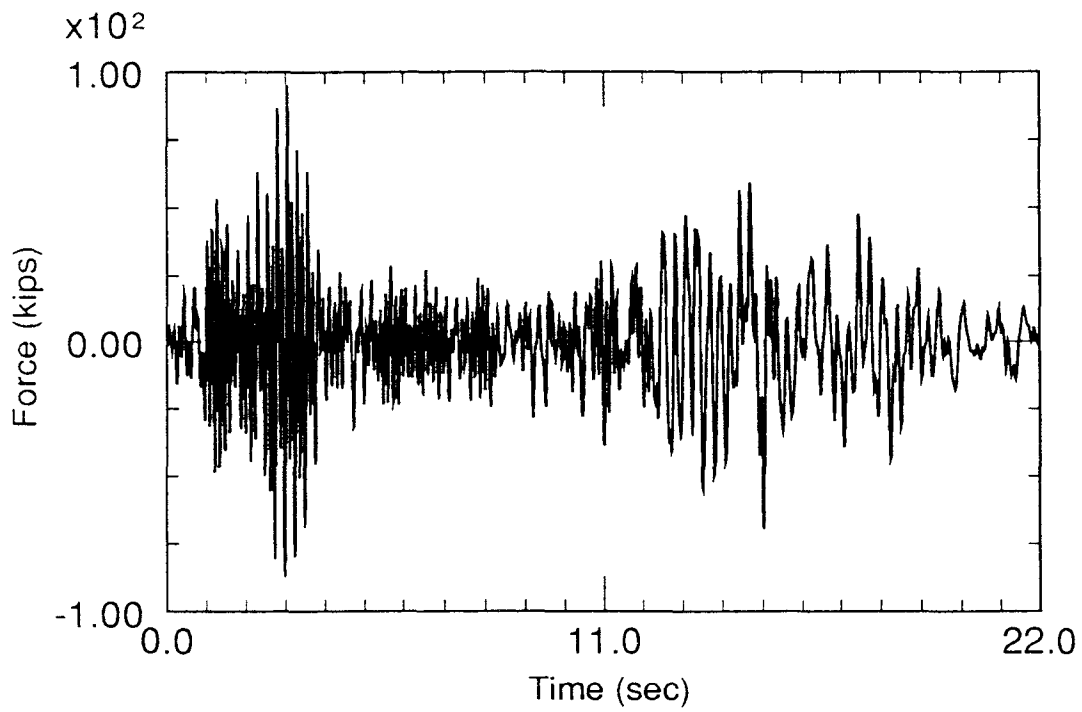


Figure 4.26b Seismic Axial Force at Shear Key (Node 2)

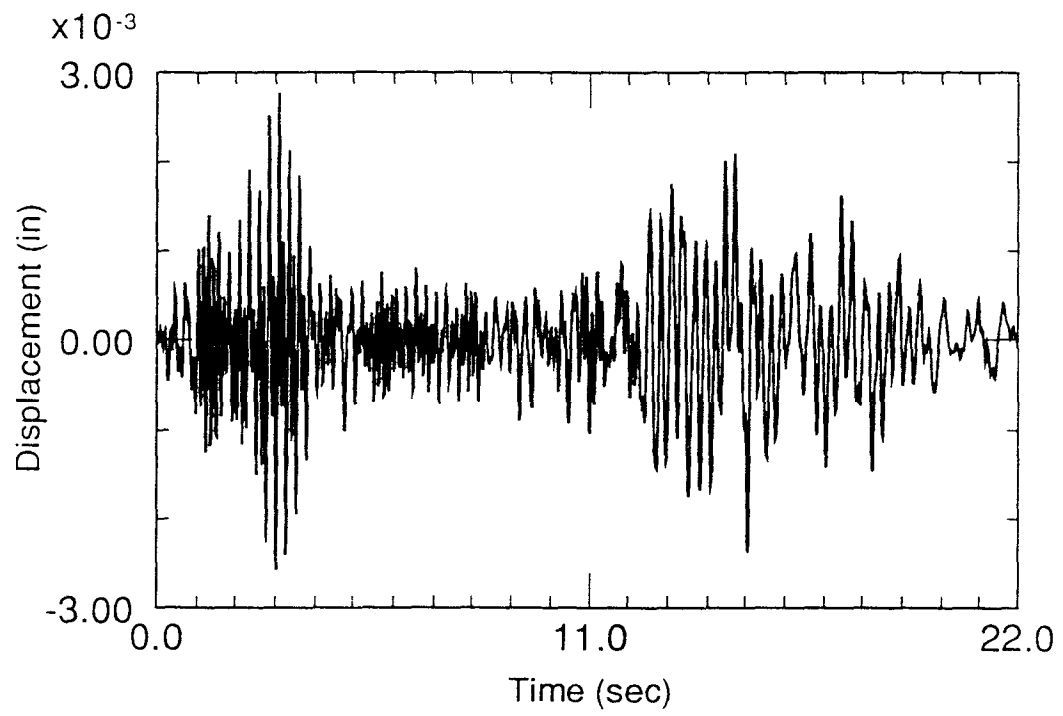


Figure 4.27 Vertical Displacement (Node 2)

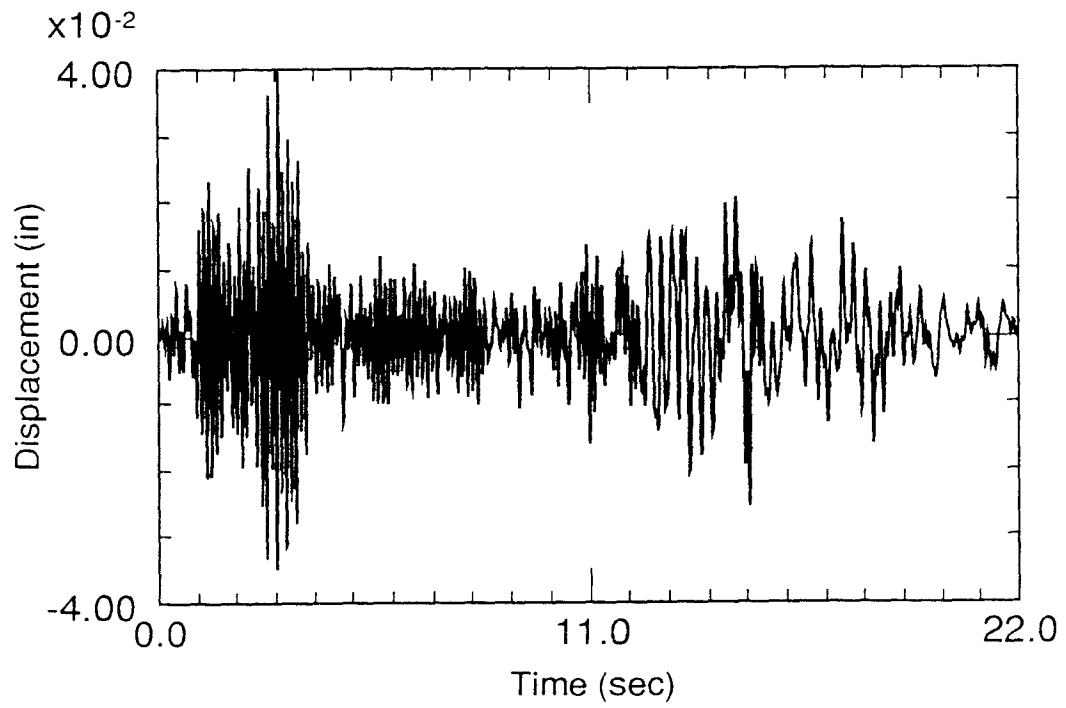


Figure 4.28 Vertical Displacement (Node 4)

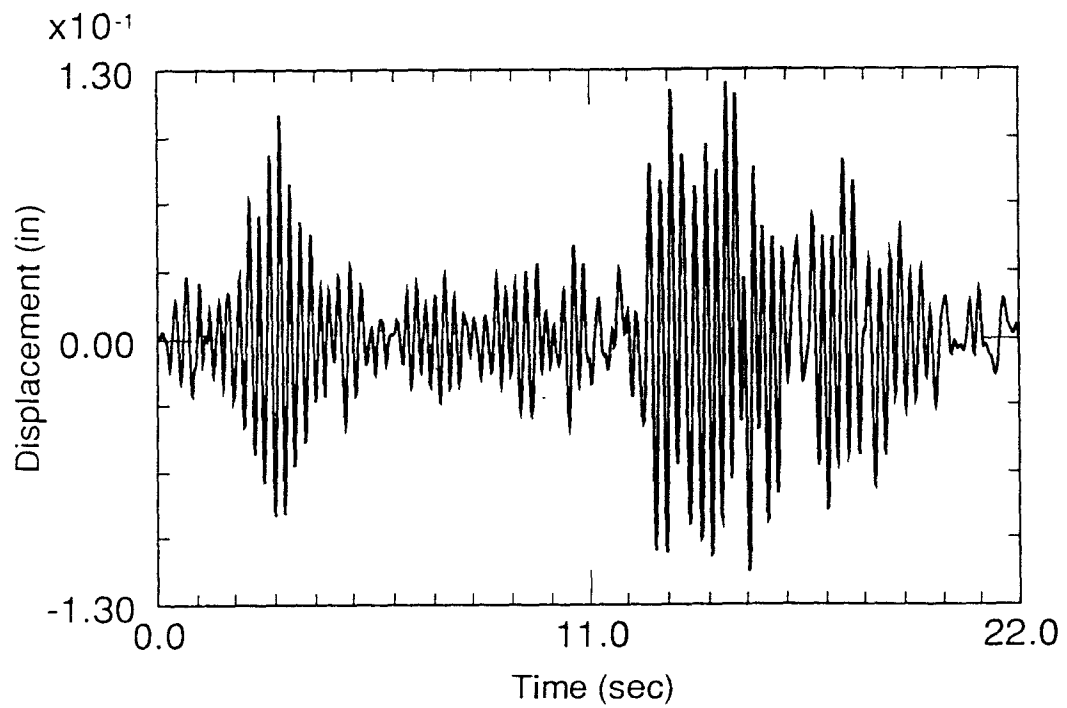


Figure 4.29 Vertical Displacement (Node 5)

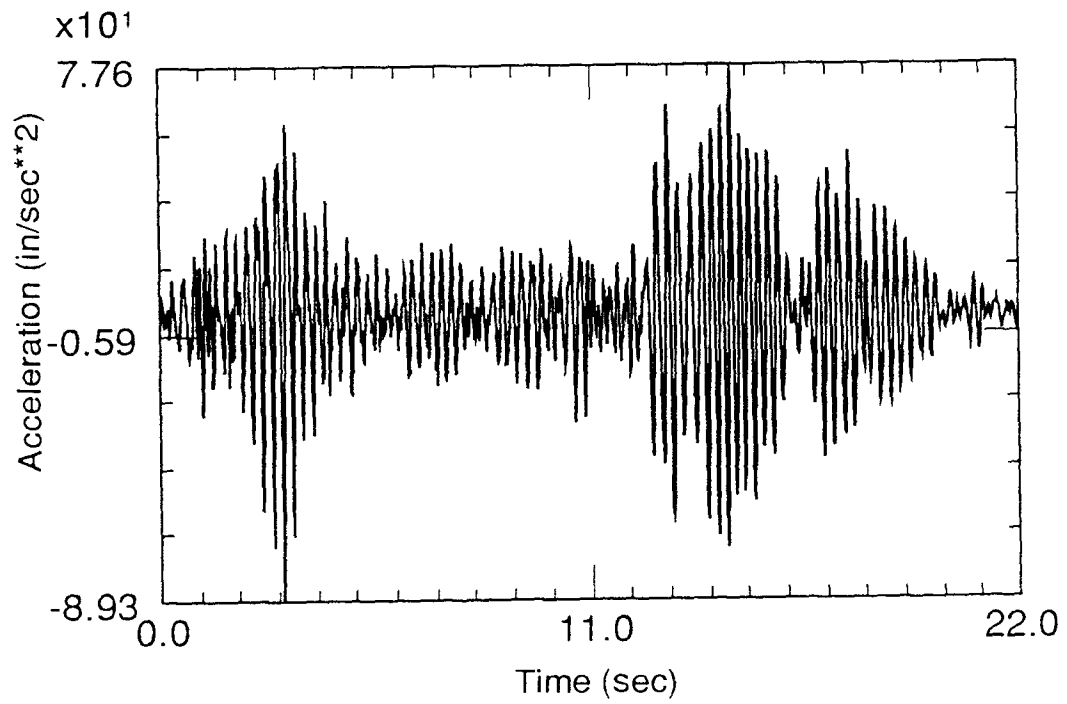


Figure 4.30 Vertical Acceleration (Node 5)

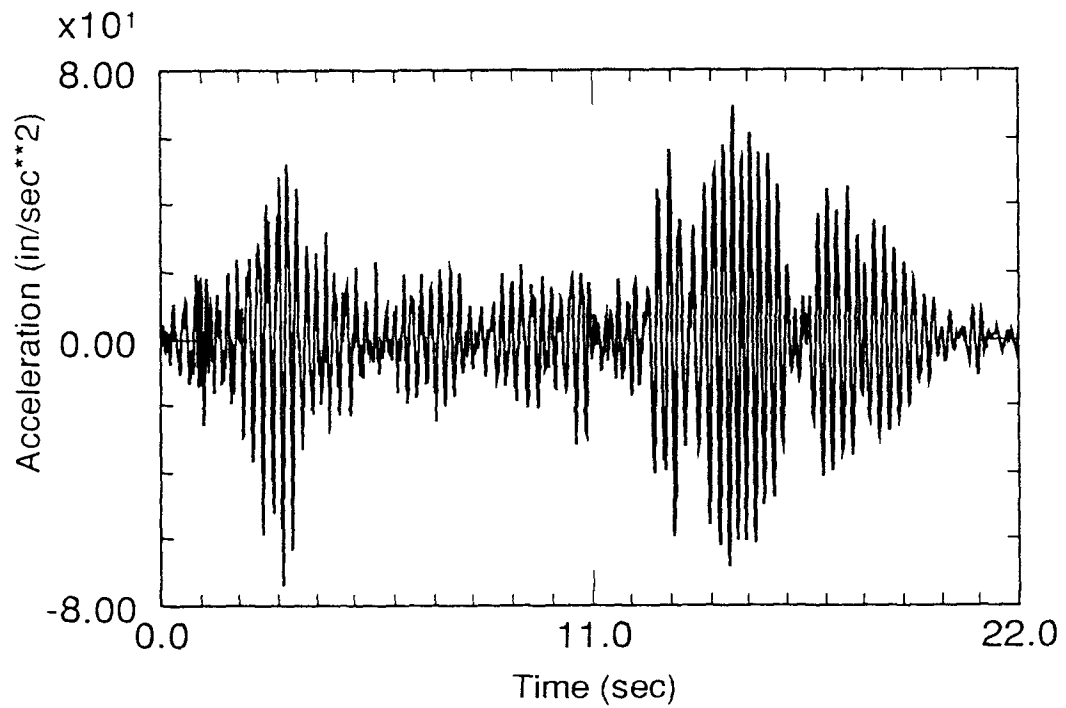


Figure 4.31 Vertical Acceleration (Node 6)

4.2 Analyses of B2 Bent

Analyses are performed on a 3-D model (consisting of two B2 bents) modeled in the same manner as for the 3-D model of B1. Figure 4.32 shows the three dimensional model.

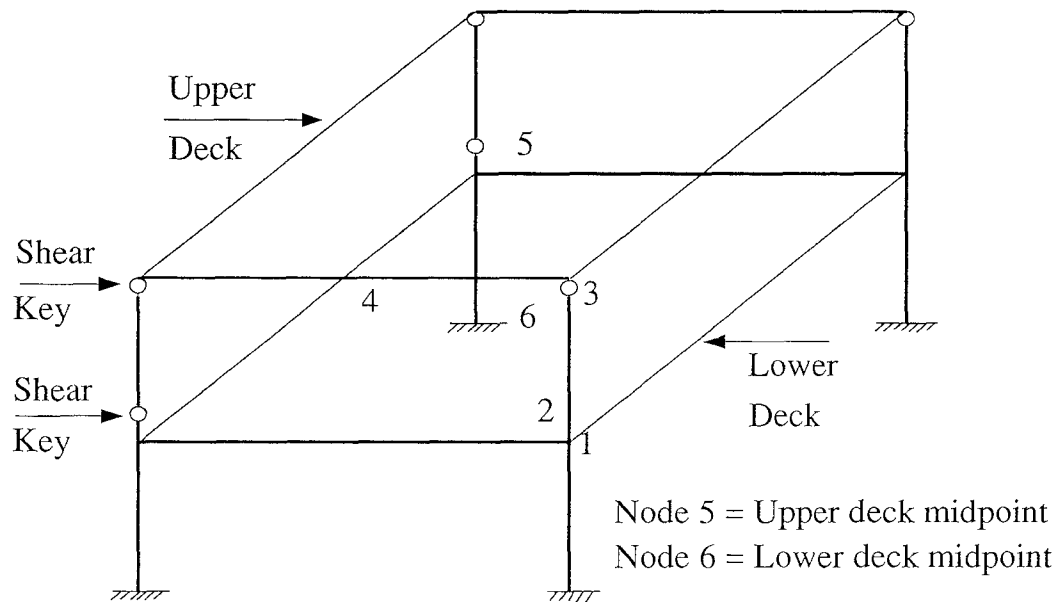


Figure 4.32 3-D Model of B2 Bent.

The results of the frequency analysis are listed in the following table:

Table 4.11 Fundamental Frequencies

Bent Height	1 st	2 nd	1 st	2 nd
	Transverse	transverse	Vertical	Vertical
46 ft	1.44	6.40	3.93	4.02
52 ft	1.38	4.84	3.92	4.01

Bent Height	1 st	1 st
	Longitudinal	Torsional
46 ft	0.70	1.66
52 ft	0.60	1.55

Linear time history analysis is performed using the same input ground motion records used for B1 bent model. The results are listed in the following tables:

Table 4.12: Maximum Lateral Displacements

Bent Height	Displacement (node 3) (in)	Displacement (node 1) (in)
46 ft	3.72 (t = 12.96 sec)	0.44 (t = 12.98 sec)
52 ft	3.60 (t = 13.00 sec)	0.68 (t = 13.02 sec)

Table 4.13: Seismic Shear and Axial Forces

Bent Height	Max. Shear (node 1) (kips)	Total Shear (node 1) (kips)	Max.Tension (node 1) (kips)	Total Axial (node 1) (kips)
46 ft	1137 (t = 12.94 sec)	1137	-80 (t = 2.84 sec)	628
52 ft	994 (t = 12.98 sec)	994	-81 (t = 2.84 sec)	627

Table 4.14: Seismic Forces

Bent Height	Max. Force (lower deck) (kips)	Force (upper deck) (kips)	Ratio
46 ft	367 (0.13W) (t = 12.98 sec)	726 (0.26W) (t = 12.98 sec)	1 : 1.98
52 ft	429 (0.15W) (t = 13.04 sec)	594 (0.21W) (t = 13.04 sec)	1 : 1.38

Table 4.15: Vertical Accelerations (Bent Height = 46 ft)

Location	Max. Vertical Acceleration (in/sec ²)	Amplification Factor
Midpoint (upper deck) (node 5)	81.5 (0.21 g)	3.51
Midpoint (Lower deck) (node 6)	74 (0.19 g)	3.19

The time history of displacements and forces (bent height = 46 ft) are shown in Figures 4.33–4.36.

As seen from the Table 4.12 and 4.13 and Figures (4.33–4.36), the maximum lateral displacements of both decks, the maximum shear forces, and the maximum tensile forces in columns (just below the shear keys) occurred during the 13th second of the ground motion (13th-14th second).

The maximum lateral displacement of the upper deck (3.72 in.) is higher than the maximum displacement of B1 bent (1.88 in.). As mentioned before B1 bent had undergone inelastic deformations in the upper story. Therefore, B2 bent is expected to have suffered inelastic deformations. The maximum seismic tensile and compressive forces, ± 81 kips, indicates that there were insignificant changes in axial forces in the upper columns. Therefore, the axial forces had no effect on this bent type. Also, the maximum vertical acceleration of columns and girders are insignificant.

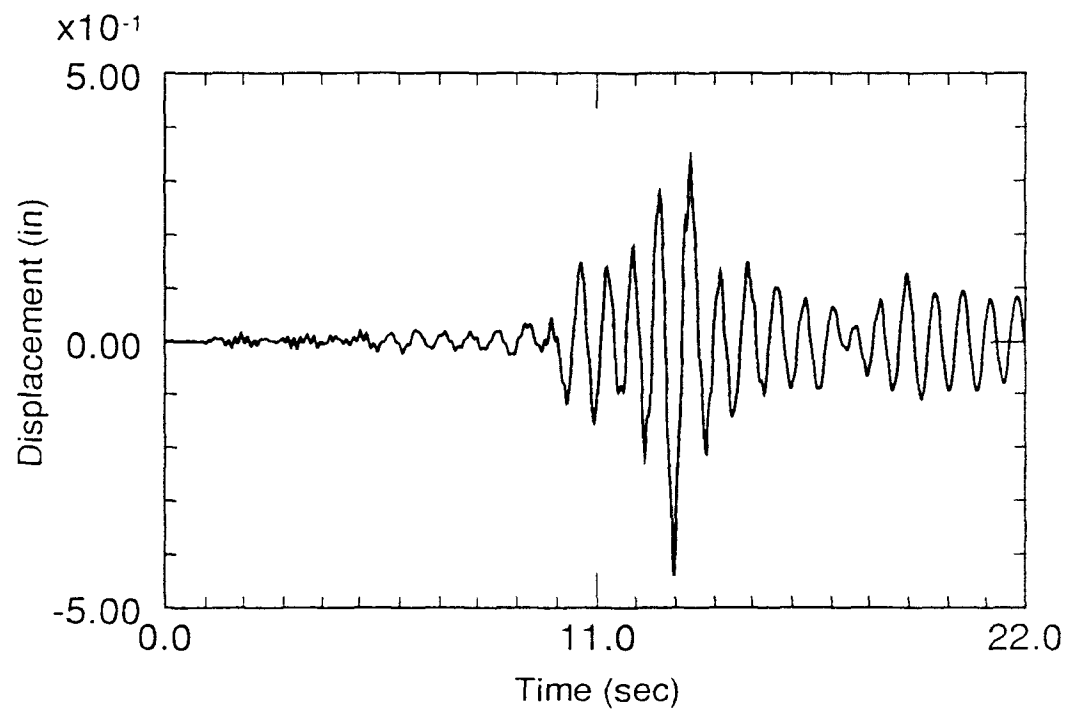


Figure 4.33 Lateral Displacement (Node 1)

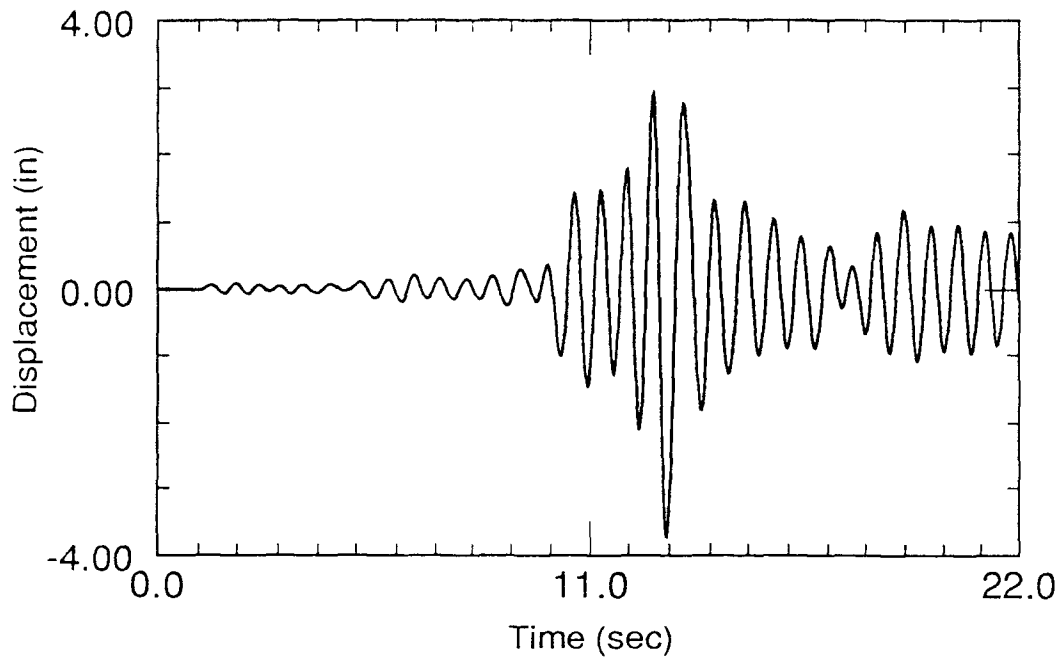


Figure 4.34 Lateral Displacement (Node 3)

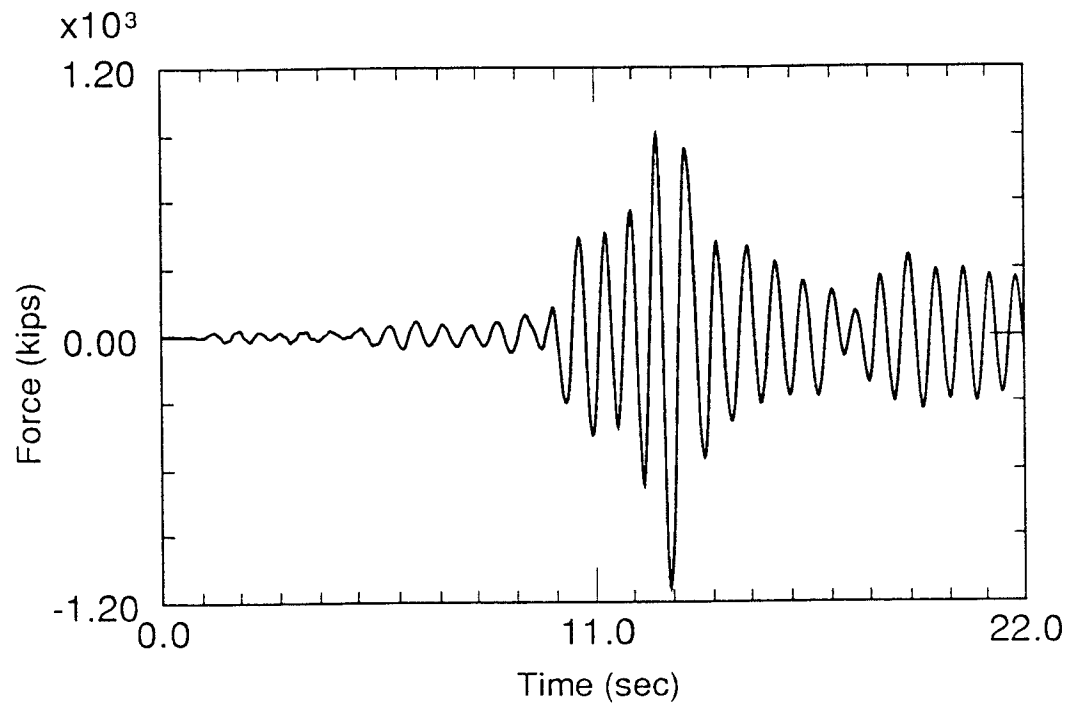


Figure 4.35 Seismic Shear Force (Node 1)

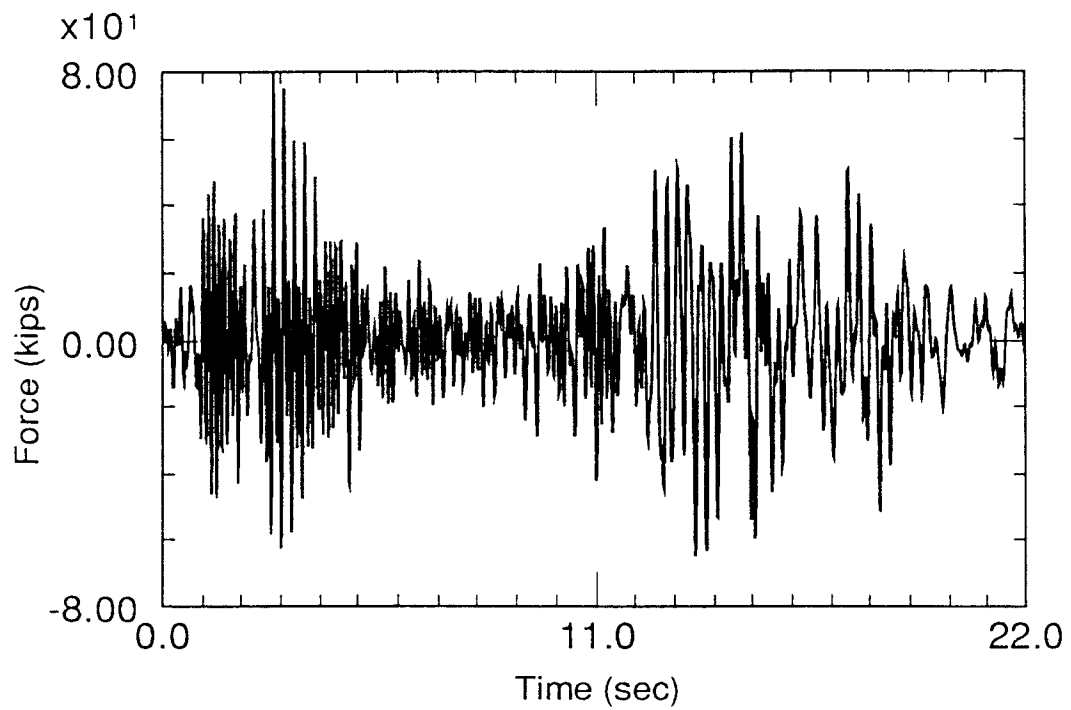


Figure 4.36 Seismic Axial Force (Node 1)

4.3 B3 bents

Analyses are performed on a 3-D model consisting of two B3 bents (shown in Figure 4.37) for bent height equal to 51.4 ft. The structure is modeled in the same manner as for B1 and B2 models.

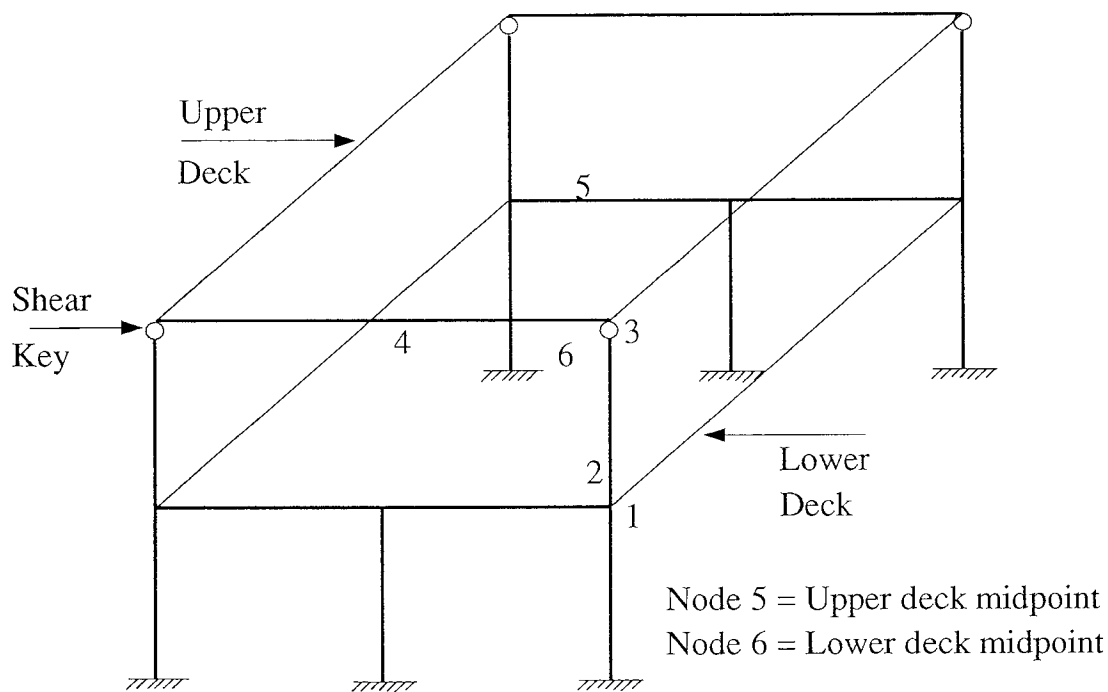


Figure 4.37 3-D Model of B3 Bents.

The results of the frequency analysis are listed in the following table:

Table 4.16: Fundamental Frequencies

Bent Height	1 st Transverse (Hz)	2 nd Transverse (Hz)	1 st Vertical (Hz)	2 nd Vertical (Hz)
51.4 ft	1.45	5.37	3.92	4.07

Bent Height	1 st. Longitudinal (Hz)	1 st. Torsional (Hz)
51.4 ft	0.76	1.76

Linear time history analyses are performed using the same input ground motion records used for B1 and B2 models. The results are listed in the following tables:

Table 4.17: Maximum Lateral Displacements

Bent Height	Displacement (node 3) (in)	Displacement (node 1) (in)
51.4 ft	3.74 (t = 12.94 sec)	0.6 (t = 13.00 sec)

Table 4.18: Seismic Shear and Axial Forces

Bent Height	Max. Shear (node 1) (kips)	Total Shear (node 1) (kips)	Max. Tension (node 1) (kips)	Total Axial (node 1) (kips)
51.4 ft	594 (t = 12.94 sec)	594	-635 (t = 13.80 sec)	73

Table 4.19: Seismic Forces

Bent Height	Max. Force (upper deck) (kips)	Force (lower deck) (kips)	Ratio
51.4 ft	542 (0.19W) (t = 13.0 sec)	624 (0.22W) (t = 13.0 sec)	1 : 1.15

The time history of displacements and forces are shown in Figures 4.38–4.41.

The maximum lateral displacement of the upper story, 3.74 in., shown in Figure 4.49, indicates inelastic deformations in the upper story.

The maximum seismic axial tension force (635 kips), shown in Figure 4.41, did not exceed the vertical compressive force (708 kips) resisted by the upper column due to gravity loads, which shows that net force acting on the upper columns during the earthquake was compressive, implying that there was no effect on the shear strength of concrete at section 2–2 by the axial force (where tension forces reduce the shear strength).

The maximum vertical accelerations of the upper and the lower decks (nodes 5 and 6) are amplified by 3.49 and 2.8 times, respectively.

A comparison of these results with the results of static analyses will be presented later.

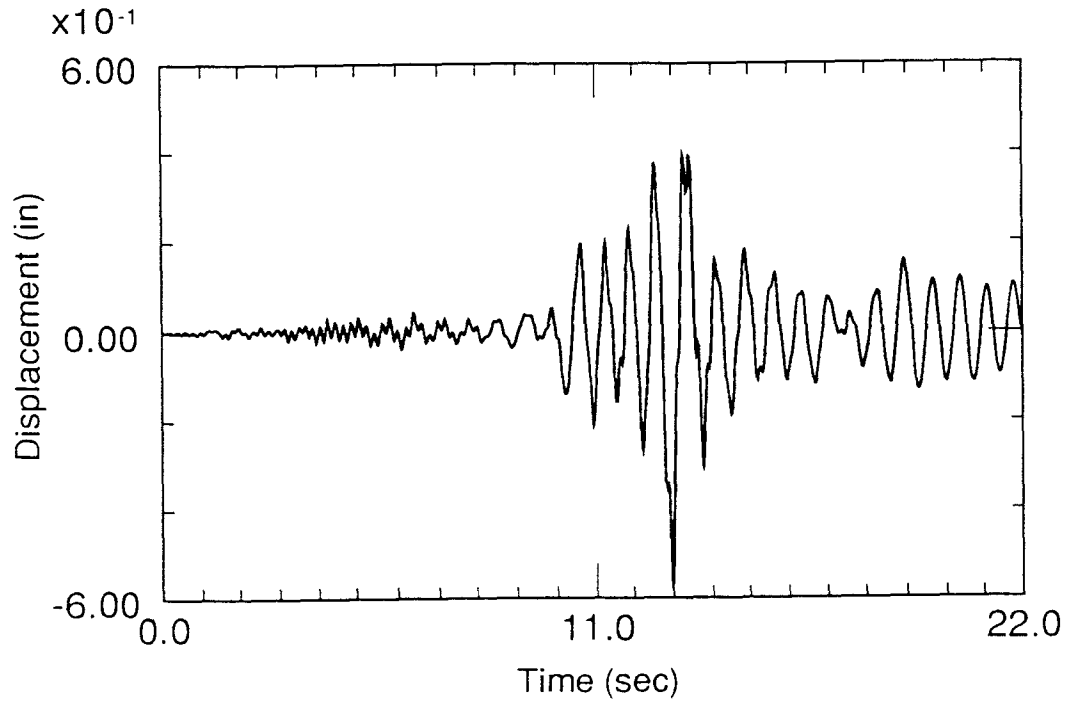


Figure 4.38 Lateral Displacement (Node 1)

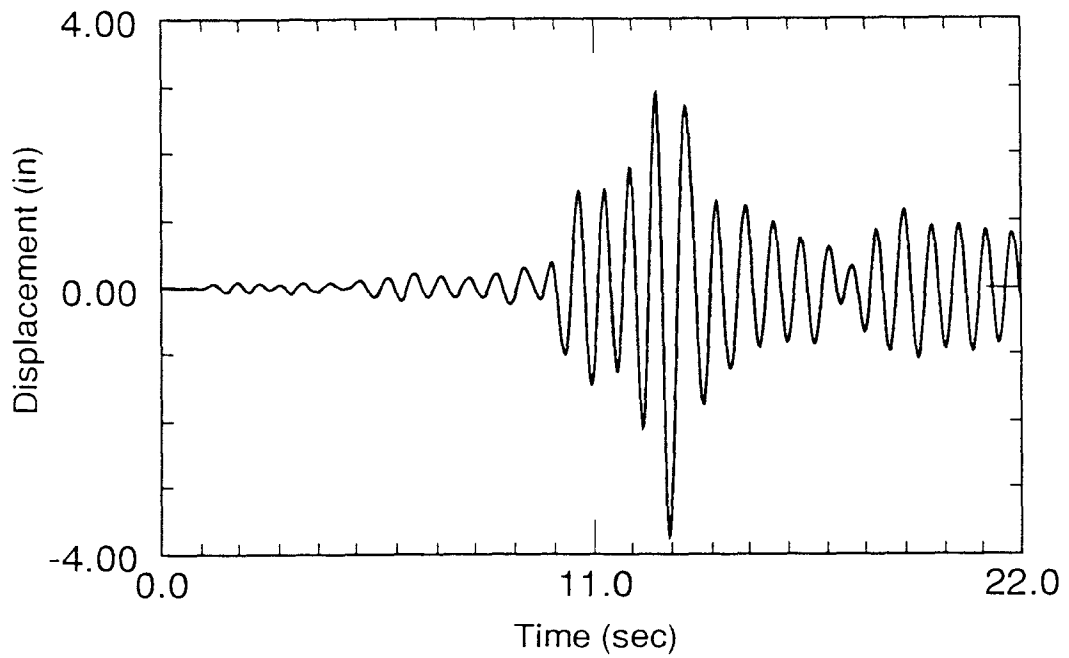


Figure 4.39 Lateral Displacement (Node 3)

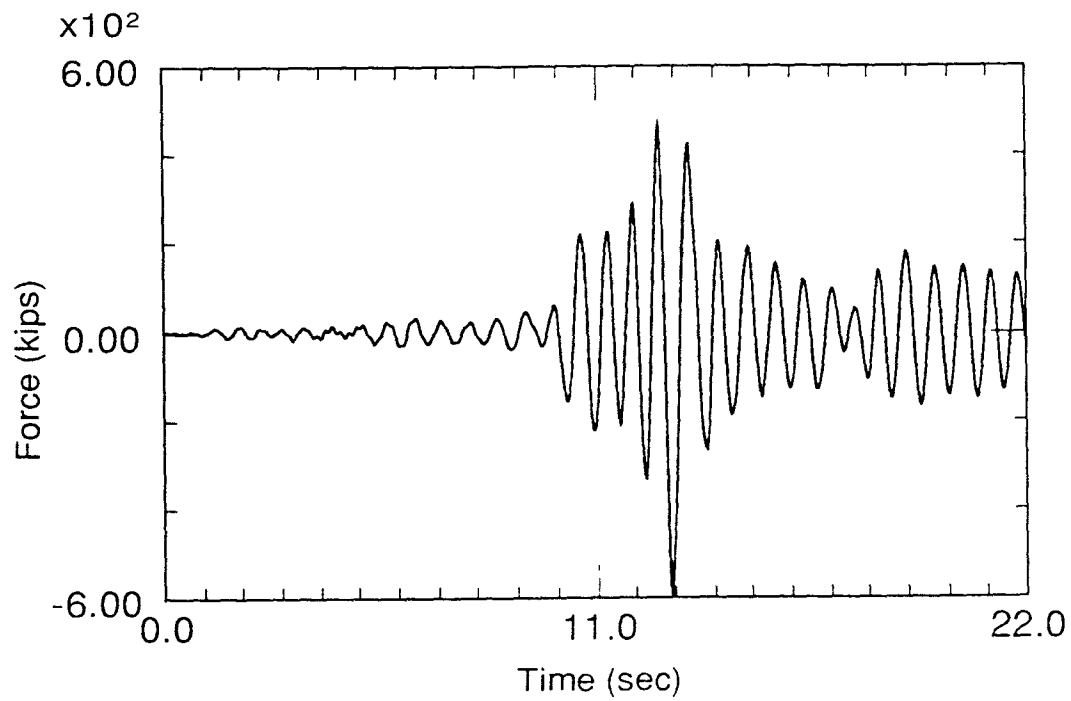


Figure 4.40 Seismic Shear Force (Node 1)

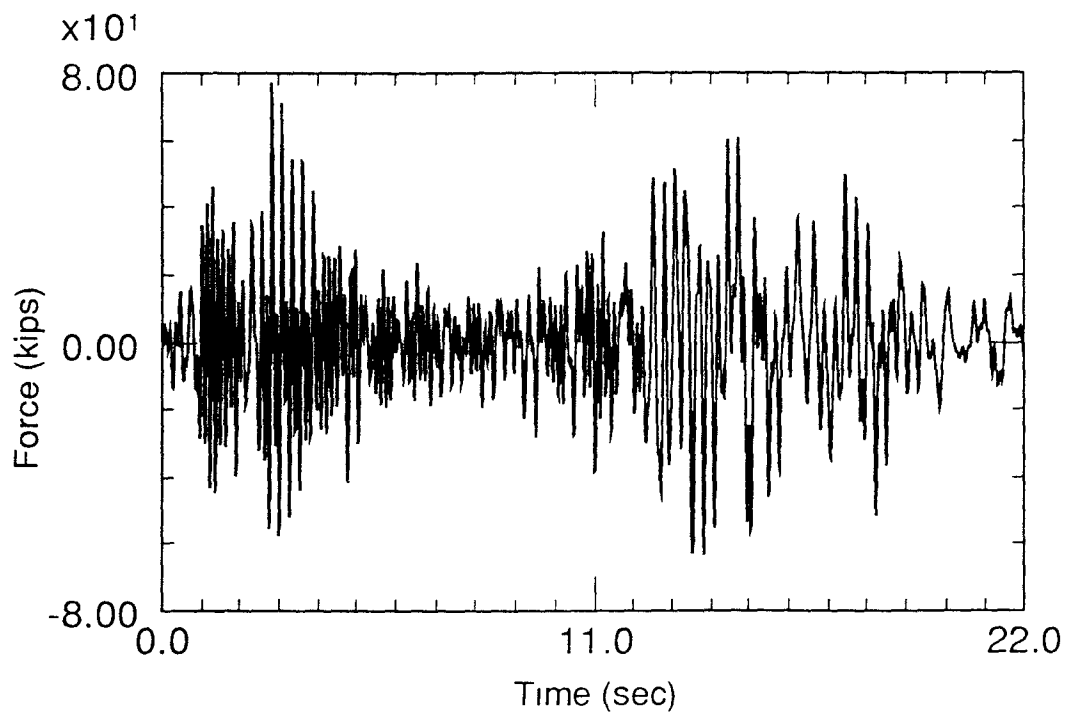


Figure 4.41 Seismic Axial Force (Node 1)

4.4 Nonlinear Analysis

4.4.1 General

A limited nonlinear analysis is performed on a 2-D model of B1 bent to show the distribution of stresses and strains in the bent. The distribution of stresses and strains in the upper columns below the shear keys are of a particular interest because of the vulnerability of that portion of the bent to shear and flexural cracking as mentioned earlier in static analyses (Chapter 3). The bent is modeled with elastic plain stress elements except for a limited portion above the shear keys that are modeled with nonlinear concrete elements. The concrete elements are a good representation of the shear keys for the reason that they crack when the tensile stresses exceed the concrete tensile strength. When the concrete elements crack, local concentration of compressive stresses might take place and that will affect the distribution of stresses and strains of that part of the structure. In the analysis, the lateral seismic forces obtained from time history analysis are applied at the upper and the lower girders (792 kips at the upper girder and 594 kips at the lower girder).

Figure 4.42 shows the distribution of the tensile stresses in the lower girder-to-column joint. Large portion of the column was subjected to tensile stresses far exceeded the tensile strength of concrete (83.7 k/ft^2). The previous stresses is expected to be reversed on the other side of the column when seismic forces are reversed due to cycling. Therefore, extensive flexural concrete cracking is expected to take place at the joint between the upper columns and the lower girder and diagonal shear cracking at the discontinuous surface of the upper columns. Due to cracking, that portion of the column became a point of weakness in the structure.

Figure 4.43 shows the stress vectors in the column indicating high tensile stress concentration at the inner side of the joint.

Figure 4.44 shows the strain distribution in the previous joint. Below the shear keys, the upper columns are subjected to strains far exceeded the tensile strain of concrete (0.000124), indicating extensive cracking at these locations.

4.5 Comparison of Static and Dynamic Analyses

4.5.1 B1 Bents

From time history analyses of B1 bents, the total shear force of the upper columns is 604 kips (Table 4.7). This force represents the seismic force F in the static analysis. For section 1–1 this force would cause extensive flexural cracking (starts at 310 kips).

For section 2–2, the force 604 kips far exceeded the 185 kips required to cause shear failure.

For section 3–3, which was already cracked due to gravity load as mentioned earlier, the force 604 kips would cause extensive flexural cracking, and yielding of steel (starts at 470 kips).

By adding the shear force due to gravity load (120 kips) to the maximum seismic shear force (604 kips), we get a total shear force of 724 kips at section 1–1. That total shear force is significantly less than 1,267 kips required to cause shear transfer failure.

From above, the maximum seismic shear force (604 kips) would not cause flexural failure at section 1–1 or section 3–3 or cause shear transfer failure at section 1–1. But it would cause shear failure at section 2–2 and extensive flexural cracking at sections 1–1 and 3–3. It would also cause steel yielding at section 3–3.

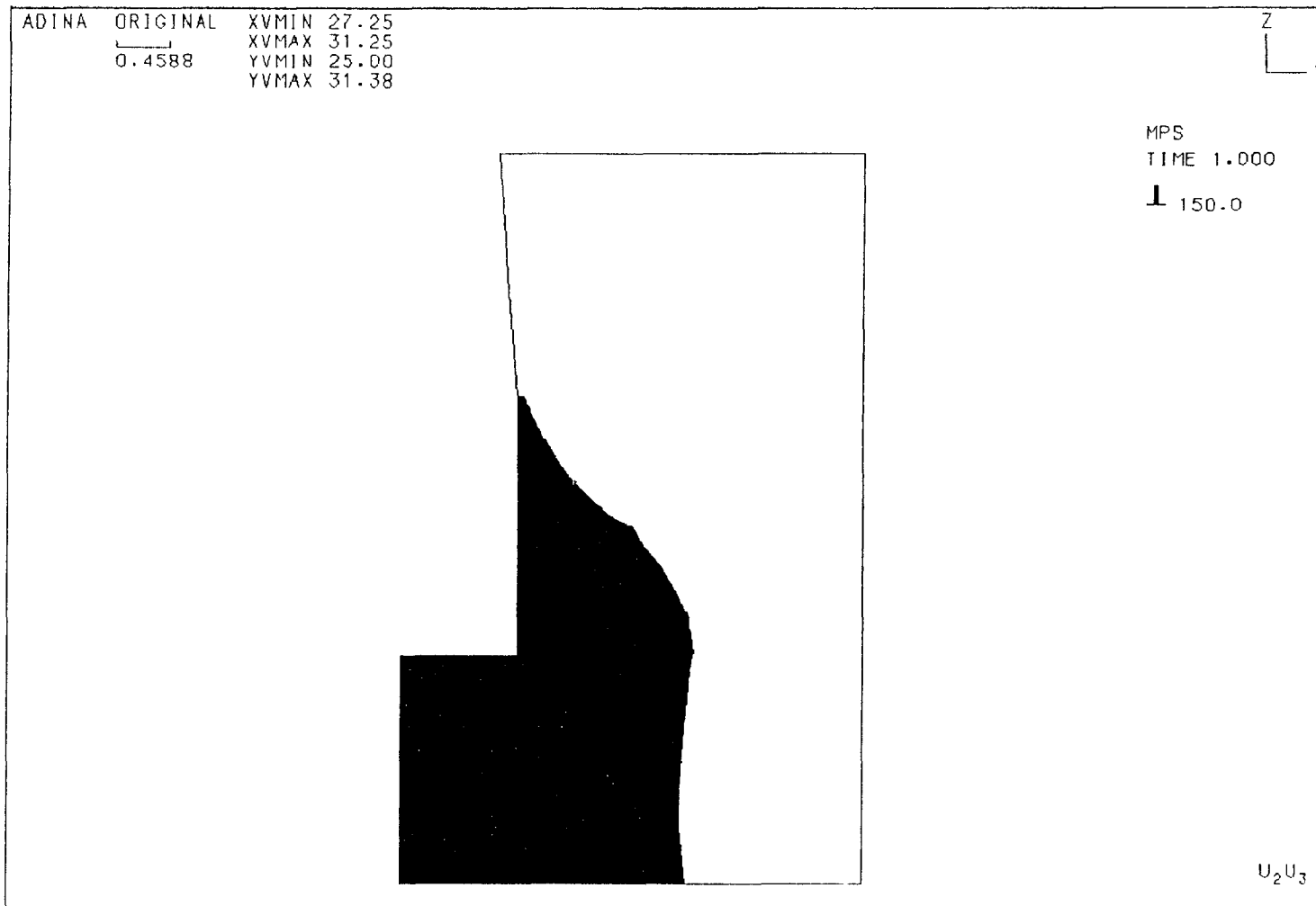


Figure 4.42 Tensile Stresses in Lower Girder-to-Column Joint

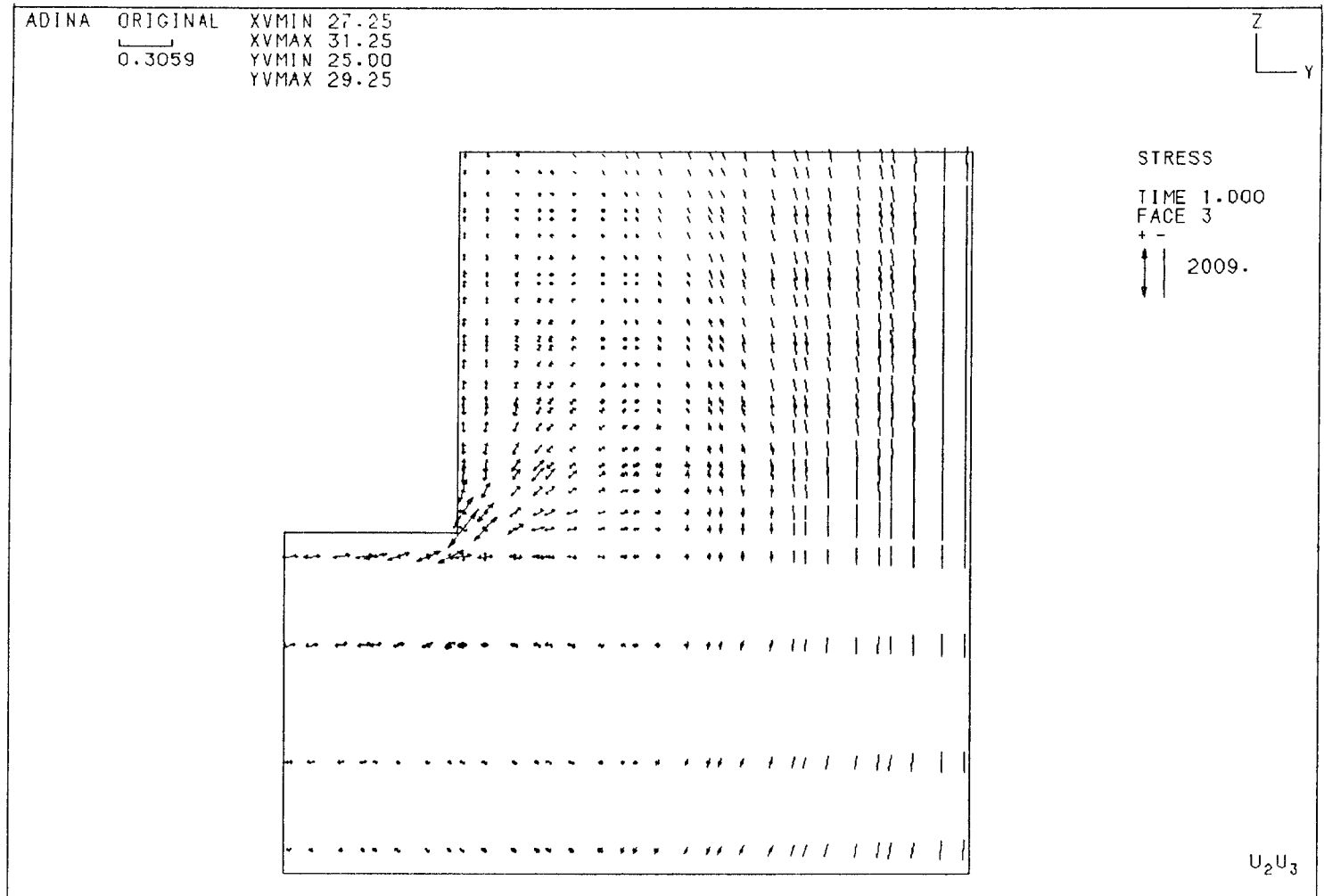


Figure 4.43 Stress Vectors in the Upper Column (Below the Shear Key)

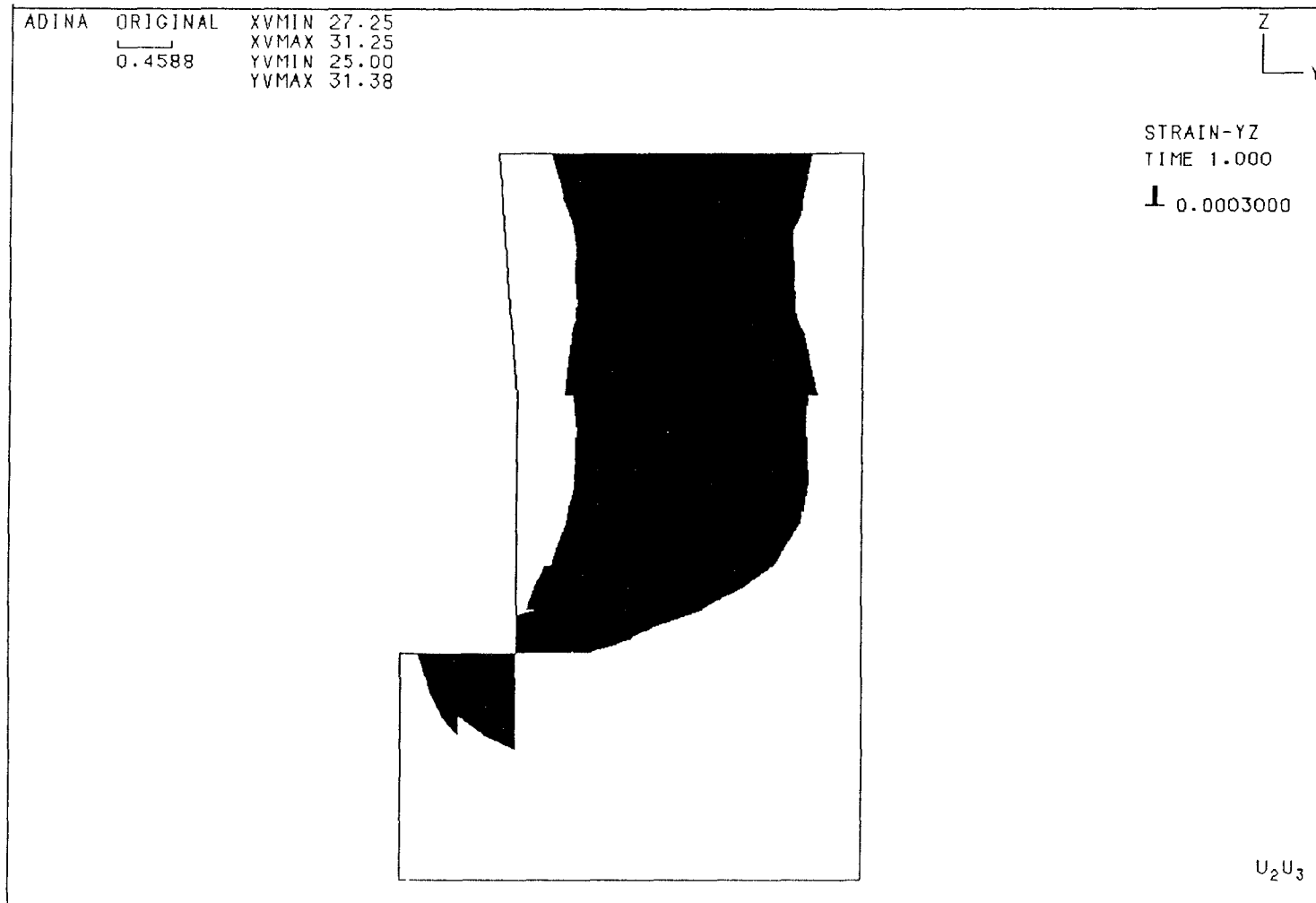


Figure 4.44 Strain Distribution in the Lower Joint

The pedestals (the part of the upper columns below the shear keys) on both sides of the bent suffered shear failure at section 2-2 and extensive flexural cracking at section 1-1 (Figure 4.45). This enabled the gravity load of the upper story to push the pedestals down and away (laterally) from the bent causing the upper deck to fall down on top of the lower deck as shown in Figure 4.46. The collapse appeared to be perfectly vertical due to the fact that the lateral displacement of the upper deck was small. The extensive cracking at section 3-3 (both sides of the section) allowed rotation of the upper columns at that location, suggesting that the upper columns pushed the pedestals in an inclined direction away from the bent.

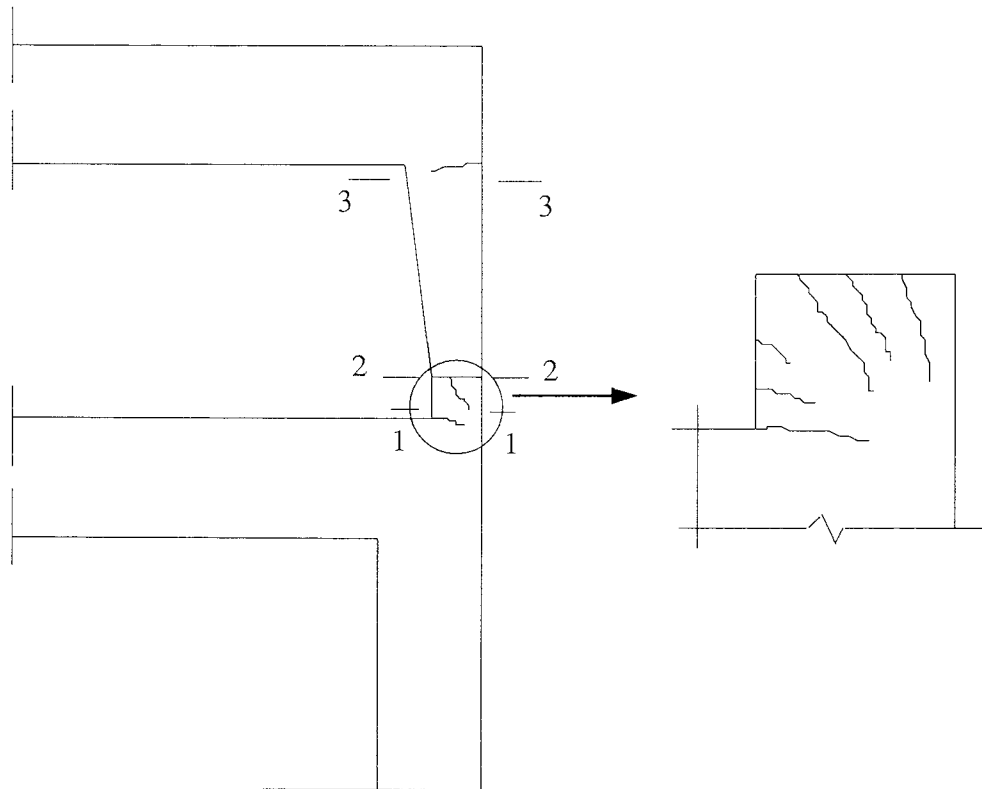


Figure 4.45 Damage to B1 Bents

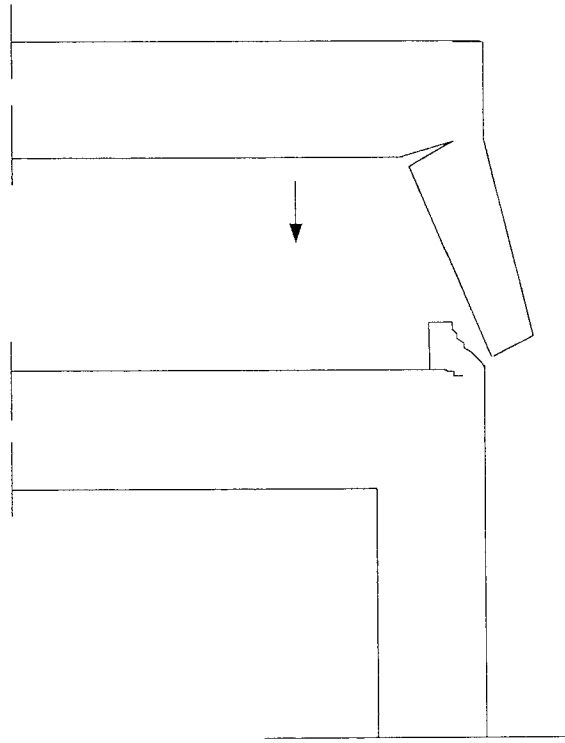


Figure 4.46 Collapse of B1 Bent

The maximum seismic axial force in the upper columns due to the vertical component of the ground motion is 70 kips = $0.025W$ = 1/10 of the gravity loads resisted by upper column, which is insignificant to cause vertical failure. But this might have contributed to pushing the pedestals downward.

4.5.2 B2 Bents

The maximum seismic shear force obtained from time history analysis in the continuous upper column is 1,137 kips. This force, which represents the force $2F$ in the static analysis, had far exceeded the force required to cause flexural failure at section 1-1 (occurs at $2F = 260$ kips). Therefore, the expected mode of failure of B2 bents is a flexural failure due to the horizontal ground motion.

4.5.3 B3 Bents

The maximum seismic shear force in the upper column is 594 kips obtained from time history analysis. This value, which represents the $0.91F$ used in static analysis, gave a value of F equal to 653 kips. This force F had exceeded the value 400 kips determined from static analysis that would cause a flexural failure at section 1-1. Therefore, a flexural failure of the upper columns and collapse of B3 bents would be expected due to the horizontal ground motion.

The fact that the two B3 bents (Bents 96 and 97) did not collapse would lead to the belief that the real intensity of the ground motion was less than the intensity of the ground motion record used in time history analyses (peak horizontal acceleration = $0.29g$).

CHAPTER 5

CONCLUSION

The existence of the shear keys in the bents throughout the structure resulted in vulnerability of the structure to shear failure. At the discontinuous surfaces, only concrete shear strength is accounted for (no contribution of steel). The shear and the axial forces exerted on a section control the concrete shear strength. While the compressive force increase the shear capacity of a section, the tensile force decrease it (see Equation 3.13, Section 3.3.5). Therefore, the combined effect of shear and axial forces on the critical sections (especially for B1 bent) was studied to determine the cause of the shear failure at the shear keys. Also, to determine whether the previous effect on the shear failure was due to the horizontal ground motion or the vertical ground motion or a contribution of both.

Time history analyses for B1 bent showed that the effect of the vertical was very limited. The maximum axial force of the upper column was 70 kips, while the maximum shear force at the shear keys was 10 kips. Assuming that the actual vertical ground acceleration was higher than the one used in analyses would not yield large forces. Therefore, the effect of the vertical motion is negligible. Also, time history analyses showed that the seismic forces due to horizontal ground motion would cause flexural failure (at the upper frame) of B2 and B3 bents. And would cause shear failure at the shear keys and flexural cracking to the upper columns (specifically below the shear keys) leading to the failure of B1 bents.

BIBLIOGRAPHY

- [1] Lew, H.S. (Editor). "Performance of Structures during the Loma Prieta Earthquake of October 17, 1989." NIST Special Publication 778 (ICCS-CTR11), U.S. Department of Commerce, National Institute of Standards and Technology (NEL), Jan. 1990.
- [2] Abolhassan, Aastaneh (Editor). "Preliminary Report on the Seismological and Engineering Aspects of the October 17, 1989 Santa Cruz (Loma Prieta) Earthquake". Report No. UCB/EERC-89/14, Earthquake Engineering Research Center, University of California, Berkeley, October 1989.
- [3] Benuska, Lee (Editor). "Loma Prieta Earthquake Reconnaissance Report," Earthquake Spectra, Supplement to Volume 6. Earthquake Engineering Research Institute, May 1990.
- [4] Housner, George W. "Competing Against Time," Report to California Governor George Deukmejian. The Governor's Board of Inquiry on the 1989 Loma Prieta Earthquake, May, 1990.
- [5] Nims, P. K., and E. Miranda. "Collapse of the Cypress Street Viaduct as a Result of the Loma Prieta Earthquake." Earthquake Engineering Research Center, Report No. UCB/EERC-89/16, November, 1989.
- [6] ADINA Engineering. "Automatic Dynamic Incremental Nonlinear Analysis."
- [7] Clough, R. W. and J. Penzien. "Dynamics of Structures," McGraw-Hill, Inc., New York, 1975.
- [8] Paz, Mario. "Structural Dynamics Theory and Computation." Van Nostrand Reinhold, New York, 1991.
- [9] Blume, J. A. , N. M. Newmark; L. H. Corning. "Design of Multistory Reinforced Concrete Buildings for Earthquake Motion," Portland Cement Association, Chicago, Illinois, 1961.
- [10] Bathe, K. J. "Finite Element Procedures in Engineering Analysis," Prentice-Hall, Inc. , Englewood Cliffs, New Jersey, 1982.
- [11] Cook, R. D. "Concepts and Applications of Finite Element Analysis," John Wiley and Sons, New York, 1981.

- [12] Wang, Chu-Kia, Charles G. Salmon. "Reinforced Concrete Design," Happer & Row, Publishers, New York, 1985.
- [13] Park, R. and T. Paulay. "Reinforced Concrete Structures," John Wiley and Sons, New York, 1975.
- [14] Hassoun, M. Nadim. "Design of Reinforced Concrete Structures," PWS Engineering, Boston 1985.